# Non-Reciprocal Heat Transfer in Quantum Systems

by

**Cahit Kargı**

A Dissertation Submitted to the
Graduate School of Sciences and Engineering
in Partial Fulfillment of the Requirements for
the Degree of

Master of Science

in

Physics

KOÇ
UNIVERSITY

June 2, 2018

**Koç University**

**Graduate School of Sciences and Engineering**

This is to certify that I have examined this copy of a master's thesis by

**Cahit Kargı**

and have found that it is complete and satisfactory in all respects,
and that any and all revisions required by the final
examining committee have been made.

Committee Members:

_____

Prof. Dr. Özgür Esat Müstecaplıoğlu (Advisor)

_____

Prof. Dr. Mauro Paternostro

_____

Assoc. Prof. Dr. Menderes Işkın

Date: _____

*To my beloved mom, a strong woman who raised me almost all alone, and through her to all women (or men), like her and in her words, "left in the dark" by being kept away from any education at all, most of whom, I believe, would do wonders with a proper education.*

# ABSTRACT

Abundance of heat makes it a good candidate as an energy resource, but our ability in manipulating heat is so limited. As a new way of heat control, thermal analogs of non-reciprocal electronic devices, such as a diode, transistor, etc., caught attention in many works. Recently, these works started to propose devices in the quantum domain, and the proposed quantum thermal devices, especially diodes as our focus in this thesis, still have optimization problems. In the cases of two interacting qubits diodes, heat rectification is absent for resonant qubits. In this thesis, we consider a quantum thermal diode composed of two interacting qubits, coupled with an optomechanical-like coupling. We derive the global master equation and calculate the heat current for both flat and Ohmic spectral densities to show the diode behavior. Quality of the diode is quantified by a measure, called rectification factor. We numerically calculate the rectification factor for a wide range of system parameters, including weak and strong coupling regimes. We show that the unit rectification factor is obtained for various parameters both in high and low temperature ranges. Most importantly, almost unit rectification is possible even when the qubits have resonant transition frequencies. We explain the physical mechanism leading to all these results, and we show that the mechanism relies on allowed transition and/or bath couplings being asymmetric. We also demonstrate that the asymmetry in transitions is achieved by an asymmetry in free Hamiltonians of subsystems and/or interaction among them. Demonstrations for the sources of asymmetry are carried with two toy models. One of them is a single qubit, which is the smallest possible diode, and the other is a three-level atom. Even though these two systems show diode behaviors, there is very little control of the rectification direction, and two interacting qubits provide versatile control of the diode.

# ÖZETÇE

Isı bolluğu onu enerji kaynağı olarak iyi bir aday yapar, ancak ısıyı manipüle etme kabiliyetimiz çok sınırlıdır. Yeni bir ısı kontrol yöntemi olarak, diyot, transistör vb. gibi karşılıklı olmayan elektronik cihazların termal analogları, birçok çalışmada dikkat çekmiştir. Son zamanlarda, bu çalışmalar kuantum alanında cihazlar önermeye başladı ve önerilen bu kuantum termal cihazları, özellikle bu tezde odaklandığımız diyotlar, hala optimizasyon problemlerine sahiptir. İki etkileşimli qubit diyotu durumunda, rezonans qubitler için ısı yönlendirmesi yoktur. Bu tez çalışmasında, optomekanik benzeri bir kavrama ile birleşen etkileşim içindeki iki qubit oluşturduğu bir kuantum termal diyodu ele alıyoruz. Global mastır denklemini türetiyoruz ve diyot davranışını göstermek için hem düz hem de Ohmik spektral yoğunlukları için ısı akımını hesaplıyoruz. Diyotun kalitesi, düzeltme faktörü olarak adlandırılan bir ölçü ile ölçülüyor. Zayıf ve güçlü qubit etkileşim rejimleri de dahil olmak üzere çok çeşitli sistem parametreleri için düzeltme faktörünü sayısal olarak hesaplıyoruz. Birim düzeltme faktörünün hem yüksek hem de düşük sıcaklık aralıklarında çeşitli parametreler için elde edildiğini göstermekteyiz. En önemlisi, qubitler rezonant frekanslara sahip olsalar bile neredeyse birim düzeltme mümkündür. Tüm bu sonuçlara yol açan fiziksel mekanizmayı açıklıyoruz ve mekanizmanın izin verilen enerji geçişleri ve/veya qubit-ısı banyosu etkileşimlerinin asimetrik olmasına bağlı olduğunu gösteriyoruz. Ayrıca geçişlerdeki asimetrinin, alt sistemlerin serbest Hamiltonlularında bir asimetri ve/veya bunların aralarındaki etkileşimi ile elde edildiğini de göstermekteyiz. Asimetri kaynaklarını iki oyuncak modeli ile örneklendiriyoruz. Bunlardan biri, mümkün olan en küçük diyot olan, tek qubit sistemi diğeri ise üç seviyeli bir atomdur. Bu iki sistem, diyot davranışları gösterse de, düzeltme yönünün çok az kontrolü vardır ve etkileşim içindeki iki qubit sistemi, diyotun çok yönlü kontrolünü sağlar.

# ACKNOWLEDGMENTS

I am grateful to Prof. Dr. Özgür Esat Müstecaplıoğlu beyond words, first of all for giving me the opportunity to be a member of QuEST group and most of all for his guidance and patience in every stage of my M.Sc. degree. His invaluable guidance in research, teachings in the courses, and the collaborations he introduced always helped me to find true inspiration and motivation. Finally, I will always feel in debt to him for his extraordinary kindness and generosity in times of real need.

I thank hospitality of CTAMOP group in Queen's University of Belfast and Nanophysics group of Reykjavík University where some parts of this work had been completed. I, beyond words, thank to Prof. Dr. Mauro Paternostro and Prof. Dr. Andrei Manolescu for always helping in many stages by various means, including their reviews on my reports and drafts. In addition to their academic support and excellence, their kind and supporting personalities gave me motivation and self-esteem in my works. I also thank to Asst. Prof. Dr. Neşe Aral for useful discussions on many biological systems.

I thank each and every member of the QuEST group, useful discussions with them taught me a lot. Emre Köse was always there to help in any means I need, and I am thankful to have such a teammate, colleague, and a good friend. M. Tahir Naseem always intrigued me with the most interesting and useful discussions. I thank many colleagues and friends from Koç University for their friendship and support.

I especially thank my fellow OFT members, Kerim Demirel, Birkan Uçar, Oğuzhan Özcan, and Tuğşad Çavuşer. They are a second family to me, and with such good friends a person would not need anything else. I am very lucky to have them

I finally acknowledge the financial support from the Koç University TÜPRAŞ Energy Center (KUTEM) through an M.Sc. degree scholarship.

# TABLE OF CONTENTS

**List of Figures** **x**

**Chapter 1: Introduction** **1**

**Chapter 2: Background** **3**

2.1 A Short Description of Open Quantum Systems . . . . . 3

2.2 Mathematical Background . . . . . 5

2.2.1 Hilbert and Banach Spaces . . . . . 5

2.2.2 Solution to a System of Differential Equations . . . . . 6

2.3 Quantum Mechanics . . . . . 7

2.3.1 Pure States . . . . . 8

2.3.2 Mixed States and the Density Matrix . . . . . 9

2.3.3 Time Evolution of Density Matrix . . . . . 10

2.3.4 Composite Systems . . . . . 11

2.4 Classical and Quantum Statistical Mechanics . . . . . 12

2.4.1 Boltzmann Probability Distribution . . . . . 13

2.4.2 Density Matrix of a System in Thermal Equilibrium . . . . . 14

2.4.3 Density Matrix of a Bosonic Thermal Bath . . . . . 16

2.5 Derivation of the Markovian Master Equation . . . . . 18

2.5.1 Quantum Dynamical Semigroup . . . . . 19

2.5.2 Interaction Picture . . . . . 20

2.5.3 Master Equation in the Interaction Picture . . . . . 22

2.5.4 Lindblad Form . . . . . 24

2.6 Quantum Thermodynamics . . . . . 32

2.7 non-Markovian Techniques . . . . . 33

**Chapter 3: Application and Numerical Implementation of Markovian Master Equation 34**

3.1 Two-Level System Thermalization . . . . . 34

3.1.1 System Description . . . . . 35

3.1.2 Pure Dephasing Term . . . . . 37

3.1.3 Population Dynamics . . . . . 38

3.1.4 Solving the Equations of Motion . . . . . 40

3.1.5 Heat Current . . . . . 45

3.2 Non-Equilibrium Two-Level System . . . . . 48

3.2.1 Master Equation . . . . . 49

3.2.2 Observable Dynamics . . . . . 51

**Chapter 4: Local vs Global Markovian Master Equations 54**

4.1 Local Approach . . . . . 54

4.1.1 Three Interacting Qubits . . . . . 54

4.1.2 Two Interacting Qubits . . . . . 59

4.2 Global Approach . . . . . 61

**Chapter 5: Quantum Thermal Diodes 65**

5.1 A Single Qubit as the Smallest Diode . . . . . 66

5.2 Diode Behavior form a Three Level Atom . . . . . 68

5.3 Two-Qubit Quantum Thermal Diode . . . . . 70

5.3.1 Dressed System Description . . . . . 71

5.3.2 Model Realizations, Comparisons, and Explanations . . . . . 73

5.3.3 Heat Currents and Thermal Diode Quality Measure . . . . . 75

5.3.4 Asymmetry in the Heat Current . . . . . 75

5.3.5 Asymmetry due to Transition Frequencies . . . . . 83

**Chapter 6: Conclusion and Outlook** **88**

6.1 Outlook . . . . . 89

**Chapter 7: Appendix** **90**

7.1 Quantum Dynamics of Three Interacting Qubits . . . . . 90

7.2 Dressing Two Interacting Qubits . . . . . 91

7.3 Dynamics of the Dressed Two Qubits . . . . . 93

7.4 Heat Currents of the Dressed Two Qubits . . . . . 94

7.4.1 Flat Spectrum . . . . . 94

7.4.2 Ohmic Spectrum . . . . . 96

**Bibliography** **99**

# LIST OF FIGURES

2.1 **Open Quantum System.** Effects of the environment, which exchanges energy with the system, is described by MME. System plus environment is considered as a closed composite . . . . . 4

3.1 **Two Level System (Qubit) Cases.** (a) Qubit with a transition frequency $\omega$ is couple to a thermal bath at temperature $T_{\mathrm{L}}$ with a rate $\kappa_{\mathrm{L}}$. (b) It is also coupled to a second thermal at temperature $T_{\mathrm{R}}$ with a rate $\kappa_{\mathrm{R}}$. . . . . 35

3.2 **Qubit Thermalization.** Populations converges to the Gibbs distribution of the bath temperature. Three different cases are as shown in the legends. Colored dots show analytical result, black solid lines are numerical. . . . . 45

3.3 **Qubit Thermalization.** Coherences dies away in every case, and this plot shows the imaginary part. Three different cases are as shown in the legends. Colored dots show analytical result, black solid lines are numerical. . . . . 46

3.4 **Qubit Thermalization.** Coherences dies away in every case, and this plot shows the real part. Three different cases are as shown in the legends. Colored dots show analytical result, black solid lines are numerical. . . . . 47

3.5 **Qubit Thermalization.** Heat flows from hot to cold. Three different cases are as shown in the legends. Colored dots show analytical result, black solid lines are numerical. . . . . 48

3.6 **Steady State Heat Current.** When $T_{\mathrm{R}} > T_{\mathrm{L}}$, $\mathcal{J}_{\mathrm{R}}^{\mathrm{ss}}$ is positive. . . . 50

4.1 **Three and Two Interacting Qubits.** Left (L) and right (R) qubits are coupled to their local baths at temperature $T_{\mathrm{L}}$ and $T_{\mathrm{R}}$ with the rates $\kappa_{\mathrm{L}}$ and $\kappa_{\mathrm{R}}$, and right qubit interacts with left qubit/s with a coupling strength $g$. . . . . 55

4.2 **Three Interacting Qubits.** Steady state heat currents from (a) hot and (b) cold baths sum to zero. Heat current maximizes at an optimized temperature as the (c) correlations, and (d) first qubit always thermalizes with its local bath. . . . . 57

4.3 **Fourier Law of Thermal Conduction.** Steady state heat current through a single qubit increases as the temperature bias $T_{\mathrm{Hot}} - T_{\mathrm{Cold}}$ is increased. . . . . 58

4.4 **Local MME Comparison.** a: When, left bath is always hotter than the right bath, which is at temperature $\langle \hat{\sigma}_z \rangle_{T_{\mathrm{R}}} = -1$ (0 K), everything, deceivingly, seem consistent. b: When right bath has a finite temperature, that is $\langle \hat{\sigma}_z \rangle_{T_{\mathrm{R}}} = -0.5$, heat current direction of (b) dipole-dipole coupling is always from hot to cold, which is violated in the (a) optomechanical like coupling case. . . . . 60

4.5 **Global MME for Two Interacting Qubits.** Steady state heat currents have the correct direction, and its non-reciprocal. . . . . 64

7.1 **ORQ Flat Spectrum Low temperature.** . . . . . 94

7.2 **ORQ Flat Spectrum High temperature.** . . . . . 95

7.3 **RQ Flat Spectrum Low temperature.** . . . . . 95

7.4 **RQ Flat Spectrum High temperature.** . . . . . 96

7.5 **ORQ Ohmic Spectrum Low temperature.** . . . . . 96

7.6 **ORQ Ohmic Spectrum High temperature.** . . . . . 97

7.7 **RQ Ohmic Spectrum Low temperature.** . . . . . 97

7.8 **RQ Ohmic Spectrum High temperature.** . . . . . 98

# Chapter 1

# INTRODUCTION

Nature is fundamentally quantum mechanical. Yet, intricate quantum mechanical behaviors, such as quantum coherence, are not present in everyday life, and our macroscopic experience is dominantly classical. This is because "quantumness" is preserved only in isolated systems (or at least in low temperatures with very small levels of noise). Therefore, quantum effects in biology [1, 2, 3] are quite surprising, since these systems are open to noisy environments. One extraordinary effect is the observation of long-lived quantum coherence in the excitation energy transfer (EET) through photosynthetic pigment-protein complexes (PPCs) [4, 5, 6, 7, 8].

Techniques from theory of open quantum systems [9, 10, 11, 12, 13] are applied to EET through PPCs to understand the effects of noise on the transport [14, 15, 16, 17, 18, 19, 20, 21]. It is shown that the exciton transport through dissipative quantum networks (at zero temperature) can be enhanced by local dephasing [15], and an optimized interplay between free Hamiltonian evolution and thermal noise is shown to increase the transport efficiency [16]. Enhancement of transport efficiency by the optimization of dynamical interplay between the Hamiltonian of a disordered system and pure dephasing is attributed to prevention from localization in disordered system [22] with fully coherent dynamics [17, 18] and quantum Zeno effect of highly incoherent dynamics [17, 18], and to line broadening [18, 19]. For the ordered systems, there is no localization to overcome, yet fully coherent dynamics is not again more efficient than the dynamics with an optimized noise [20]. This is related to an optimization between the destruction of dark states by noise and quantum Zeno effect caused by the excessive amount of noise [19, 20]. Also, a structured noise, that is a non-Markovian

environment composed of local oscillators on each transport site, has also shown to be beneficial for the transport efficiency [19, 23, 24, 25, 26, 27, 28, 29]. It is argued that the vibrational modes open up additional transport pathways, or dynamically adjust the resonances to provide directionality in the transport network [24, 26, 27, 28]. These vibrational modes are also shown to support the lifetime of coherences to the observed time-scales [23, 24, 25, 29, 30].

The noise-assisted transport idea proved in the works above is experimentally tested and verified in various platforms [31, 32, 33, 34, 35, 36], yet there is still debate on the role of coherence on the transport in Photosynthesis [37, 38]. Also, it has been shown that introducing a sink, which is the common point in almost all of the above studies, contradicts the second law of thermodynamics [39]. Therefore, adopting the thermodynamical measures [40] to analyze the transport [28, 21] in a thermodynamically consistent way, we shift our attention to quantum thermal non-reciprocal devices, which are required to turn waste heat into useful resource [41, 42, 43, 44] not only in energy-harvesting [45, 46], but also in information processing [47, 48] and heat engines [49, 50]. Quantum non-reciprocal devices are theoretically proposed [51, 52, 53, 54, 55, 56], and experimental works realized a single-photon optical diode [57], a heat switch from coupled superconducting qubits [58], and photonic heat valve [59].

This thesis first presents the background required for open quantum systems and the derivation of Markovian master equation (MME), which is the main tool used in almost all of the above theoretical studies. Then, toy model examples of MME are presented to demonstrate what is MME and how to solve it. Finally, the working principle of a quantum thermal diode of two interacting qubits [54, 55, 56] is explained together with a discussion on how would a non-Markovian environment affect the diode behavior.

Chapter 2

# BACKGROUND

This chapter presents the required background from both quantum and statistical mechanics. It starts with very basic but useful mathematical definitions and also presents a method to solve coupled first order linear homogeneous differential equations. Then, density matrix formalism is introduced by considering ensemble average of an observable for a mixed state, which is a statistical ensemble of pure states. Rigorous terminology divides the naming into two as density operator and density matrix, which is a matrix representation of the operator in a chosen basis, we use the name density matrix for both cases. It is already obvious that the statistical ideas play a key role here. Therefore, this chapter also introduces required background from both classical and quantum statistical mechanics. Another use of them is to reduce the dynamics of system-environments composite to only the system of interest by removing the environment degrees of freedom with the use of their statistical properties. This is done by deriving the quantum master equation in Born-Markov approximation. Finally, a short review of quantum thermodynamics and non-Markovian methods are presented.

## *2.1 A Short Description of Open Quantum Systems*

Generic example is a system interacting with an environment at temperature $T$, as shown in Fig. 2.1. The whole configuration, the system S plus the environment, is closed, and its dynamics is described by the Liouville - von Neumann equation, which is derived in the subsequent sections,

$$i\hbar\frac{d}{dt}\hat{\rho}(t) = \left[\hat{H}, \hat{\rho}(t)\right], \tag{2.1}$$

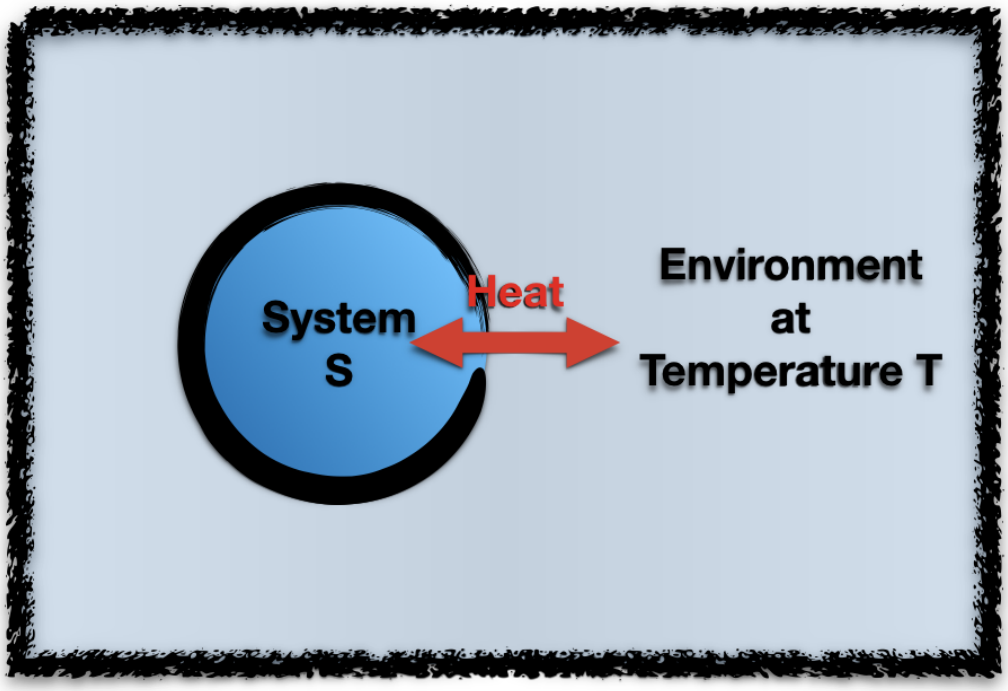


Figure 2.1: **Open Quantum System.** Effects of the environment, which exchanges energy with the system, is described by MME. System plus environment is considered as a closed composite

where $\hat{\rho}$ is the density matrix introduced in the subsequent sections, and $\hat{H}$ is the total Hamiltonian given as

$$\hat{H} = \hat{H}_{\mathrm{S}} + \hat{H}_{\mathrm{R}} + \hat{H}_{\mathrm{I}}, \tag{2.2}$$

where $\hat{H}_{\mathrm{S}}$, $\hat{H}_{\mathrm{R}}$, and $\hat{H}_{\mathrm{I}}$ are respectively the system, environment, and system-environment interaction Hamiltonians. When only the system S is of interest, its state $\hat{\rho}_{\mathrm{S}}(t)$ is obtained by tracing out the environment degrees of freedom

$$\hat{\rho}_{\mathrm{S}}(t) = \mathrm{Tr}_{\mathrm{R}}\left[\hat{\rho}(t)\right]. \tag{2.3}$$

However, obtaining $\hat{\rho}(t)$ requires Eq. 2.1 to be solved, and it is not possible for most systems. Therefore, Markovian master equation technique is developed to describe the time evolution of $\hat{\rho}_{\mathrm{S}}$ by applying second order perturbation to 2.1 under Born-Markov approximations, which is justified in weak system-environment coupling. Subsequent sections present the derivation and description of involved approximations. Once the environment degrees of freedom are traced out, dynamics of the system S is given by an equation of the form

$$i\hbar\frac{d}{dt}\hat{\rho}_{\mathrm{S}}(t) = \left[\hat{H}_{\mathrm{S}}, \hat{\rho}_{\mathrm{S}}\right] + \hat{\mathcal{L}}[\hat{\rho}_{\mathrm{S}}], \tag{2.4}$$

where $\hat{\mathcal{L}}$ is called Liouville super-operator (Liouvillian) adding the effects of environment to the unitary dynamics of S. Here, the term super-operator means an operator (Liouvillian) that acts on other operators (density operator/matrix). The rest of this section is basically all about obtaining the super-operator $\hat{\mathcal{L}}$ both in its general form and for specific systems.

## *2.2 Mathematical Background*

This section involves two parts. The first part summarizes the mathematical definitions used in the Quantum mechanics, which are also useful in rigorous mathematical approaches to open quantum systems. The second part introduces a method to solve coupled differential equations, which is adopted in solving the Quantum master equations.

### *2.2.1 Hilbert and Banach Spaces*

A vector space $\mathbb{V}$ is a set that is closed under vector addition and vector multiplication, and it is defined by a set of axioms [60, 61, 62, 63]. A Banach space $\mathbb{B}$ is a complete vector space with a norm $\|.\|$ [12, 60, 63], and Hilbert spaces $\mathbb{H}$ are Banach spaces with a norm given $\|f\| = \sqrt{\langle f, f\rangle}$, where $\langle f, g\rangle$ is an inner product of the two vectors $f$ and $g$ [60, 62, 63]. Completeness of a vector space means that all Cauchy sequences converge to a limit [60, 63].

An example of Hilbert spaces is the space of square integrable functions $\mathbb{L}^2$ [64], meaning that the integral of $f^2$ over the whole real line is finite for any function $f \in \mathbb{L}^2$. The norm for $\mathbb{L}^2$ is

$$\langle f, g \rangle = \int_{-\infty}^{\infty} f(x)g(x)dx, \tag{2.5}$$

where $f, g \in \mathbb{L}^2$. Such functions are used as the wave functions (solutions to Schrödinger equation) of quantum systems [64]. A More abstract version is to use a ket $|.\rangle$ to represent the state of a system, and an element in the dual space called bra $\langle .|$ is used to define the inner product$\langle .\rangle$ [65].

Observable of a quantum systems, more precisely the expectation value $\langle \hat{O} \rangle$ of an operator $\hat{O}$, is obtained by applying the corresponding operator $\hat{O}$ of an observable to a state $|.\rangle$ and then taking the inner product with dual of the state $\langle .|$ [61, 64, 65]

$$\langle \hat{O} \rangle = \langle . | \, \hat{O} \, | . \rangle \, . \tag{2.6}$$

Operators form a Banach space with an operator norm, which tells the unitarity of an operator [12, 63]. I do not present the definition of operator norm here, but unitary operators have norms equal to 1. If an operator has a norm less than 1, it is called as contraction [12, 63].

### *2.2.2 Solution to a System of Differential Equations*

Here, solution for a specific system of differential equations (SDE) is presented to be used in solving the MME. Consider the following SDE

$$\begin{aligned} \dot{x}_1 &= M_{11}x_1 + \quad \cdots \quad + M_{1n}x_n, \\ &\vdots \\ \dot{x}_n &= M_{n1}x_1 + \quad \cdots \quad + M_{nn}x_n, \end{aligned} \tag{2.7}$$

which can be written in the matrix form as follows [66, 67, 68]

$$\overbrace{\begin{bmatrix} \dot{x}_1 \\ \vdots \\ \dot{x}_n \end{bmatrix}}^{\dot{\boldsymbol{X}}} = \overbrace{\begin{bmatrix} M_{11} & \cdots & M_{1n} \\ \vdots & \ddots & \vdots \\ M_{n1} & \cdots & M_{nn} \end{bmatrix}}^{\boldsymbol{M}} \overbrace{\begin{bmatrix} x_1 \\ \vdots \\ x_n \end{bmatrix}}^{\boldsymbol{X}} \implies \dot{\boldsymbol{X}} = \boldsymbol{M}\boldsymbol{X}. \tag{2.8}$$

There are two ways to solve the Eq. 2.8. First solution is written trivially as

$$\boldsymbol{X} = e^{\boldsymbol{M}t}\boldsymbol{C}, \tag{2.9}$$

where $\boldsymbol{C}$ is a column matrix (a vector) of constants to be determined from the initial values [66, 67, 68]. If the matrix $\boldsymbol{M}$ is diagonal, which means the equations are not coupled to begin with, the matrix exponential and the solution is trivial. For a coupled system, there are two ways to proceed after this point. First one is to expand the exponential as a power series, which can be used easily in the numerical calculations

$$e^{\boldsymbol{M}t} = \sum_{k=0}^{\infty} \frac{t^k}{k!}\boldsymbol{M}^t. \tag{2.10}$$

Second method is to first diagonalize the matrix $\boldsymbol{M}$ and then exponentiating it [66, 67, 68]. Diagonalization of a matrix can be performed by finding its eigenvalues, which is a part of the second way to solve Eq. 2.8. Using the eigenvalues $k_j$ and eigenvectors $\boldsymbol{k}$ of the matrix $\boldsymbol{M}$, we can also write the solution of Eq. 2.8 as

$$\boldsymbol{X} = \sum_{j=1}^{n} c_j e^{k_j t}\boldsymbol{k}, \tag{2.11}$$

where $c_j$ are integration constant to be determined from initial conditions. I will use and further explain these techniques in the subsequent chapters.

## *2.3 Quantum Mechanics*

There are three equivalent ways to describe the dynamics of a quantum mechanical system. These are commonly called as Schrödinger, Heisenberg, and Dirac (or interaction) pictures. In this thesis and in general, Schrödinger picture is used extensively, but interaction picture is useful in the derivation of MME and is explained in the subsequent sections. I do not present these pictures in detail, but it can be found in standard text books [61, 65, 69, 70]. In the Schrödinger picture, state of a closed quantum system is represented by its wave-function, which evolves under a

unitary dynamics determined by the system Hamiltonian. Quantum mechanics is intrinsically probabilistic and the probability of an observable to have a certain value is obtained by its expectation values. However, in realistic systems, there are also classical uncertainties, and these are incorporated into quantum mechanics with density matrices [65, 71, 72, 73, 74].

In this section, pure and mixed states are introduced to lead our way to density matrix formalism, and then the dynamics of this statistical treatment is derived. Also, density matrix of a composite system and its reduction to a subsystem density matrix with a partial trace operation is described. This section is a combination of summaries for the topics from standard books [61, 64, 65, 69, 70, 71, 72, 73, 74, 75].

### *2.3.1 Pure States*

For a closed quantum system with a given Hamiltonian $\hat{H}$, eigenstates $|\psi_i\rangle$ of the Hamiltonian (i.e. energy eigenstates) describe a basis for the Hilbert space of states. Eigenstates are obtained form the eigenvalue equation

$$\hat{H}\,|\psi_i\rangle = E_i\,|\psi_i\rangle\,, \tag{2.12}$$

where $E_i$ is the eigenenergy for the eigenstate $|\psi_i\rangle$. A pure state $|\Psi\rangle$ is a normalized superposition of the eigenstates, which can be written for a Hilbert space with dimension $d$ as

$$|\Psi\rangle = \sum_{i=0}^{d} c_i\,|\psi_i\rangle\,,$$

where the $c_i$ are complex numbers, and the normalization condition is

$$\langle\Psi|\Psi\rangle = 1 \Longleftrightarrow \sum_{i=0}^{d} |c_i|^2 = 1.$$

Time evolution of a pure state is given by the Schrödinger equation

$$i\hbar\frac{\partial}{\partial t}\,|\Psi(t)\rangle = \hat{H}(t)\,|\Psi(t)\rangle\,. \tag{2.13}$$

Schrödinger equation will be used to obtain Liouville - von Neumann equation, which describes the time evolution of density matrix. In order to introduce density matrix

formalism, final concept needed from the pure state description is expectation value for an observable $O$, which is calculated as

$$\langle \hat{O} \rangle = \langle \Psi | \hat{O} | \Psi \rangle \, .$$

### *2.3.2 Mixed States and the Density Matrix*

If a quantum system is a statistical ensemble of pure states $|\Psi_j\rangle$ with corresponding weights $w_j$, state of the system cannot anymore be described by a single state vector. Yet, using the statistical weights $w_j$, we can write the expectation of an observable as the ensemble average

$$[\hat{O}] \equiv \sum_j w_j \, \langle \Psi_j | \hat{O} | \Psi_j \rangle \, . \tag{2.14}$$

Using the completeness relation for a basis of the Hilbert space

$$\sum_{b'} |b'\rangle \, \langle b'| = \mathbb{1}.$$

Eq. 2.14 can be rewritten as

$$\begin{aligned} [\hat{O}] &= \sum_j w_j \, \langle \Psi_j | \left( \sum_{b'} |b'\rangle \, \langle b'| \right) \hat{O} \left( \sum_{b''} |b''\rangle \, \langle b''| \right) |\Psi_j\rangle \\ &= \sum_{b'} \sum_{b''} \left( \sum_j w_j \, \langle b''|\Psi_j\rangle \, \langle \Psi_j|b'\rangle \right) \langle b'|\hat{O}|b''\rangle \\ &= \sum_{b'} \sum_{b''} \langle b''| \left( \sum_j w_j \, |\Psi_j\rangle \, \langle \Psi_j| \right) |b'\rangle \, \langle b'|\hat{O}|b''\rangle \, . \end{aligned} \tag{2.15}$$

At this stage, we can define the density matrix as

$$\hat{\rho} = \sum_j w_j \, |\Psi_j\rangle \, \langle \Psi_j| \, . \tag{2.16}$$

As shown below, this operator is used to calculate the ensemble average of a mixed state for any observable. Also, elements of the matrix representation, called the density matrix, in any basis $|b'\rangle$ is found as

$$\rho_{b''b'} = \langle b''|\hat{\rho}|b'\rangle = \sum_j w_j \, \langle b''|\Psi_j\rangle \, \langle \Psi_j|b'\rangle \, . \tag{2.17}$$

Diagonal elements of this matrix give population for the corresponding eigenstate, and off-diagonal elements are the correlations between eigenstates, called coherences.Now, using the density matrix, we write ensemble average as

$$[\hat{O}] = \sum_{b'} \sum_{b''} \langle b'' | \hat{\rho} \overbrace{|b'\rangle \langle b'|}^{\mathbb{1}} \hat{A} |b''\rangle \sum_{b''} \langle b'' | \hat{\rho}\hat{A} | b'' \rangle = \mathrm{Tr}(\hat{\rho}\hat{A}). \tag{2.18}$$

Final relation tells that the ensemble average of a mixed state for any observable $\hat{A}$ is found by the trace of $\hat{\rho}\hat{A}$ in any basis.

### *2.3.3 Time Evolution of Density Matrix*

We have introduced the formalism that properly describes a mixed state. Now, we use this formalism to describe the time evolution of mixed states. Here, we still consider a closed system so that dynamics of the pure states are described with the Schrödinger equation. Then, from an initial state $\hat{\rho}(t_0)$, density matrix at a later time $t$ is written as

$$\hat{\rho}(t_0) = \sum_j \omega_j |\Psi_j, t_0\rangle \langle \Psi_j, t_0| \qquad \rightarrow \qquad \hat{\rho}(t) = \sum_j \omega_j |\Psi_j, t\rangle \langle \Psi_j, t| \,. \tag{2.19}$$

Taking time derivative of both sides in the second expression of Eq. 2.19, we write

$$\frac{d}{dt}\hat{\rho}(t) = \sum_j \omega_j \frac{\partial}{\partial t} \left( |\Psi_j, t\rangle \langle \Psi_j, t| \right) = \sum_j \omega_j \left( \frac{\partial}{\partial t} \left( |\Psi_j, t\rangle \right) \langle \Psi_j, t| + |\Psi_j, t\rangle \frac{\partial}{\partial t} \left( \langle \Psi_j, t| \right) \right). \tag{2.20}$$

We have the time derivative for a ket in Eq. 2.13, and it is given for a bra as

$$-i\hbar \frac{\partial}{\partial t} \langle \Psi(t)| = \langle \Psi(t)| \hat{H}(t). \tag{2.21}$$

Then, by multiplying Eq. 2.20 with $i\hbar$ and substituting time derivatives of bra and ket states Eq. 2.13 and 2.20, we obtain the following relation

$$i\hbar \frac{d}{dt}\hat{\rho}(t) = \sum_j \omega_j \left[ \hat{H} |\Psi_j, t\rangle \langle \Psi_j, t| - |\Psi_j, t\rangle \langle \Psi_j, t| \hat{H} \right] = -\left[ \hat{\rho}, \hat{H} \right] = \left[ \hat{H}, \hat{\rho} \right], \tag{2.22}$$

called the Liouville - von Neumann equation describing time evolution of a quantum statistical system.

### *2.3.4 Composite Systems*

Almost all systems of interest comprise multiple components. Therefore, this section is about the density matrix of composite systems. State of a system with two constituents, A and B, is written as (by direct product)

$$|\Psi_{\mathrm{A+B}}\rangle = \sum_{i,j} \alpha_{i,j} \, |a_i, b_j\rangle \,, \tag{2.23}$$

where, $\alpha_{i,j} = \langle a_i, b_j | \Psi_{\mathrm{A+B}} \rangle$ and $|a_i, b_j\rangle = |a_i\rangle \otimes |b_j\rangle$. Normalization of the composite state $|\Psi_{\mathrm{A+B}}\rangle$ means that

$$\sum_{i,j} |\alpha_{i,j}|^2 = 1.$$

If the factorization $\alpha_{i,j} = \alpha_i^{(\mathrm{A})} \alpha_j^{(\mathrm{B})}$ is possible, then

$$|\Psi_{\mathrm{A+B}}\rangle = \left[ \sum_i \alpha_i^{(\mathrm{A})} \, |a_i\rangle \right] \left[ \sum_j \alpha_j^{(\mathrm{B})} \, |b_j\rangle \right] \equiv |\Psi_{\mathrm{A}}\rangle \otimes |\Psi_{\mathrm{B}}\rangle \,,$$

factorization of the state into states of the subsystems is also possible. The state of a composite system that cannot be factorized into a product state of its subsystem states is called an entangled state. Finally, the density matrix of the composite system is just again the outer product of system states $\hat{\rho}_{\mathrm{A+B}} = |\Psi_{\mathrm{A+B}}\rangle \langle \Psi_{\mathrm{A+B}}|$.

In the open quantum systems, we are interested in dynamics of the system in a thermal bath, and MME is derived by tracing out the bath degrees of freedom by taking partial trace. Assume that we are interested in the properties of system A, and let $\mathrm{Tr}_{\mathrm{B}}$ denote the operation of trace only over the subsystem B (partial trace).

Density matrix of system A (so the state) is obtained as follows

$$\begin{aligned}
\mathrm{Tr_B}\left[|\Psi_{\mathrm{A+B}}\rangle\langle\Psi_{\mathrm{A+B}}|\right] &= \mathrm{Tr_B}\left[\left(\sum_i \alpha_i |a_i\rangle \sum_j \alpha_j |b_j\rangle\right)\left(\sum_k \alpha_k^* \langle a_k| \sum_l \alpha_l^* \langle b_l|\right)\right] \\
&= \sum_{i,k} \alpha_i \alpha_k^* |a_i\rangle\langle a_k| \,\mathrm{Tr_B}\left(\sum_{j,l} \alpha_j \alpha_l^* |b_j\rangle\langle b_l|\right) \\
&= \sum_{i,k} |a_i\rangle\langle a_k| \sum_{j,l} \alpha_i \alpha_j \alpha_k^* \alpha_l^* \delta_{j,l} \\
&= \sum_{i,k} |a_i\rangle\langle a_k| \underbrace{\sum_j \alpha_{i,j}\alpha_{j,k}^*}_{c_{ik}} = \sum_{i,k} c_{ik} |a_i\rangle\langle a_k| = \hat{\rho}_{\mathrm{A}}, \qquad (2.24) \\
\Longrightarrow \mathrm{Tr_B}\left[\hat{\rho}_{\mathrm{A+B}}\right] &= \hat{\rho}_{\mathrm{A}}. \qquad (2.25)
\end{aligned}$$

One additional assumption above is that the composite state is factorisable, which guarantees that $\mathrm{Tr_A}\left[\hat{\rho}_{\mathrm{A+B}}\right] \otimes \mathrm{Tr_B}\left[\hat{\rho}_{\mathrm{A+B}}\right] = \hat{\rho}_{\mathrm{A+B}}$, but procedure is the same for any composite state.

In above calculation, it may seem unambiguous whether or not the $c_{ik}$'s give the correct matrix coefficients. Assume that expectation value of an observable $\hat{O}_{\mathrm{A}}$ of system A is calculated as

$$\begin{aligned}
\langle\hat{O}_{\mathrm{A}}\rangle &= \langle\Psi_{\mathrm{A+B}}|\hat{O}_{\mathrm{A}}|\Psi_{\mathrm{A+B}}\rangle = \sum_{i,j,k,l} \alpha_{k,l}^* \alpha_{i,j} \langle a_k|\hat{O}|a_i\rangle \underbrace{\langle b_l|b_j\rangle}_{\delta_{j,l}} = \sum_{i,j,k} \alpha_{k,j}^* \alpha_{i,j} \langle a_k|\hat{O}|a_i\rangle \\
\langle\hat{O}_{\mathrm{A}}\rangle &= \sum_{i,k} c_{ik} \langle a_k|\hat{O}_{\mathrm{A}}|a_i\rangle . \qquad (2.26)
\end{aligned}$$

By using the density matrix of system A given by the Eq. 2.24, this expectation value is also calculated using the Eq. 2.18 as

$$[\hat{O}_{\mathrm{A}}] = \mathrm{Tr}\left(\hat{\rho}_{\mathrm{A}}\hat{O}_{\mathrm{A}}\right) = \sum_i \langle a_i|\hat{\rho}_{\mathrm{A}}\hat{O}_{\mathrm{A}}|a_i\rangle = \sum_{i,k} \langle a_i|\hat{\rho}_{\mathrm{A}}|a_k\rangle \langle a_k|\hat{O}_{\mathrm{A}}|a_i\rangle . \qquad (2.27)$$

In the second line, resolution of identity is used. Comparing Eq. 2.26 and 2.27, it is seen that $\langle a_i|\hat{\rho}_{\mathrm{A}}|a_k\rangle = c_{ik}$, which is the same in Eq. 2.24.

## *2.4 Classical and Quantum Statistical Mechanics*

This section firstly presents a derivation for Boltzmann probability distribution, and then, by introducing a measure of disorder for the density matrix together with the

defining properties of equilibrium, it is shown that the elements of density matrix in thermal equilibrium are simply Boltzmann probabilities. Finally, density matrix for a thermal bath of bosons is defined. This section is a combination of summaries for the topics from standard books [65, 74, 75, 76, 77, 78, 79].

### *2.4.1 Boltzmann Probability Distribution*

In classical thermodynamics and statistical mechanics, entropy is defined respectively as

$$dS = \frac{đQ_{\text{rev}}}{T}, \tag{2.28}$$

$$S = k_B \ln(\Omega), \tag{2.29}$$

where $đQ_{\text{rev}}$ is the infinitesimal heat reversibly given to the system at the temperature $T$, and $\Omega = e^{S/k_B}$ is the number of possible micro-states for a given macro-state for discrete systems and phase space volume containing the states satisfying macroscopic constraints for continuous systems. Total energy $U_{\text{T}} = U_{\text{R}} + U_{\text{A}}$ of a system A and its environment R is constant, and the number of states is written as a function of system energy $U_{\text{A}}$ as

$$\Omega(U_{\text{A}}) = \Omega_{\text{A}}(U_{\text{A}}) \times \Omega_{\text{R}}(U_{\text{T}} - U_{\text{A}}). \tag{2.30}$$

The first law of thermodynamics, which is about the conservation of energy, is mathematically stated as

$$dU = đQ + đW, \tag{2.31}$$

$$dU = đQ + \sum_i J_i dx_i, \tag{2.32}$$

where $J_i$ are generalized forces with their conjugate general displacements $dx_i$, and $đQ$ is infinitesimal heat. Then, using the entropy definition given in Eq. 2.28, we obtain a relation for the number of states for a specific energy $U$ by firstly obtaining a relation for the temperature as follows

$$\frac{1}{T} = \left(\frac{\partial S}{\partial U}\right)_{x_i} = k_B \left(\frac{\partial \ln \Omega}{\partial U}\right)_{x_i}, \tag{2.33}$$

$$\Omega = \gamma e^{U/k_B T}. \tag{2.34}$$

Then, for a particular energy $E_i$ of the system A, we have the number of states from Eq. 2.30 as

$$\Omega(E_i) = 1 \times \Omega_{\mathrm{R}}(U_{\mathrm{T}} - U_{\mathrm{A}}) = \gamma e^{(U_{\mathrm{T}} - E_i)/k_B T}. \tag{2.35}$$

From this relation, we write the total number of accessible micro-states of a discrete system as

$$N_{\mathrm{total}} = \sum_j \Omega(E_j) = \gamma e^{U_{\mathrm{T}}/k_B T} \sum_j e^{-E_j/k_B T}. \tag{2.36}$$

The basic assumption of classical statistical mechanics is that all the possible quantum states are equally probable, equal a priori. Therefore, the probability of system A having the particular energy $E_i$ is the ratio of number of micro-states with this energy to total number of micro-states, which is given by

$$p_i = \frac{\Omega(E_i)}{\sum_j W(E_j)} = \frac{e^{-E_i/k_B T}}{\sum_j e^{-E_j/k_B T}} = \frac{e^{-E_i/k_B T}}{Z}, \tag{2.37}$$

where the partition function $Z \equiv \sum_j e^{-E_j/k_B T}$ is defined. Eq. 2.37 is the Boltzmann probability distribution, and it will give us an intuition about the elements of density matrix for a system in equilibrium with a thermal bath through their structural similarity.

### *2.4.2 Density Matrix of a System in Thermal Equilibrium*

Defining properties of equilibrium include, maximized entropy, definite system energy, and steady probability distribution. We make use of these properties to derive the density matrix of a system in thermal equilibrium. For this purpose, let us first introduce a measure of disorder for the system

$$\sigma = -\operatorname{Tr}\left(\hat{\rho} \ln \hat{\rho}\right). \tag{2.38}$$

Meaning of $\sigma$ is rather clear if we use the basis in which $\hat{\rho}$ is diagonal

$$\sigma = -\sum_j \rho_{jj}^{(\mathrm{diag})} \ln \rho_{jj}^{(\mathrm{diag})}. \tag{2.39}$$

Since each element $\rho_{jj}^{(\mathrm{diag})}$ is a real number between 0 and 1, $\sigma$ is positive semidefinite. For a completely random ensemble, every state (with N number of them) is populated equally $\rho_{jj}^{\mathrm{diag}} = \frac{1}{N}$, then

$$\sigma = -\sum_{j=1}^{N} \frac{1}{N} \ln\left(\frac{1}{N}\right). \tag{2.40}$$

If the state is normalized $\sum_j \rho_{jj}^{\mathrm{diag}} = 1$, the maximum value is $\sigma = 1$. For a pure state, $\sigma$ has its lowest value 0, because only one of the states $j$ is occupied, the rest of $\rho_{jj}^{\mathrm{diag}}$ will be zero and for that one particular occupied state $\rho_{ii}^{(\mathrm{diag})} = 1 \implies \ln \rho_{ii}^{\mathrm{diag}} = 0$, so $\sigma_{\mathrm{pure}} = 0$. Simply by stating that entropy is a measure of this order in thermodynamic, here is a good position to introduce von-Neumann entropy

$$S = k_B \sigma. \tag{2.41}$$

Now, we use the properties of thermal equilibrium stated above

- Entropy is maximized $\implies$ $\delta\sigma = 0$,
- Energy is definite $\implies$ $[\hat{H}] = \mathrm{Tr}(\hat{\rho}\hat{H}) = U$,
  $\implies$ $\delta[\hat{H}] = \sum_k \delta\rho_{kk} E_k$,
- Probabilities are steady $\implies$ $\delta \,\mathrm{Tr}\,\hat{\rho} = \sum_k \delta\rho_{kk} = 0$.

We can combine all there conditions with the use of Lagrange multipliers as

$$\sum_k \overbrace{\delta\rho_{kk} \ln \rho_{kk} + \delta\rho_{kk}}^{\delta\sigma} + \overbrace{\delta\rho_{kk}\beta E}^{\beta\delta[\hat{H}]} + \overbrace{\gamma\delta\rho_{kk}}^{\gamma\delta tr\rho}, \tag{2.42}$$

which is equal to zero and is written as

$$\sum_k \delta\rho_{kk} \left[\ln \rho_{kk} + 1 + \beta E_k + \gamma\right] = 0, \tag{2.43}$$

Eq. 2.43 is zero independent of $\delta\rho_{kk}$. Therefore, we must have

$$\ln \rho_{kk} + 1 + \beta E_k + \gamma = 0, \tag{2.44}$$

which gives the following relation for diagonal density matrix elements

$$\rho_{kk} = \exp(-\beta E_k - \gamma - 1) = \frac{e^{-\beta E_k}}{e^{\gamma+1}}. \tag{2.45}$$

Since the partition function is a normalization factor the probabilities, and diagonal density matrix elements are populations, we define $Z$ from the normalization condition as

$$\sum_j \rho_{jj} = 1 = e^{-\gamma-1}\left(\sum_j e^{-\beta E_j}\right) Z \equiv e^{\gamma+1} = \left(\sum_j e^{-\beta E_j}\right). \tag{2.46}$$

Then, diagonal density matrix elements in Eq. 2.45 are written as

$$\rho_{kk} = \frac{e^{-\beta E_k}}{Z} = \frac{e^{-\beta E_k}}{\sum_j e^{-\beta E_j}}. \tag{2.47}$$

These matrix element have the same form as in Eq. 2.37, which means that probability distributions in the thermal state are the same. Therefore, we can identify $\beta$ as $k_B T$ and finally write the density matrix of a system in thermal equilibrium as

$$\hat{\rho} = \frac{\exp\left(-\beta \hat{H}\right)}{Z}, \tag{2.48}$$

with the partition function defined as $Z = \mathrm{Tr}\left(e^{-\beta \hat{H}}\right)$.

### *2.4.3 Density Matrix of a Bosonic Thermal Bath*

This bath model can be used for a bath of photon or phonon gas. Let us consider a bath of bosons at temperature $T$, the probability $p_n$, that a certain mode of the field is excited with $n$ photons is obtained from Boltzmann probability distribution as

$$p_n = \frac{e^{-E_n k_B T}}{\sum_m e^{-E_m/k_B T}}. \tag{2.49}$$

Here, $E_n = \hbar\omega_n\left(n + \frac{1}{2}\right)$ is the quantized energy levels of the bosonic field, and the $\frac{1}{2}$ term is called the zero-point (or vacuum) energy. Using the short hand $A = \exp\left(-\frac{\hbar\omega_n}{k_B T}\right)$ together with the geometric series relation

$$a + ar + ar^2 + ... = \sum_{k=0}^{\infty} ar^k = \frac{a}{1-r} \quad \text{for} \quad |r| < 1, \tag{2.50}$$

we first write the probabilities as $p_n = \frac{A^n}{\sum_m A^m}$, and use $\sum_m A^m = \frac{1}{1-A}$ to write te probabilities as

$$p_n = (1-A)\,A^n = \left[1 - \exp\left(-\frac{\hbar\omega_n}{k_B T}\right)\right] \exp\left(-\frac{n\hbar\omega_n}{k_B T}\right), \tag{2.51}$$

Therefore, the density matrix for a single-mode thermal filed, which is a mixed state of number states with the Boltzmann is given by

$$\begin{aligned}
\hat{\rho}_{\text{thermal}} &= \sum_n p_n \left|n\right\rangle \left\langle n\right| = \left[1 - \exp\left(-\frac{\hbar\omega_n}{k_B T}\right)\right] \sum_n \exp\left(-\frac{n\hbar\omega_n}{k_B T}\right) \left|n\right\rangle \left\langle n\right| \\
&= \left[1 - \exp\left(-\frac{\hbar\omega_n}{k_B T}\right)\right] \sum_n \exp\left(-\frac{\hbar\omega_n \hat{a}^\dagger \hat{a}}{k_B T}\right) \left|n\right\rangle \left\langle n\right| \\
\hat{\rho}_{\text{thermal}} &= \left[1 - \exp\left(-\frac{\hbar\omega_n}{k_B T}\right)\right] \exp\left(-\frac{\hbar\omega_n \hat{a}_n^\dagger \hat{a}_n}{k_B T}\right).
\end{aligned} \tag{2.52}$$

This can be put into more compact form as in Eq. 2.48

$$\hat{\rho} = \frac{e^{-\beta\hbar\omega_n \hat{a}^\dagger \hat{a}}}{\text{Tr}\left(e^{-\beta\hbar\omega_n \hat{a}^\dagger \hat{a}}\right)}.$$

Another form of the thermal bath density matrix is obtained by first calculating the average number of photons as

$$\begin{aligned}
\bar{n} &= \sum_m m p_m = (1-A)\sum_m m A^m = (1-A)A\frac{\partial}{\partial A}\sum_m A^m (1-A)A\frac{\partial}{\partial A}\left(\frac{1}{1-A}\right) \\
&= (1-A)\frac{-A}{(1-A)^2} = \frac{A}{1-A} \\
\bar{n} &= \frac{\exp\left(-\frac{\hbar\omega_n}{k_B T}\right)}{1 - \exp\left(-\frac{\hbar\omega_n}{k_B T}\right)} = \frac{1}{\exp\left(\frac{\hbar\omega_n}{k_B T}\right) - 1}.
\end{aligned} \tag{2.53}$$

Then, using the probabilities in Eq. 2.49, density matrix of a thermal field is written as

$$\hat{\rho}_{\text{thermal}} = \sum_n \frac{\bar{n}^n}{(1+\bar{n})^{n+1}} \left|n\right\rangle \left\langle n\right|. \tag{2.54}$$

This can be generalized to multi-mode thermal bath of bosons using the multi-mode Fock states, $\left|n_k^1\right\rangle \otimes \left|n_k^2\right\rangle \otimes \left|n_k^3\right\rangle \otimes \cdots \equiv \left|n_k^1 n_k^2 n_k^3 \ldots n_k^l \ldots\right\rangle \equiv \bigotimes_l \left|n_k^l\right\rangle \equiv \left|\{n_k\}\right\rangle$, where

subscript represents a certain multi-mode state, and superscripts are for the individual modes. Then from the basic definition of density matrix, it is written as

$$\hat{\rho}_{\text{multi}} = \sum_k p_k \left|\{n_k\}\right\rangle \left\langle\{n_k\}\right|, \tag{2.55}$$

where the probability of a certain multi-mode state is just multiplication of the probabilities for individual modes $p_k = p_k^1 \times p_k^2 \times \cdots = \prod_l p_k^l$ also written as

$$p_k = \prod_l \left[1 - \exp\left(-\frac{\hbar\omega_l}{k_B T}\right)\right] \exp\left(-\frac{n_l^k \hbar\omega_l}{k_B T}\right). \tag{2.56}$$

Substituting this Eq. 2.56 in, multi-mode thermal bath density matrix is written as

$$\hat{\rho}_{\text{multi}} = \sum_{\{n_k\}} \prod_l \left[1 - \exp\left(-\frac{\hbar\omega_l}{k_B T}\right)\right] \exp\left(-\frac{n_k^l \hbar\omega_l}{kBT}\right) \left|\{n_k\}\right\rangle \left\langle\{n_k\}\right|, \tag{2.57}$$

$$\hat{\rho}_{\text{multi}} = \prod_l e^{-\hbar\omega_l \hat{a}_l^\dagger \hat{a}_l / k_B T} \left(1 - e^{-\hbar\omega_l / k_B T}\right). \tag{2.58}$$

Finally, the average number of excitations for a certain mode is calculated by the sum of excitation number in a multi-mode state times the probability of that multi-mode state over all the multi-mode states as

$$\bar{n}^l = \sum_k n_k^l p_k. \tag{2.59}$$

We will make use of this density matrix and the average excitation number when we are tracing out the environment degrees of freedom deriving the MME.

## *2.5 Derivation of the Markovian Master Equation*

This section first summarizes the quantum dynamical semigroup [10, 11, 12, 80, 81, 82] and then provides the microscopic derivation of master equation in Born-Markov approximation (MME) using the interaction picture [78, 79, 83, 84]. Finally, by considering a specific model, harmonic oscillator in a bosonic thermal bath, the MME is put into Lindblad form [80, 81, 84]. This section is a combination of summaries for the topics from above references.

### *2.5.1 Quantum Dynamical Semigroup*

Dynamical semigroup concept is used for classical Markov processes, and the word "semi" means that the process is irreversible. In other words, one-parameter family describing the conditional transition probabilities of a Markov process is defined only for positive time differences $\tau = t_2 - t_1$, where $t_2 > t_1$. Quantum dynamical semigroup is the direct generalization of the same ideas to quantum Markov processes used to describe the open quantum systems (OQS). Using this direct analogy, quantum MME is written from the classical master equation of a Markov process by replacing the classical probability distribution with a density matrix as

$$\frac{d}{dt}\hat{\rho}(t) = \hat{\mathcal{L}}\hat{\rho}(t). \tag{2.60}$$

Formal solution of the Eq. 2.60 is just $\Lambda(\tau)\hat{\rho}(t_{\text{initial}})$, where $\tau \equiv t_{\text{final}} - t_{\text{initial}}$. One-parameter family of maps $\{\Lambda(\tau), \tau \geq 0\}$ are used to describe the dynamics of an OQS, and they satisfy the following properties

- $\Lambda(t_1)\Lambda(t_2) = \Lambda(t_1 + t_2)$ - semigroup property (Markovian)
- $\text{Tr}\left(\Lambda(\tau)\hat{\rho}(t_{\text{initial}})\right) = \text{Tr}\left(\hat{\rho}\right)$ - Trace preservation
- $\Lambda(\tau)\hat{\rho}(t_{\text{initial}}) \geq 0$ - Positivity (for $\hat{\rho} \geq 0$)
- $\lim_{\tau \to 0} \Lambda(\tau)\hat{\rho}(t_{\text{initial}}) = \hat{\rho}(t_{\text{initial}})$ - Continuity

Positivity is replaced by a stronger condition, complete positivity, to properly treat the entangled states. After this point, I just summarize the quantum dynamical semigroup technique by writing the MME for a single qubit, but more detail on quantum dynamical semigroup can be found in Refs. [10, 11, 12, 80, 81, 82]. Considering a open quantum system associated with a $n$-dimensional Hilbert space $\mathbb{H}$, completely positive dynamical map (omitting $(t_{\text{initial}})$) is written by a Kraus decomposition as

$$\Lambda(\tau)\hat{\rho} = \sum_{\alpha} \hat{W}_{\alpha}\hat{\rho}\hat{W}_{\alpha}^{\dagger}, \tag{2.61}$$

where $\hat{W}_\alpha$ are bounded operators on $\mathbb{H}$ with $\sum_\alpha \hat{W}_\alpha^\dagger \hat{W}_\alpha = \mathbb{1}$. Then, using the above properties of the dynamical mapping together with this decomposition and a complete basis of orthonormal operators $\{\hat{F}_i, i = 1, \cdots, n^2\}$ for the Liouville space [85, 86] corresponding to the considered finite dimensional $\hat{\mathbb{H}}$, most general form of $\mathcal{L}$ is derived to be

$$\hat{\mathcal{L}}\hat{\rho} = -i\left[\hat{H}, \hat{\rho}\right] + \sum_{i,j=1}^{n^2-1} \kappa_{ij} \overbrace{\left(\hat{F}_i \hat{\rho} \hat{F}_j^\dagger - \frac{1}{2}\{\hat{F}_j^\dagger \hat{F}_i, \hat{\rho}\}\right)}^{\hat{\mathcal{D}}[\hat{F}]}, \tag{2.62}$$

where $\hat{H}$ is Hamiltonian of the system, $\hat{\mathcal{D}}[\hat{F}]$ is the Lindblad dissipator of the operator $\hat{F}$, $\kappa_{ij}$ are positive constants to be determined from environment correlations and system-environment coupling strength, and the identity operator $\mathbb{1}$ of $\{\hat{F}_i, i = 1, \cdots, n^2\}$ is discarded in the sum. For a two level with the following Hamiltonian

$$\hat{H}_{\text{TLS}} = \frac{\omega}{2}\hat{\sigma}_z, \tag{2.63}$$

basis of the corresponding Liouville space can be $\{\mathbb{1}, \hat{\sigma}_+, \hat{\sigma}_-, \hat{\sigma}_z\}$, where $\hat{\sigma}$'s are Pauli spin operators. Then, master equation of a two level system is written as

$$\dot{\hat{\rho}} = -\frac{i}{\hbar}\left[\hat{H}_{\text{TLS}}, \hat{\rho}\right] + \kappa_- \hat{\mathcal{D}}[\hat{\sigma}_-] + \kappa_+ \hat{\mathcal{D}}[\hat{\sigma}_+] + \kappa_z \hat{\mathcal{D}}[\hat{\sigma}_z], \tag{2.64}$$

where $\kappa$'s are determined by bath correlations, which obey the (Kubo-Martin-Schwinger) KMS conditions for a thermal bath. Terms in this equation are detailedly discussed in the subsequent chapter.

### *2.5.2 Interaction Picture*

Until this point we made use of Schrödinger picture, and now interaction is introduced to be used for the derivation of MME. As the name suggests, interaction picture is useful when there is interaction such tthat the total Hamiltonian can be split into a free part $\hat{H}_0$ and an interaction part $\hat{H}_{\text{I}}(t)$

$$\hat{H}(t) = \hat{H}_0 + \hat{H}_{\text{I}}(t). \tag{2.65}$$

Evolution of a pure state is unitary for a closed system, and it is described by the unitary-evolution operator $\hat{U}(t,t_0)$ as

$$|\Psi(t)\rangle = \hat{U}(t,t_0)\,|\Psi(t_0)\rangle \qquad \text{with} \qquad \hat{U}(t_0,t_0) = \mathbb{1}. \tag{2.66}$$

Using this relation, time evolution of a density matrix is rewritten in terms of unitary evolution operator as

$$\begin{aligned} \hat{\rho}(t) &= \sum_j p_j\,|\Psi_j,t\rangle\,\langle\Psi_j,t| = \sum_n p_n \hat{U}(t,t_0)\,|\Psi_j,t_0\rangle\,\langle\Psi_j,t_0|\,\hat{U}^\dagger(t,t_0) \\ &= \hat{U}(t,t_0)\hat{\rho}(t_0)\hat{U}^\dagger(t,t_0). \end{aligned} \tag{2.67}$$

Substituting the unitary evolution relation Eq. 2.66 into the Schrödinger equation Eq. 2.13, we get the equation of motion for unitary evolution operator as

$$i\hbar\frac{\partial}{\partial t}\hat{U}(t,t_0) = \hat{H}(t)\hat{U}(t,t_0), \tag{2.68}$$

which has a solution in terms of a Hamiltonian, that commutes at different times, as

$$\hat{U}(t,t_0) = \exp\left[\frac{1}{i\hbar}\int_{t_0}^{t} dt'\,\hat{H}(t')\right]. \tag{2.69}$$

Then, by partitioning the Hamiltonian as in Eq. 2.65, the unitary operation is divided into two parts as

$$\hat{U}(t,t_0) = \overbrace{\exp\left[\frac{1}{i\hbar}\hat{H}_0(t-t_0)\right]}^{\hat{U}_0(t,t_0)}\overbrace{\exp\left[\frac{1}{i\hbar}\int_{t_0}^{t} dt'\,H_{\rm I}(t')\right]}^{\hat{U}_{\rm I}(t,t_0)}, \tag{2.70}$$

Now, we are in a position to define the observables and density matrix in the interaction picture using expectation value of an observable $\hat{O}$. Using partitioned unitary operator, expectation value of an observable $\hat{O}(t)$ is written as

$$\begin{aligned} \langle\hat{O}(t)\rangle &\equiv \langle\hat{O}\rangle_t = \mathrm{Tr}(\hat{O}\hat{\rho}(t)) = tr(\hat{O}\hat{U}(t,t_0)\hat{\rho}(t_0)\hat{U}^\dagger(t,t_0)) \\ \langle\hat{O}\rangle_t &= \mathrm{Tr}\left(\hat{O}\hat{U}_0(t,t_0)\hat{U}_{\rm I}(t,t_0)\hat{\rho}(t_0)\hat{U}_{\rm I}^\dagger(t,t_0)\hat{U}_0^\dagger(t,t_0)\right). \end{aligned} \tag{2.71}$$

t Using the cyclic property of trace that is $\mathrm{Tr}(ABC) = \mathrm{Tr}(BCA) = \mathrm{Tr}(CAB)$, we get

$$\langle\hat{O}\rangle_t = \mathrm{Tr}\left(\hat{O}_{\rm I}(t)\hat{\rho}_{\rm I}(t)\right),$$

where $\hat{O}_{\rm I}(t) = \hat{U}_0^\dagger(t,t_0)\hat{O}\hat{U}_0(t,t_0)$ and $\hat{\rho}_{\rm I}(t) = \hat{U}_{\rm I}(t,t_0)\hat{\rho}(t_0)\hat{U}_{\rm I}^\dagger(t,t_0)$, or alternatively $\hat{\rho}_{\rm I}(t) = \hat{U}_0^\dagger(t,t_0)\hat{\rho}(t)\hat{U}_0(t,t_0)$.

These equations are constructed in a way that at time $t = t_0$ interaction picture observables and density matrix coincide with the corresponding operators in Schrödinger picture. Above relations tell that, in the interaction picture, observable operators are evolved by free Hamiltonian, and density matrix is evolved by interaction Hamiltonian, which can also be obtained by the transformation of Schrödinger picture density matrix using free evolution unitary operator. It is straightforward to show that the interaction picture Hamiltonian $\tilde{\hat{H}}_{\rm I}(t)$, which evolves the interaction picture states, is obtained from the interaction Hamiltonian by the transformation

$$\begin{aligned}
\hat{\tilde{H}}(t) &= \hat{U}_0^\dagger(t,t_0)\hat{H}(t)\hat{U}_0(t,t_0 = \hat{U}_0^\dagger(t,t_0)(\hat{H}_0 + H_{\rm I}(t))\hat{U}_0(t,t_0) \\
&= \underbrace{\hat{U}_0^\dagger(t,t_0)\hat{H}_0\hat{U}_0(t,t_0)}_{\hat{H}_0} + \underbrace{\hat{U}_0^\dagger(t,t_0)\hat{H}_{\rm I}(t)\hat{U}_0(t,t_0)}_{\hat{\tilde{H}}_{\rm I}(t)} \\
\hat{\tilde{H}}(t) &= \hat{H}_0 + \hat{\tilde{H}}_{\rm I}(t). \qquad (2.72)
\end{aligned}$$

In the third line, free unitary evolution operators had no effect on free Hamiltonian, because they commute, and the order can be changed to cancel unitary operators.

### *2.5.3 Master Equation in the Interaction Picture*

In Schrödinger picture, we have $i\hbar\dot{\rho}(t) = \left[\hat{H}, \hat{\rho}(t)\right]$ for the time evolution a density matrix, and the density matrix transforms into interaction picture as, $\hat{\rho}_{\rm I}(t) = \hat{U}_0^\dagger(t,t_0)\hat{\rho}(t)\hat{U}_0(t,t_0)$, more explicitly,

$$\hat{\rho}_{\rm I}(t) = \exp(-\frac{\hat{H}_0(t-t_0)}{i\hbar})\hat{\rho}(t)\exp(\frac{\hat{H}_0(t-t_0)}{i\hbar}).$$

Differentiating the both sides of this relation and substituting the relation for $\dot{\hat{\rho}}$ together with the interaction picture Hamiltonian in Eq. 2.72, we obtain the equation

of motion for the interaction picture density matrix as

$$\begin{aligned}\dot{\hat{\rho}}_{\mathrm{I}}(t) &= -\frac{1}{i\hbar}\left[\hat{H}_0, \hat{\rho}_{\mathrm{I}}(t)\right] + \overbrace{\exp(-\frac{\hat{H}_0(t-t_0)}{i\hbar})\frac{\partial\hat{\rho}(t)}{\partial t}\exp(\frac{\hat{H}_0(t-t_0)}{i\hbar})}^{\frac{1}{i\hbar}\left[\hat{U}_0^\dagger\hat{H}(t)\hat{U}_0, \hat{U}_0\hat{\rho}\hat{U}_0^\dagger\right]=\frac{1}{i\hbar}\left[\hat{\tilde{H}}(t), \hat{\rho}_{\mathrm{I}}(t)\right]} \\ &= \frac{1}{i\hbar}\left[\tilde{H}(t) - \hat{H}_0, \hat{\rho}_{\mathrm{I}}(t)\right] = \frac{1}{i\hbar}\left[\hat{\tilde{H}}_{\mathrm{I}}(t), \hat{\rho}_{\mathrm{I}}(t)\right] \end{aligned} \tag{2.73}$$

From this equation, we will obtain the master equation by a direct (formal) integration and substitute it back to get

$$\hat{\rho}_{\mathrm{I}}(t) = \hat{\rho}_{\mathrm{I}}(0) + \frac{1}{i\hbar}\int_0^t \left[\hat{\tilde{H}}_{\mathrm{I}}(t'), \hat{\rho}_{\mathrm{I}}(t')\right] dt', \tag{2.74}$$

$$\dot{\hat{\rho}}_{\mathrm{I}}(t) = \frac{1}{i\hbar}\left[\hat{\tilde{H}}_{\mathrm{I}}(t), \hat{\rho}_{\mathrm{I}}(0)\right] - \frac{1}{\hbar^2}\int_0^t \left[\hat{\tilde{H}}_{\mathrm{I}}(t), \left[\hat{\tilde{H}}_{\mathrm{I}}(t'), \hat{\rho}_{\mathrm{I}}(t')\right]\right] dt'. \tag{2.75}$$

In addition to the approach that we follow to derive the MME here, time-dependent perturbation by means of Dyson series (essentially the same with our method but with a subtle difference), projection operators approach, and other methods are also used [87, 88, 89, 90].

Now, consider that $\hat{\rho}_{\mathrm{I}}(t)$ represents the state of a system S plus an environment R composite, and we are interested in the subsystem S. Then, we obtain the density matrix of subsystem $\hat{\rho}_{\mathrm{S_I}}(t)$ by tracing over environment degrees of freedom as

$$\dot{\hat{\rho}}_{\mathrm{S_I}}(t) = \frac{1}{i\hbar}\,\mathrm{Tr_R}\left[\hat{\tilde{H}}_{\mathrm{I}}(t), \hat{\rho}_{\mathrm{I}}(0)\right] - \frac{1}{\hbar^2}\int_0^t \mathrm{Tr_R}\left[\hat{\tilde{H}}_{\mathrm{I}}(t), \left[\hat{\tilde{H}}_{\mathrm{I}}(t'), \hat{\rho}_{\mathrm{I}}(t')\right]\right] dt'. \tag{2.76}$$

After this point, we will make a set of assumptions to simplify the master equation. First, we will assume that $\left[\hat{\tilde{H}}_{\mathrm{I}}(t), \hat{\rho}_{\mathrm{I}}(0)\right] = 0$, which may not be considered as an approximation, since it could explicitly be included in the derivation by removing a term from interaction Hamiltonian and adding it to system Hamiltonian. Second assumption is the Born approximation, which depends on the coupling between system and environment being weak so that no further correlation is build up between S and R other than the initial correlations, and the environment density matrix is practically not affected by the interactions, i.e. stays the same over time. This assumption enables us to factorize the density matrix $\rho_{\mathrm{I}}(0)$ at $t = 0$ and $\rho_{\mathrm{I}}(t)$ at any later time,

if it is initially separable as

$$\hat{\rho}_{\mathrm{I}}(0) = \hat{\rho}_{\mathrm{S_I}}(0)\hat{R}_0, \tag{2.77}$$

$$\hat{\rho}_{\mathrm{I}}(t) = \hat{\rho}_{\mathrm{S_I}}(t)\hat{R}_0, \tag{2.78}$$

where $\hat{R}_0$ is the density matrix of the environment, which does not change over time scales of observation. Last assumption, namely Markov approximation, is to reduce the master equation into a true (time-local) differential equation. Assumption is that the correlation functions of the environment vary at a time scale much shorter than the characteristic time of the dynamics of S. In other words, environment memory time is much shorter than system response time. With this assumption, time-nonlocal part of density matrix is removed by the replacement $\rho_{\mathrm{S_I}}(t^{'}) \rightarrow \rho_{\mathrm{S_I}}(t)$. Then, we finally obtain the master equation in Born-Markov approximation as

$$\dot{\hat{\rho}}_{\mathrm{S_I}}(t) = -\frac{1}{\hbar^2}\int_0^t \mathrm{Tr_R}\left[\hat{\tilde{H}}_{\mathrm{I}}(t), \left[\hat{\tilde{H}}_{\mathrm{I}}(t^{'}), \hat{\rho}_{\mathrm{S_I}}(t)R_0\right]\right] dt^{'}. \tag{2.79}$$

### *2.5.4 Lindblad Form*

Despite being derived with critical assumptions, Eq. 2.79 has a rather general form, and it is applicable for many systems, since it makes no assumptions on the type of system-environment interaction. In this part, starting from the master equation only in Born approximation, that is Eq. 2.76 without the commutator and with a separable $\hat{\rho}_{\mathrm{I}}(t)$, we first make us of a specific model to further simplify the form of master equation, and then we will put it into Lindblad form.

Before continuing with the derivation, a digression to motivate all these long calculations seems appropriate here. For a single quantum system, deriving the master equation with all these details is useful to ease the derivation of MME for composite interacting quantum systems. Details on this are presented in the subsequent chapters, but we highlight the key points, which give useful insights and intuitions for the derivation of composite system MMEs, along with the derivation.

*A Specific Form of Interaction*

Before focusing on our specific model, let us first assume an interaction Hamiltonian of the form

$$\hat{H}_{\rm I} = \hbar \sum_i \hat{s}_i \hat{\Gamma}_i, \tag{2.80}$$

where $\hat{s}_i$ are system, and $\hat{\Gamma}_i$ are environment operators. Then, the master equation in Born approximation is obtained by transforming the interaction Hamiltonian into interaction picture and substituting it into Eq. 2.76 as

$$\begin{aligned}
\hat{\tilde{H}}_{\rm I}(t) &= \hbar \sum_i e^{(i/\hbar)(\hat{H}_{\rm S}+H_{\rm R})t} \hat{s}_i \hat{\Gamma}_i e^{-(i/\hbar)(\hat{H}_{\rm S}+H_{\rm R})t} \\
&= \hbar \sum_i \overbrace{\left(e^{(i/\hbar)(\hat{H}_{\rm S}+H_{\rm R})t} \hat{s}_i e^{-(i/\hbar)(\hat{H}_{\rm S}+H_{\rm R})t}\right)}^{\hat{\tilde{s}}_i(t)} \overbrace{\left(e^{(i/\hbar)(\hat{H}_{\rm S}+H_{\rm R})t} \hat{\Gamma}_i e^{-(i/\hbar)(\hat{H}_{\rm S}+H_{\rm R})t}\right)}^{\hat{\tilde{\Gamma}}_i(t)}, \\
\dot{\hat{\rho}}_{\rm S_I}(t) &= -\sum_{i,j} \int_0^t {\rm Tr}_{\rm R}\left[\hat{\tilde{s}}_i(t)\hat{\tilde{\Gamma}}_i(t), \left[\hat{\tilde{s}}_j(t')\hat{\tilde{\Gamma}}_j(t'), \hat{\rho}_{\rm S_I}(t')R_0\right]\right] dt' \\
&= -\sum_{i,j} \int_0^t dt' \Big\{ \left(\hat{\tilde{s}}_i(t)\hat{\tilde{s}}_j(t')\hat{\rho}_{\rm S_I}(t') - \hat{\tilde{s}}_j(t')\hat{\rho}_{\rm S_I}(t')\hat{\tilde{s}}_i(t)\right) \langle \hat{\tilde{\Gamma}}_i(t)\hat{\tilde{\Gamma}}_j(t')\rangle_{\rm R} \\
&\quad + \left(\hat{\rho}_{\rm S_I}(t')\hat{\tilde{s}}_j(t')\hat{\tilde{s}}_i(t) - \hat{\tilde{s}}_i(t)\hat{\rho}_{\rm S_I}(t')\hat{\tilde{s}}_j(t')\right) \langle \hat{\tilde{\Gamma}}_j(t')\hat{\tilde{\Gamma}}_i(t)\rangle_{\rm R} \Big\},
\end{aligned} \tag{2.81}$$

where we have used the cyclic property of trace, and the correlation functions are given as

- $\langle \hat{\tilde{\Gamma}}_i(t)\hat{\tilde{\Gamma}}_j(t')\rangle_{\rm R} = {\rm Tr}_{\rm R}\left[R_0 \hat{\tilde{\Gamma}}_i(t)\hat{\tilde{\Gamma}}_j(t')\right]$,
- $\langle \hat{\tilde{\Gamma}}_j(t')\hat{\tilde{\Gamma}}_i(t)\rangle_{\rm R} = {\rm Tr}_{\rm R}\left[R_0 \hat{\tilde{\Gamma}}_j(t')\hat{\tilde{\Gamma}}_i(t))\right]$.

*A Harmonic Oscillator in a Bath of Bosons*

Now, we will make us of the above approach for a harmonic oscillator in a bosonic thermal bath for which the Hamiltonian is

$$\hat{H} = \hat{H}_{\rm S} + \hat{H}_{\rm R} + \hat{H}_{\rm I},$$

where free system Hamiltonians are respectively given for the system and bath as

$$\hat{H}_{\rm S} = \hbar\omega\hat{a}^\dagger\hat{a}, \tag{2.82}$$

$$\hat{H}_{\rm R} = \sum_j \hbar\omega_j\hat{b}_j^\dagger\hat{b}_j, \tag{2.83}$$

and the interaction between them are given as $\hat{H}_{\rm I} = \sum_j \hbar g_j\left(\hat{a}^\dagger\hat{b}_j + \hat{a}\hat{b}_j^\dagger\right)$. Here, $\hat{a}$ and $\hat{a}^\dagger$ are respectively bosonic annihilation and creation operators of the Harmonic oscillator system, and they obey the commutation relation $\left[\hat{a},\hat{a}^\dagger\right] = \mathbb{1}$. These operators for the bosonic bath are respectively $\hat{b}$ and $\hat{b}^\dagger$. Finally, $\omega$ and $\omega_j$ are the frequencies of Harmonic oscillator system and $jth$ mode of the bosonic bath, respectively.

Our interaction Hamiltonian includes two pairs of operators, so the summation index $i$ in Eq. 2.80 runs from 1 to 2. Therefore, when the summation in Eq. 2.81 is distributed explicitly into the integral, there appear 8 terms in parentheses of environmental correlations, but only 4 of them would have non-vanishing correlations. In order to explicitly calculate them, let us first identify the related operators and transform them into interaction picture, and then let us write the full form of master equation. First, we identify the operators as

$$\hat{s}_1 = \hat{a} \qquad \text{and} \qquad \hat{\Gamma}_1 = \hat{\Gamma}^\dagger \equiv \sum_j g_j b_j^\dagger,$$

$$\hat{s}_2 = \hat{a}^\dagger \qquad \text{and} \qquad \hat{\Gamma}_2 = \hat{\Gamma} \equiv \sum_j g_j b_j.$$

Then, transform the operators into interaction picture,

$$\hat{\tilde{s}}_1(t) = e^{i\omega_0\hat{a}^\dagger\hat{a}t}\hat{a}e^{-i\omega_0\hat{a}^\dagger\hat{a}t} = \hat{a}e^{-i\omega_0 t}, \tag{2.84}$$

$$\hat{\tilde{s}}_2(t) = e^{i\omega_0\hat{a}^\dagger\hat{a}t}\hat{a}^\dagger e^{-i\omega_0\hat{a}^\dagger\hat{a}t} = \hat{a}^\dagger e^{i\omega_0 t}, \tag{2.85}$$

$$\begin{aligned}\hat{\tilde{\Gamma}}_1(t) &= \hat{\tilde{\Gamma}}^\dagger(t) = \exp\left(i\sum_n \omega_n\hat{b}_n^\dagger\hat{b}_n t\right)\left(\sum_j g_j\hat{b}_j^\dagger\right)\exp\left(-i\sum_m \omega_n\hat{b}_m^\dagger\hat{b}_m t\right)\\ &= \sum_j g_j\hat{b}_j^\dagger e^{i\omega_j t},\end{aligned} \tag{2.86}$$

$$\begin{aligned}\hat{\tilde{\Gamma}}_2(t) &= \hat{\tilde{\Gamma}}(t) = \exp\left(i\sum_n \omega_n\hat{b}_n^\dagger\hat{b}_n t\right)\left(\sum_j g_j\hat{b}_j\right)\exp\left(-i\sum_m \omega_n\hat{b}_m^\dagger\hat{b}_m t\right)\\ &= \sum_j g_j\hat{b}_j e^{-i\omega_j t},\end{aligned} \tag{2.87}$$

where we used the fact that operators of different environment oscillators commute.

One of the most useful point in this derivation is the identification of interaction picture coupling operators Eq. 2.84 and 2.85. Importance of this identification is apparent in the end result, and we emphasize its importance there.

Finally, by substituting the Eq. 2.84 - 2.87 in Eq. 2.81, we obtain the master equation as

$$\begin{aligned}
\dot{\hat{\rho}}_{\mathrm{S_I}}(t) \;=\; & -\int_0^t dt' \Big\{ \Big(\hat{a}\hat{a}\hat{\rho}_{\mathrm{S_I}}(t') - \hat{a}\hat{\rho}_{\mathrm{S_I}}(t')\hat{a}\Big) e^{-i\omega_0(t+t')} \langle \hat{\tilde{\Gamma}}^\dagger(t)\hat{\tilde{\Gamma}}^\dagger(t')\rangle_{\mathrm{R}} \\
& + \Big(\hat{\rho}_{\mathrm{S_I}}(t')\hat{a}\hat{a} - \hat{a}\hat{\rho}_{\mathrm{S_I}}(t')\hat{a}\Big) e^{-i\omega_0(t+t')} \langle \hat{\tilde{\Gamma}}^\dagger(t')\hat{\tilde{\Gamma}}^\dagger(t)\rangle_{\mathrm{R}} \\
& + \Big(\hat{a}\hat{a}^\dagger\hat{\rho}_{\mathrm{S_I}}(t') - \hat{a}^\dagger\hat{\rho}_{\mathrm{S_I}}(t')\hat{a}\Big) e^{-i\omega_0(t-t')} \langle \hat{\tilde{\Gamma}}^\dagger(t)\hat{\tilde{\Gamma}}(t')\rangle_{\mathrm{R}} \\
& + \Big(\hat{\rho}_{\mathrm{S_I}}(t')\hat{a}^\dagger\hat{a} - \hat{a}\hat{\rho}_{\mathrm{S_I}}(t')\hat{a}^\dagger\Big) e^{-i\omega_0(t-t')} \langle \hat{\tilde{\Gamma}}(t')\hat{\tilde{\Gamma}}^\dagger(t)\rangle_{\mathrm{R}} \\
& + \Big(\hat{a}^\dagger\hat{a}\hat{\rho}_{\mathrm{S_I}}(t') - \hat{a}\hat{\rho}_{\mathrm{S_I}}(t')\hat{a}^\dagger\Big) e^{i\omega_0(t-t')} \langle \hat{\tilde{\Gamma}}(t)\hat{\tilde{\Gamma}}^\dagger(t')\rangle_{\mathrm{R}} \\
& + \Big(\hat{\rho}_{\mathrm{S_I}}(t')\hat{a}\hat{a}^\dagger - \hat{a}^\dagger\hat{\rho}_{\mathrm{S_I}}(t')\hat{a}\Big) e^{i\omega_0(t-t')} \langle \hat{\tilde{\Gamma}}^\dagger(t')\hat{\tilde{\Gamma}}(t)\rangle_{\mathrm{R}} \\
& + \Big(\hat{a}^\dagger\hat{a}^\dagger\hat{\rho}_{\mathrm{S_I}}(t') - \hat{a}^\dagger\hat{\rho}_{\mathrm{S_I}}(t')\hat{a}^\dagger\Big) e^{i\omega_0(t+t')} \langle \hat{\tilde{\Gamma}}(t)\hat{\tilde{\Gamma}}(t')\rangle_{\mathrm{R}} \\
& + \Big(\hat{\rho}_{\mathrm{S_I}}(t')\hat{a}^\dagger\hat{a}^\dagger - \hat{a}^\dagger\hat{\rho}_{\mathrm{S_I}}(t')\hat{a}^\dagger\Big) e^{i\omega_0(t+t')} \langle \hat{\tilde{\Gamma}}(t')\hat{\tilde{\Gamma}}(t)\rangle_{\mathrm{R}} \,, \Big\}, \qquad (2.88)
\end{aligned}$$

where four distinct correlation functions are

- $\langle \hat{\tilde{\Gamma}}^\dagger(t)\hat{\tilde{\Gamma}}^\dagger(t')\rangle_{\mathrm{R}} = \sum_{j,k} g_j g_k e^{i\omega_j t} e^{i\omega_k t'} \,\mathrm{Tr}_{\mathrm{R}}\left(R_0 \hat{b}_j^\dagger \hat{b}_k^\dagger\right)$,
- $\langle \hat{\tilde{\Gamma}}(t)\hat{\tilde{\Gamma}}(t')\rangle_{\mathrm{R}} = \sum_{j,k} g_j g_k e^{-i\omega_j t} e^{-i\omega_k t'} \,\mathrm{Tr}_{\mathrm{R}}\left(R_0 \hat{b}_j \hat{b}_k\right)$,
- $\langle \hat{\tilde{\Gamma}}^\dagger(t)\hat{\tilde{\Gamma}}(t')\rangle_{\mathrm{R}} = \sum_{j,k} g_j g_k e^{i\omega_j t} e^{-i\omega_k t'} \,\mathrm{Tr}_{\mathrm{R}}\left(R_0 \hat{b}_j^\dagger \hat{b}_k\right)$,
- $\langle \hat{\tilde{\Gamma}}(t)\hat{\tilde{\Gamma}}^\dagger(t')\rangle_{\mathrm{R}} = \sum_{j,k} g_j g_k e^{-i\omega_j t} e^{i\omega_k t'} \,\mathrm{Tr}_{\mathrm{R}}\left(R_0 \hat{b}_j \hat{b}_k^\dagger\right)$.

First two of these correlations are zero, and they eliminate the first and last two terms in the master equation Eq.2.88. They (two are given below the others are calculated

similarly) are calculated using multi-mode Fock states as

$$\begin{aligned}
\mathrm{Tr_R}\left(\hat{R}_0\hat{b}_j^\dagger\hat{b}_k^\dagger\right) &= \sum_i \langle\{n_i\}|\hat{R}_0\hat{b}_j^\dagger\hat{b}_k^\dagger|\{n_i\}\rangle = \sum_i \langle\{n_i\}|\hat{R}_0\sqrt{n_i^j+1}\sqrt{n_i^k+1}|\{n_i\}^{k+1,j+1}\rangle \\
&= \sum_i \sqrt{(n_i^j+1)(n_i^k+1)}\,\langle\{n_i\}|\prod_{\mathrm{I}}\frac{e^{-\hbar\omega_{\mathrm{I}}\hat{b}_{\mathrm{I}}^\dagger\hat{b}_{\mathrm{I}}/k_BT}}{(1-e^{-\hbar\omega_l/k_BT})^{-1}}|\{n_i\}^{k+1,j+1}\rangle \\
&= \sum_i \prod_{\mathrm{I}}\frac{e^{-\hbar\omega_{\mathrm{I}}n_l^{i,k+1,j+1}/k_BT}}{(1-e^{-\hbar\omega_{\mathrm{I}}/k_BT})^{-1}}\sqrt{(n_i^j+1)(n_i^k+1)}\underbrace{\langle\{n_i\}|\{n_i\}^{k+1,j+1}\rangle}_{=0} = 0, \\
\implies \langle\hat{\tilde{\Gamma}}^\dagger(t)\hat{\tilde{\Gamma}}^\dagger(t')\rangle_{\mathrm{R}} &= 0, \qquad (2.89)
\end{aligned}$$

where we used the orthogonality of multi-mode Fock states. Also, orthogonality of multi-mode states is used in a way that superscripts read the modified mode of the certain state $|\{n_i\}\rangle$, and $+/-$ means excitation number is increased/decreased.

Other correlations are related to the average excitation number of the bath and are calculated as

$$\begin{aligned}
\mathrm{Tr_R}\left(\hat{R}_0\hat{b}_j^\dagger\hat{b}_k\right) &= \sum_i \langle\{n_i\}|\hat{R}_0\hat{b}_j^\dagger\hat{b}_k|\{n_i\}\rangle = \sum_i \langle\{n_i\}|\hat{R}_0\sqrt{n_i^j}\sqrt{n_i^k}|\{n_i\}^{k-1,j+1}\rangle \\
&= \sum_i \sqrt{n_i^j n_i^k}\,\langle\{n_i\}|\prod_{\mathrm{I}}\frac{e^{-\hbar\omega_{\mathrm{I}}\hat{b}_{\mathrm{I}}^\dagger\hat{b}_{\mathrm{I}}/k_BT}}{(1-e^{-\hbar\omega_{\mathrm{I}}/k_BT})^{-1}}|\{n_i\}^{k-1,j+1}\rangle \\
&= \sum_i \underbrace{\prod_{\mathrm{I}}\frac{e^{-\hbar\omega_l n_{\mathrm{I}}^{i,k-1,j+1}/k_BT}}{(1-e^{-\hbar\omega_{\mathrm{I}}/k_BT})^{-1}}}_{p_{i,k-1,j+1}}\sum_i \sqrt{n_i^j n_i^k}\underbrace{\langle\{n_i\}|\{n_i\}^{k-1,j+1}\rangle}_{=\delta_{j,k}}, \\
\implies \mathrm{Tr_R}\left(\hat{R}_0\hat{b}_j^\dagger\hat{b}_k\right) &= \delta_{j,k}e^{-\hbar\omega_j/k_BT}e^{-\hbar\omega_k/k_BT}\sum_i n_i^j p_i = \delta_{j,k}\bar{n}^j. \qquad (2.90)
\end{aligned}$$

In above calculation, the exponential part is due to probability correction, and Kronecker delta is deliberately kept, since there is a further sum on $j$ and $k$. Finally, the correlation function becomes

$$\langle\hat{\tilde{\Gamma}}^\dagger(t)\hat{\tilde{\Gamma}}(t')\rangle_{\mathrm{R}} = \sum_{j,k} g_j g_k e^{i\omega_j t}e^{-i\omega_k t'}\delta_{j,k}\bar{n}^j = \sum_j |g_j|^2\, e^{i\omega_j(t-t')}\bar{n}(\omega_j,T).$$

Similarly, the others are calculated as

$$\langle\hat{\tilde{\Gamma}}(t)\hat{\tilde{\Gamma}}(t')\rangle_{\mathrm{R}} = 0, \tag{2.91}$$

$$\langle\hat{\tilde{\Gamma}}^{\dagger}(t')\hat{\tilde{\Gamma}}(t)\rangle_{\mathrm{R}} = \sum_j |g_j|^2 e^{-i\omega_j(t-t')}\bar{n}(\omega_j,T), \tag{2.92}$$

$$\langle\hat{\tilde{\Gamma}}(t)\hat{\tilde{\Gamma}}^{\dagger}(t')\rangle_{\mathrm{R}} = \sum_j |g_j|^2 e^{-i\omega_j(t-t')}\left[\bar{n}(\omega_j,T)+1\right], \tag{2.93}$$

$$\langle\hat{\tilde{\Gamma}}(t')\hat{\tilde{\Gamma}}^{\dagger}(t)\rangle_{\mathrm{R}} = \sum_j |g_j|^2 e^{i\omega_j(t-t')}\left[\bar{n}(\omega_j,T)+1\right]. \tag{2.94}$$

The non-vanishing environment correlation functions still involve a summation over the modes. Since there are infinite number of modes, sum is changed to an integral by introducing the density of states $g(\omega)$ such that $g(\omega)d\omega$ is the number of modes with frequencies in the interval $\omega$ to $\omega+d\omega$. Then, defining $t-t'\equiv\tau$, non-vanishing correlations are written as

$$\langle\hat{\tilde{\Gamma}}^{\dagger}(t)\hat{\tilde{\Gamma}}(t-\tau)\rangle_{\mathrm{R}} = \int_0^{\infty} d\omega e^{i\omega\tau}g(\omega)\,|g_w|^2\,\bar{n}(\omega,T), \tag{2.95}$$

$$\langle\hat{\tilde{\Gamma}}(t-\tau)\hat{\tilde{\Gamma}}^{\dagger}(t)\rangle_{\mathrm{R}} = \int_0^{\infty} d\omega e^{i\omega\tau}g(\omega)\,|g_w|^2\,[\bar{n}(\omega,T)+1], \tag{2.96}$$

$$\langle\hat{\tilde{\Gamma}}(t)\hat{\tilde{\Gamma}}^{\dagger}(t-\tau)\rangle_{\mathrm{R}} = \int_0^{\infty} d\omega e^{-i\omega\tau}g(\omega)\,|g_w|^2\,[\bar{n}(\omega,T)+1], \tag{2.97}$$

$$\langle\hat{\tilde{\Gamma}}^{\dagger}(t-\tau)\hat{\tilde{\Gamma}}(t)\rangle_{\mathrm{R}} = \int_0^{\infty} d\omega e^{-i\omega\tau}g(\omega)\,|g_w|^2\,\bar{n}(\omega,T). \tag{2.98}$$

Then, the master equation in Born approximation with non-vanishing correlations is

$$\begin{aligned}\dot{\hat{\rho}}_{\mathrm{S_I}}(t) = -\int_0^t d\tau\Big\{ &\left(\hat{a}\hat{a}^{\dagger}\hat{\rho}_{\mathrm{S_I}}(t-\tau)-\hat{a}^{\dagger}\hat{\rho}_{\mathrm{S_I}}(t-\tau)\hat{a}\right)e^{-i\omega_0\tau}\,\langle\hat{\tilde{\Gamma}}^{\dagger}(t)\hat{\tilde{\Gamma}}(t-\tau)\rangle\\ &+\left(\hat{\rho}_{\mathrm{S_I}}(t-\tau)\hat{a}^{\dagger}\hat{a}-\hat{a}\hat{\rho}_{\mathrm{S_I}}(t-\tau)\hat{a}^{\dagger}\right)e^{-i\omega_0\tau}\,\langle\hat{\tilde{\Gamma}}(t-\tau)\hat{\tilde{\Gamma}}^{\dagger}(t)\rangle\\ &+\left(\hat{a}^{\dagger}\hat{a}\hat{\rho}_{\mathrm{S_I}}(t-\tau)-\hat{a}\hat{\rho}_{\mathrm{S_I}}(t-\tau)\hat{a}^{\dagger}\right)e^{i\omega_0\tau}\,\langle\hat{\tilde{\Gamma}}(t)\hat{\tilde{\Gamma}}^{\dagger}(t-\tau)\rangle\\ &+\left(\hat{\rho}_{\mathrm{S_I}}(t-\tau)\hat{a}\hat{a}^{\dagger}-\hat{a}^{\dagger}\hat{\rho}_{\mathrm{S_I}}(t-\tau)\hat{a}\right)e^{i\omega_0\tau}\,\langle\hat{\tilde{\Gamma}}^{\dagger}(t-\tau)\hat{\tilde{\Gamma}}(t)\rangle\Big\}.\end{aligned} \tag{2.99}$$

*Markov Approximation*

With out any detailed discussion on time scales, stating that if $\tau$ is in the order of environment memory time, Markov approximation, which is to assume that $t >> \tau$,

will be the replacement of $\hat{\rho}_{\mathrm{S_I}}(t-\tau) \rightarrow \hat{\rho}_{\mathrm{S_I}}(t)$ and the extension of $\tau$ integration to infinity as the limit $t \rightarrow \infty$. With these replacements, master equation in Born-Markov approximation is written in a more compact form as

$$\begin{aligned}\dot{\hat{\rho}}_{\mathrm{S_I}} &= \kappa_1(\hat{a}\hat{\rho}_{\mathrm{S_I}}\hat{a}^\dagger - \hat{a}^\dagger\hat{a}\hat{\rho}_{\mathrm{S_I}} - \hat{\rho}_{\mathrm{S_I}}\hat{a}\hat{a}^\dagger + \hat{a}^\dagger\hat{\rho}_{\mathrm{S_I}}\hat{a}) + \kappa_1^*(\hat{a}^\dagger\hat{\rho}_{\mathrm{S_I}}\hat{a} - \hat{a}\hat{a}^\dagger\hat{\rho}_{\mathrm{S_I}} - \hat{\rho}_{\mathrm{S_I}}\hat{a}^\dagger\hat{a} + \hat{a}\hat{\rho}_{\mathrm{S_I}}\hat{a}^\dagger) \\ &\quad +\kappa_2(\hat{a}\hat{\rho}_{\mathrm{S_I}}\hat{a}^\dagger - \hat{a}^\dagger\hat{a}\hat{\rho}_{\mathrm{S_I}}) + \kappa_2^*(\hat{a}\hat{\rho}_{\mathrm{S_I}}\hat{a}^\dagger - \hat{\rho}_{\mathrm{S_I}}\hat{a}^\dagger\hat{a}), \qquad (2.100)\end{aligned}$$

where the coefficient are given as,

$$\kappa_1 = \lim_{t\to\infty}\int_0^t d\tau \int_0^\infty d\omega e^{-i(\omega-\omega_0)\tau} g(\omega)\left|g_\omega\right|^2, \qquad (2.101)$$

$$\kappa_2 = \lim_{t\to\infty}\int_0^t d\tau \int_0^\infty d\omega e^{-i(\omega-\omega_0)\tau} g(\omega)\left|g_\omega\right|^2 \bar{n}(\omega,T). \qquad (2.102)$$

These integrals are easier to carry, if time integral is taken first. Then, with the use of Cauchy principal value of an improper integral and residue theorem, these factors are found to be

$$\kappa_1 = \pi g(\omega_0)\left|g_{\omega_0}\right|^2 + i\Delta \equiv \frac{\kappa}{2} + i\Delta, \qquad (2.103)$$

$$\kappa_2 = \pi g(\omega_0)\left|g_{\omega_0}\right|^2 \bar{n}(\omega,T) + i\Delta' \equiv \frac{\kappa}{2}\bar{n} + i\Delta', \qquad (2.104)$$

where we defined

$$\Delta \equiv P\int_0^\infty d\omega \frac{g(\omega)\left|g_\omega\right|^2}{\omega_0-\omega}, \qquad (2.105)$$

$$\Delta' \equiv P\int_0^\infty d\omega \frac{g(\omega)\left|g_\omega\right|^2}{\omega_0-\omega}\bar{n}(\omega,T). \qquad (2.106)$$

Substituting these in and reorganizing the master equation Eq. 2.100, we get

$$\begin{aligned}\dot{\hat{\rho}}_{\mathrm{S_I}} = -i\Delta\left[\hat{a}^\dagger\hat{a},\rho_{\mathrm{S}}\right] &+ \frac{\kappa}{2}(2\hat{a}\hat{\rho}_{\mathrm{S_I}}\hat{a}^\dagger - \hat{a}^\dagger\hat{a}\hat{\rho}_{\mathrm{S_I}} - \hat{\rho}_{\mathrm{S_I}}\hat{a}^\dagger\hat{a}) \\ &+ \kappa\bar{n}(\hat{a}\hat{\rho}_{\mathrm{S_I}}\hat{a}^\dagger + \hat{a}^\dagger\hat{\rho}_{\mathrm{S_I}}\hat{a} - \hat{a}^\dagger\hat{a}\hat{\rho}_{\mathrm{S_I}} - \hat{\rho}_{\mathrm{S_I}}\hat{a}\hat{a}^\dagger). \qquad (2.107)\end{aligned}$$

*Lindblad Form*

The density matrix in Eq. 2.107 is still in the interaction picture, and it is transformed into the Schrödinger picture as

$$\hat{\rho}_{\mathrm{S_I}} = e^{(i/\hbar)\hat{H}_{\mathrm{S}}t}\hat{\rho}_{\mathrm{S}}(t)e^{-(i/\hbar)\hat{H}_{\mathrm{S}}t}. \qquad (2.108)$$

Then, its time derivative is written as

$$\dot{\hat{\rho}}_{\mathrm{S_I}} = \frac{1}{i\hbar}\left[\hat{H}_{\mathrm{S}}, \hat{\rho}_{\mathrm{S}}\right] + e^{(i/\hbar)\hat{H}_{\mathrm{S}}t}\dot{\hat{\rho}}_{\mathrm{S}}(t)e^{-(i/\hbar)\hat{H}_{\mathrm{S}}t}. \tag{2.109}$$

Substituting the Eq. 2.108 and 2.109 into the Eq. 2.107 and reorganizing it to leave only $\dot{\hat{\rho}}_{\mathrm{S}}$ on the left hand side, each right hand term gets multiplied by unitary operators from both sides. Commutator relation would not be effected by that, and the other operators transform as

$$\begin{aligned} e^{-(i/\hbar)\hat{H}_{\mathrm{S}}t}\hat{a}\hat{\rho}_{\mathrm{S_I}}\hat{a}^\dagger e^{(i/\hbar)\hat{H}_{\mathrm{S}}t} &= e^{-(i/\hbar)\hat{H}_{\mathrm{S}}t}\hat{a}\left(e^{(i/\hbar)\hat{H}_{\mathrm{S}}t}\hat{\rho}_{\mathrm{S}}e^{-(i/\hbar)\hat{H}_{\mathrm{S}}t}\right)\hat{a}^\dagger e^{(i/\hbar)\hat{H}_{\mathrm{S}}t} \\ &= \left(e^{-(i/\hbar)\hat{H}_{\mathrm{S}}t}\hat{a}e^{(i/\hbar)\hat{H}_{\mathrm{S}}t}\right)\hat{\rho}_{\mathrm{S}}\left(e^{-(i/\hbar)\hat{H}_{\mathrm{S}}t}\hat{a}^\dagger e^{(i/\hbar)\hat{H}_{\mathrm{S}}t}\right) \\ &= \hat{a}\hat{\rho}_{\mathrm{S}}\hat{a}^\dagger. \end{aligned} \tag{2.110}$$

Finally, the master equation in Born-Markov approximation becomes

$$\begin{aligned} \dot{\hat{\rho}}_{\mathrm{S}} = -i\omega_0^{'}\left[\hat{a}^\dagger\hat{a}, \rho_{\mathrm{S}}\right] &+ \frac{\kappa}{2}(2\hat{a}\hat{\rho}_{\mathrm{S}}\hat{a}^\dagger - \hat{a}^\dagger\hat{a}\hat{\rho}_{\mathrm{S}} - \hat{\rho}_{\mathrm{S}}\hat{a}^\dagger\hat{a}) \\ &+ \kappa\bar{n}(\hat{a}\hat{\rho}_{\mathrm{S}}\hat{a}^\dagger + \hat{a}^\dagger\hat{\rho}_{\mathrm{S}}\hat{a} - \hat{a}^\dagger\hat{a}\hat{\rho}_{\mathrm{S}} - \hat{\rho}_{\mathrm{S}}\hat{a}\hat{a}^\dagger). \end{aligned} \tag{2.111}$$

where $\omega_0^{'} \equiv \omega_0 + \Delta$ is the shifted energy level due to system-environment coupling, called Lamb shift. Finally, it will be put into Lindblad form by using the commutation relation of harmonic oscillator creation and annihilation operators. Also, neglecting the energy shift, it is written as

$$\dot{\hat{\rho}}_{\mathrm{S}} = -\frac{i}{\hbar}\left[\hat{H}_{\mathrm{S}}, \rho_{\mathrm{S}}\right] + \frac{\kappa}{2}(\bar{n}+1)(2\hat{a}\hat{\rho}_{\mathrm{S}}\hat{a}^\dagger - \hat{a}^\dagger\hat{a}\hat{\rho}_{\mathrm{S}} - \hat{\rho}_{\mathrm{S}}\hat{a}^\dagger\hat{a}) + \frac{\kappa}{2}\bar{n}(2\hat{a}^\dagger\hat{\rho}_{\mathrm{S}}\hat{a} - \hat{a}\hat{a}^\dagger\hat{\rho}_{\mathrm{S}} - \hat{\rho}_{\mathrm{S}}\hat{a}\hat{a}^\dagger). \tag{2.112}$$

This form is important mainly because of two points. First is the meaning of each term on the right-hand side. Unitary evolution Eq. 2.22 of the system-environment composite is reduced to the unitary evolution of the system plus the second and third terms both of which have dephasing effects while the latter de-excites and the former excites the system. They reflect the environmental effects on the open system, and their role is demonstrated in the next chapter using the single qubit case.

The second and more important point is better explained by writing the MME

Eq. 2.112 in a more compact form with Lindblad dissipator, defined in Eq. 2.62,

$$\dot{\hat{\rho}}_{\mathrm{S}} = -\frac{i}{\hbar}\left[\hat{H}_{\mathrm{S}}, \rho_{\mathrm{S}}\right] + \kappa(\bar{n}+1)(\hat{\mathcal{D}}[\hat{a}]) + \kappa\bar{n}(\hat{\mathcal{D}}[\hat{a}^{\dagger}]), \tag{2.113}$$

where Lindblad dissipator are respectively written using the operators in Eq. 2.84 and 2.85, and the average excitation number $\bar{n}$ is calculated using the frequency of their phase in Eq. 2.84 and 2.85. Since, they are not used at any other point in the derivation, if we identify the interaction picture coupling operators of a composite system by dressing it, we trivially write the MME using those operators as above with coefficients $(1+\bar{n})$ and $\bar{n}$ for negative and positive phases, respectively. Deriving the MME of a composite system, an additional approximation is used in some cases, called the secular approximation. All these are detailedly discussed in the subsequent chapters.

## *2.6 Quantum Thermodynamics*

In this section, we briefly introduce the quantum counter-parts of classical thermodynamical laws and definitions. We do not detailedly discuss them, but more details are presented in many works [91, 90, 92, 93, 94, 95]. Zeroth law of thermodynamics is about the transitivity of thermal equilibrium and enables the definition of temperature. In quantum thermodynamics, it is imposed by the requirement of no energy flow between subsystems in thermal equilibrium, which is equivalent to tensor product state of subsystems satisfy the KMS condition. First law is again on the conservation of energy, which requires definitions of heat and work. These are defined for a quantum system by writing the expectation value of its Hamiltonian as

$$\langle \hat{H} \rangle = \text{constant} = \mathrm{Tr}\left[\hat{\rho}\hat{H}\right], \tag{2.114}$$

and imposing that its time derivative should be constant

$$\frac{d}{dt}\langle \hat{H} \rangle = \underbrace{\mathrm{Tr}\left[\dot{\hat{\rho}}\hat{H}\right]}_{\mathcal{J}} + \underbrace{\mathrm{Tr}\left[\hat{\rho}\dot{\hat{H}}\right]}_{\mathcal{W}}, \tag{2.115}$$

where $\mathcal{J}$ and $\mathcal{W}$ are respectively defined as heat and work. With these definitions at hand, finally we define second law, which is about the direction of heat flow, as

$$\frac{dS(\hat{\rho})}{dt} - \sum_{i=1}^{N} \frac{\mathcal{J}_i(t)}{T_i} \geq 0, \tag{2.116}$$

which impose that sum of all the steady state (entropy is maximized, so $\dot{S} = 0$) heat currents to the system should be zero. This form of second law also satisfy the heat current direction, which is always from hot to cold.

## *2.7 non-Markovian Techniques*

We will not make use of non-Markovian techniques in this thesis, but we present a short discussion on the implications of non-Markovianity on the quantum thermal diode. Therefore, very short review together with some key references on non-Markovian master equations is presented here. MME is derived by considering a weak system-environment coupling, and non-Markovian approach is adopted, if the system is not weakly coupled to its environment. An exact solution would be non-Markovian, and there are techniques to carry non-Markovian analysis without exactly solving it. Two extensive reviews on non-Markovian dynamics are Refs. [96, 97], and a very short list of non-Markovian methods is: (i) perturbative approaches, like time-convolutionless (TCL), Nakajima-Zwanzig time-nonlocal ME [98], (ii) a non-perturbative method [99], (iii) method of correlated projection superoperators [100], (iv) dynamics using time-evolving matrix product operators [101], and (v) Quantum-trajectory approach [102]. Among many works on non-Markovian ME's, particularly important ones for quantum thermal diode analysis are Refs. [103, 104] for two interacting qubits and Refs. [105, 106, 107] for a single qubit.

Chapter 3

# APPLICATION AND NUMERICAL IMPLEMENTATION OF MARKOVIAN MASTER EQUATION

In this chapter, MME is analyzed using two different cases of a single two-level system (qubit), as shown in Fig. 3.1, to better understand its structure and to exemplify the numerical implementation method. The first case is a qubit coupled with a single thermal bath, which demonstrates the thermalization process and is shown in Fig. 3.1 (a). Second case is with two thermal baths at different temperatures, as shown in Fig. 3.1 (b), and it is a good example to introduce steady state heat currents.

## *3.1 Two-Level System Thermalization*

In this part, we consider the case depicted in Fig. 3.1 (a). MME for a two level system (qubit) is obtained by mathematical means in Eq. 2.64 with some undetermined coefficients, $\kappa_+, \kappa_-, \kappa_z$. After deriving the MME for a harmonic oscillator Eq. 2.113, we claimed that the coefficients are determined by the interaction picture operators with which the system couples to the environment. Qubit-bosonic field interaction Hamiltonian obtained in rotating wave approximation is called as Jaynes-Cummings model [108] and is given by

$$\hat{H}_{\mathrm{I}} = \hbar g(\hat{\sigma}_+ \otimes \hat{a} + \hat{\sigma}_- \otimes \hat{a}^\dagger), \tag{3.1}$$

where $g$ is the qubit-field coupling strength. By a straight transformation of the coupling operators $\hat{\sigma}_-$ and $\hat{\sigma}_+$ to interaction picture, we would see that the coefficients $\kappa_-$ and $\kappa_+$ should respectively be $\kappa_{\mathrm{L}}(1+\bar{n}_{\mathrm{L}})$ and $\kappa_{\mathrm{L}}\bar{n}_{\mathrm{L}}$, if our claim is true. Here, the constant $\kappa_{\mathrm{L}}$ is determined by the qubit-environment coupling strength $g$. In order to

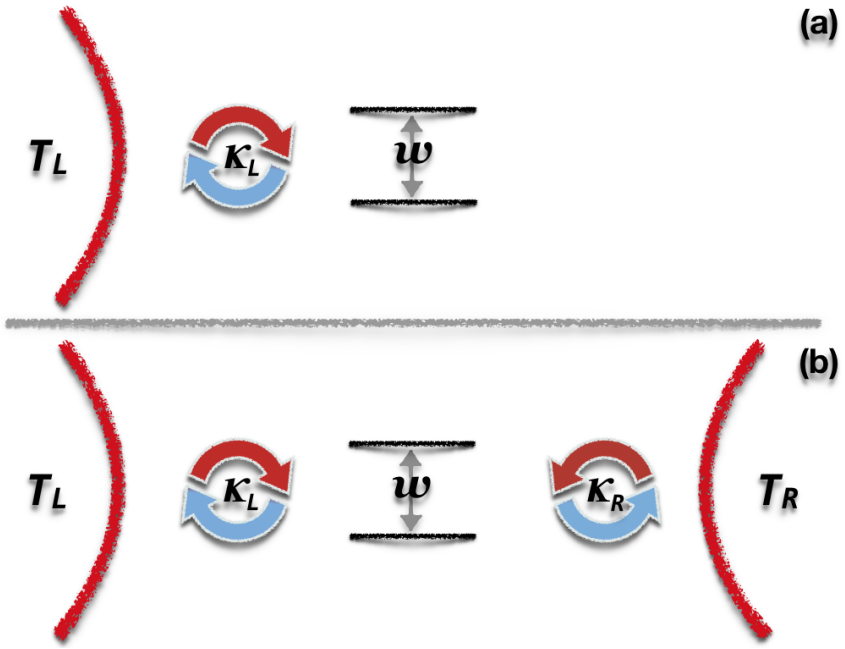


Figure 3.1: **Two Level System (Qubit) Cases.** (a) Qubit with a transition frequency $\omega$ is couple to a thermal bath at temperature $T_{\mathrm{L}}$ with a rate $\kappa_{\mathrm{L}}$. (b) It is also coupled to a second thermal at temperature $T_{\mathrm{R}}$ with a rate $\kappa_{\mathrm{R}}$.

demonstrate that these are indeed the correct coefficients, we use the fact that qubit has to equilibrate with its environment at temperature $T_{\mathrm{L}}$. Before doing that, we first describe the qubit system more detailedly and then show that the term with $\kappa_z$ in Eq. 2.64 is a pure-dephasing term, which is energy conserving.

### *3.1.1 System Description*

In all the below qubit thermalization calculations, we use the matrix representation of density matrix, and we calculate the dynamical evolution of the matrix elements. Since we look for a thermal qubit at the end, it is better to use energy basis for which the eigenenergy probabilities, in this case, diagonal elements, have to satisfy the Gibbs distribution of temperature $T_{\mathrm{L}}$. We start by defining the ground and excited states

of the qubit, respectively, as follows

$$|e\rangle = \begin{pmatrix} 1 \\ 0 \end{pmatrix}, \qquad \text{and} \qquad |g\rangle = \begin{pmatrix} 0 \\ 1 \end{pmatrix},$$

with their respective eigenenergies as $E_e = \frac{1}{2}\hbar\omega$ and $E_g = -\frac{1}{2}\hbar\omega$. Then, creation and annihilation operators are defined as

$$\hat{\sigma}_- \equiv |g\rangle\langle e| = \begin{pmatrix} 0 \\ 1 \end{pmatrix}\begin{pmatrix} 1 & 0 \end{pmatrix} = \begin{pmatrix} 0 & 0 \\ 1 & 0 \end{pmatrix},$$

$$\hat{\sigma}_+ \equiv |e\rangle\langle g| = \begin{pmatrix} 1 \\ 0 \end{pmatrix}\begin{pmatrix} 0 & 1 \end{pmatrix} = \begin{pmatrix} 0 & 1 \\ 0 & 0 \end{pmatrix}.$$

Using these, we write the matrix representations of the other Pauli spin operators in the chosen basis as

$$\hat{\sigma}_z = \hat{\sigma}_+\hat{\sigma}_+ - \hat{\sigma}_-\hat{\sigma}_+ = \begin{pmatrix} 1 & 0 \\ 0 & -1 \end{pmatrix}, \tag{3.2}$$

$$\hat{\sigma}_y = i(\hat{\sigma}_- - \hat{\sigma}_+) = \begin{pmatrix} 0 & -i \\ i & 0 \end{pmatrix}, \tag{3.3}$$

$$\hat{\sigma}_x = \hat{\sigma}_+ + \hat{\sigma}_- = \begin{pmatrix} 0 & 1 \\ 1 & 0 \end{pmatrix}, \tag{3.4}$$

Finally, we write a pure qubit state as the super-position of energy eigenstates as

$$|\Psi\rangle = C_e\,|e\rangle + C_g\,|g\rangle\,,$$

where $C_e$ and $C_g$ are complex numbers such that $|C_e|^2 + |C_g|^2 = 1$. Then, the elements of this density matrix is calculated as follows

$$\hat{\rho}_\Psi = |\Psi\rangle\langle\Psi| = \begin{pmatrix} \rho_{ee} = \langle e|\hat{\rho}|e\rangle = |C_e|^2 & \rho_{eg} = \langle e|\hat{\rho}|g\rangle = C_e C_g^* \\ \\ \rho_{ge} = \langle g|\hat{\rho}|e\rangle = C_g C_e^* & \rho_{gg} = \langle g|\hat{\rho}|g\rangle = |C_g|^2 \end{pmatrix}.$$

As mentioned earlier and is seen from above equation, diagonal elements of the density matrix are the corresponding populations, and off-diagonal elements, called coherences, contain phase information of the state. What an environment cause is

the erasion of this phase information, which is called as de-phasing, and change the pure state to a mixed with populations satisfying the probabilities imposed by the environment temperature (for the thermalization case).

### *3.1.2 Pure Dephasing Term*

Qubit MME Eq. 2.64 contains the term $\kappa_z \hat{\mathcal{D}}[\hat{\sigma}_z]$, which is an energy conserving pure dephasing. This means that it has no effect on populations of the density matrix written in energy basis, and it only erases the coherences. Such terms are easily identified by the commutation of the operator in Lindblad dissipators, $\hat{\sigma}_z$ in this case, and the system Hamiltonian, $\frac{\hbar}{2}\omega\hat{\sigma}_z$ in this case, being zero. In other words, if an operator $\hat{O}$ commutes with the Hamiltonian $\hat{H}$, meaning $\left[\hat{H}, \hat{O}\right] = 0$, then the Lindblad dissipator $\hat{\mathcal{D}}[\hat{O}]$ only dephases the system. Now, we show that this is indeed the case by writing the dissipator explicitly in the matrix form as

$$\begin{aligned}
\hat{\mathcal{D}}[\hat{\sigma}_z] &= \hat{\sigma}_z\hat{\rho}\hat{\sigma}_z - \frac{1}{2}(\overbrace{\hat{\sigma}_z\hat{\sigma}_z}^{\mathbb{1}}\hat{\rho} + \hat{\rho}\overbrace{\hat{\sigma}_z\hat{\sigma}_z}^{\mathbb{1}}) \\
&= \begin{pmatrix} 1 & 0 \\ 0 & -1 \end{pmatrix}\begin{pmatrix} \rho_{ee} & \rho_{eg} \\ \rho_{ge} & \rho_{gg} \end{pmatrix}\begin{pmatrix} 1 & 0 \\ 0 & -1 \end{pmatrix} - \begin{pmatrix} \rho_{ee} & \rho_{eg} \\ \rho_{ge} & \rho_{gg} \end{pmatrix} \\
&= \begin{pmatrix} \rho_{ee} & -\rho_{eg} \\ -\rho_{ge} & \rho_{gg} \end{pmatrix} - \begin{pmatrix} \rho_{ee} & \rho_{eg} \\ \rho_{ge} & \rho_{gg} \end{pmatrix} \\
&= -2\begin{pmatrix} 0 & \rho_{eg} \\ \rho_{ge} & 0 \end{pmatrix}. \qquad (3.5)
\end{aligned}$$

On the left hand side of the MME Eq. 2.64, we have

$$\begin{pmatrix} \dot{\rho}_{ee} & \dot{\rho}_{eg} \\ \dot{\rho}_{ge} & \dot{\rho}_{gg} \end{pmatrix},$$

then we see that the Eq. 3.5 contributes only to the equations of motion for the coherences, and it is given as

$$\dot{\rho}_{eg} = f(\hat{\rho}) - 2\kappa_z\rho_{eg},$$
$$\dot{\rho}_{ge} = g(\hat{\rho}) - 2\kappa_z\rho_{ge},$$

where $f(\hat{\rho})$ and $g(\hat{\rho})$ represent the terms due to other parts of the right hand side of MME, which are examined in the subsequent section. Here, it is obvious that the term $\hat{\mathcal{D}}[\hat{\sigma}_z]$ brings a damping term into the coherence equation of motions.

### *3.1.3 Population Dynamics*

Here, effects of the remaining terms in MME are shown by calculating each individual parts of the terms in their matrix form. An example of such calculation for the first term in $\hat{\mathcal{D}}[\hat{\sigma}_-]$ is as follows

$$\hat{\sigma}_-\hat{\rho}\hat{\sigma}_+ = \begin{pmatrix} 0 & 0 \\ 1 & 0 \end{pmatrix} \begin{pmatrix} \rho_{ee} & \rho_{eg} \\ \rho_{ge} & \rho_{gg} \end{pmatrix} \begin{pmatrix} 0 & 1 \\ 0 & 0 \end{pmatrix} = \begin{pmatrix} 0 & 0 \\ 0 & \rho_{ee} \end{pmatrix}.$$

After calculating all such parts of the terms and combining them all, effects of the terms are obtained as

$$-i\left[\hat{H}_{\mathrm{TLS}}, \hat{\rho}\right] = -i\omega \begin{pmatrix} 0 & -\rho_{eg} \\ \rho_{ge} & 0 \end{pmatrix}, \tag{3.6}$$

$$\kappa_-\hat{\mathcal{D}}[\hat{\sigma}_-] = \kappa_-(2\hat{\sigma}_-\hat{\rho}\hat{\sigma}_+ - \hat{\sigma}_+\hat{\sigma}_-\hat{\rho} - \hat{\rho}\hat{\sigma}_+\hat{\sigma}_-) = \kappa_- \begin{pmatrix} -2\rho_{ee} & -\rho_{eg} \\ -\rho_{ge} & 2\rho_{ee} \end{pmatrix}, \tag{3.7}$$

$$\kappa_+\hat{\mathcal{D}}[\hat{\sigma}_+] = \kappa_+(2\hat{\sigma}_+\hat{\rho}\hat{\sigma}_- - \hat{\sigma}_-\hat{\sigma}_+\hat{\rho} - \hat{\rho}\hat{\sigma}_-\hat{\sigma}_+) = \kappa_+ \begin{pmatrix} 2\rho_{gg} & -\rho_{eg} \\ -\rho_{ge} & -2\rho_{gg} \end{pmatrix}, \tag{3.8}$$

where, also in the rest of the thesis, we take $\hbar = k_B = 1$. One remark here is that all the right hand side terms Eq. 3.5 - 3.8 have zero trace, and the populations are uncoupled from the coherences. Therefore, each term, so does their sum, is trace preserving, which means sum of the diagonal terms remains the same. It is obviously seen and also well-known that the unitary part Eq. 3.6 brings an oscillatory behavior to the coherences. The other two terms Eqns 3.7 and 3.8, on the other hand, gives population equations of motion as

$$\dot{\rho}_{ee} = -2\kappa_-\rho_{ee} + 2\kappa_+\rho_{gg}, \tag{3.9}$$

$$\dot{\rho}_{gg} = 2\kappa_-\rho_{ee} - 2\kappa_+\rho_{gg}. \tag{3.10}$$

Since the dynamical mapping is completely positive and trace preserving, probabilities are conserved, meaning $\rho_{gg} + \rho_{ee} = 1$. This can be used to easily uncouple and solve the differential equations in Eq. 3.9 and 3.10. However, we are interested in their steady state solutions, which are obtained again using the condition $\rho_{gg} + \rho_{ee} = 1$ with $\dot{\rho}_{ee} = \dot{\rho}_{gg} = 0$ and are given as

$$\rho_{ee}^{\text{ss}} = \frac{\kappa_+}{\kappa_+ + \kappa_-},$$
$$\rho_{gg}^{\text{ss}} = \frac{\kappa_-}{\kappa_+ + \kappa_-}.$$

Imposing that the qubit have to thermalize at the temperature $T_{\text{L}}$, we write their ratio, which have to satisfy Gibbs distribution, as

$$\frac{\rho_{ee}^{\text{ss}}}{\rho_{gg}^{\text{ss}}} = \frac{\kappa_+}{\kappa_-} = e^{(E_g - E_e)/T_{\text{L}}} = e^{-\omega/T_{\text{L}}},$$

which is also know as detailed balance. Again with the use of $\rho_{gg} + \rho_{ee} = 1$, we easily find that $\rho_{ee}^{\text{ss}} = c\bar{n}_{\text{L}}$ and $\rho_{ee}^{\text{ss}} = c(1 + \bar{n}_{\text{L}})$, where c is a constant required for normalization. Then, using these we find the rates as $\kappa_+ = \kappa_{\text{L}}\bar{n}_{\text{L}}$ and $\kappa_+ = \kappa_{\text{L}}(1 + \bar{n}_{\text{L}})$, which agrees with our claim, and we drop the subscript L after this point. So far, we show that the unitary part and the last term of Eq. 2.64 are energy conserving terms and have no effect on population dynamics, and the other terms of right hand side of Eq. 2.64 determine the population dynamics. Therefore, we write MME by ignoring the energy conserving terms and keeping the other terms with their determined coefficients as

$$\dot{\hat{\rho}} = \kappa(1+\bar{n})\hat{\mathcal{D}}[\hat{\sigma}_-] + \kappa\bar{n}\hat{\mathcal{D}}[\hat{\sigma}_+] = \begin{pmatrix} -\kappa(1+\bar{n})\rho_{ee} + \kappa\bar{n}\rho_{gg} & -\frac{1}{2}\kappa(1+2\bar{n})\rho_{eg} \\ -\frac{1}{2}\kappa(1+2\bar{n})\rho_{ge} & -\kappa(1+\bar{n})\rho_{ee} + \kappa\bar{n}\rho_{gg} \end{pmatrix}. \tag{3.11}$$

Now, we further investigate these terms, and their effects are best understood by considering them individually. For example, if the only right hand side term of MME was $\kappa(1 + \bar{n})\hat{\mathcal{D}}[\hat{\sigma}_-]$ term, it would read as

$$\begin{pmatrix} \dot{\rho}_{ee} & \dot{\rho}_{eg} \\ \dot{\rho}_{ge} & \dot{\rho}_{gg} \end{pmatrix} = \frac{\kappa}{2}(\bar{n}+1) \begin{pmatrix} -2\rho_{ee} & -\rho_{eg} \\ -2\rho_{ge} & 2\rho_{ee} \end{pmatrix}.$$

It is quite obvious here that the excited stated population is decreasing while the ground state is getting populated with the same rate. Also, it is obvious that the coherences die, since their rate is proportional to the negative of them. In short, this term de-excites and de-phases the system. Similar approach to $\kappa(\bar{n})\hat{\mathcal{D}}[\hat{\sigma}_+]$ term is used to understand its effects. Starting with the assumption that only right hand side term was $\kappa(\bar{n})\hat{\mathcal{D}}[\hat{\sigma}_+]$, master equation would read

$$\begin{pmatrix} \dot{\rho}_{ee} & \dot{\rho}_{eg} \\ \dot{\rho}_{ge} & \dot{\rho}_{gg} \end{pmatrix} = \frac{\kappa}{2}\bar{n} \begin{pmatrix} 2\rho_{gg} & -\rho_{eg} \\ -2\rho_{ge} & -2\rho_g \end{pmatrix}.$$

We here see that this term does exact opposite of the $\kappa(1+\bar{n})\hat{\mathcal{D}}[\hat{\sigma}_-]$ term to the populations, which means it populates excited states. However, the coherences again dies away. In short, this term excites and de-phases the system.

To sum up, $\hat{\mathcal{D}}[\hat{\sigma}_-]$ and $\hat{\mathcal{D}}[\hat{\sigma}_+]$ respectively de-excites and excites the system, while both of them erase the coherences. Their coefficients $(1+\bar{n})$ and $\bar{n}$ determines a balance between the de-excitation and excitation processes, which is also known as detailed balance. Combined effect of all the terms on coherences is that they die away (gets damped) with an oscillatory behavior (under damping).

### *3.1.4 Solving the Equations of Motion*

In the previous part, we obtained equations of motion for each density matrix element, and we can easily solve the equations of motion by straightforward decoupling. Even though the process to obtain equations of motions and solving them is straightforward algebra, it is a rather long one even for such a small system, whose matrix is just two-by-two. Therefore, other approaches, either numerical or analytical, are required for bigger systems, especially for the ones, like a harmonic oscillator, with an infinite number of density matrix elements.

One of the analytical approaches is to obtain the equations of motion for the expectation values of the relevant observables, which is discussed and demonstrated in the next section. For a system of coupled first order ordinary differential equations, we already introduce a method in the Sec. 2.2.2, and we show in above analysis that

density matrix elements make up such a system. Only difference here is that, instead of the variable vector $\boldsymbol{X}$ and coefficient matrix $\boldsymbol{M}$, we here respectively have the density matrix $\hat{\rho}$ and the Liouville super-operator (Liouvillian) $\hat{\mathcal{L}}$.

The Liouvillian $\hat{\mathcal{L}}$ and the density matrix $\hat{\rho}$ become respectively a matrix and vector in the Liouville (super)space [85, 86] corresponding to the system Hilbert space $\hat{\mathbb{H}}$. This transformation is known as vectorization (vecing or flattening) of the density matrix [109, 110, 111, 112], and its derivation starts by projecting the master equation into the basis used to write the density matrix, which is energy basis in our case. The detailed calculations and explanations about the vecing are given the Refs. [109, 110, 111, 112].

We here describe the vectorization method by considering an $n$-dimensional Hilbert space $\mathbb{H}$ and apply it to the two level system example. In the method, we first flatten the $n \times n$ density matrix $\hat{\rho}$ to an $n^2$ vector $\vec{\rho}$ by moving columns of the $\hat{\rho}$ below each other as

$$\hat{\rho} = \begin{pmatrix} \rho_{11} & \cdots & \rho_{1n} \\ \vdots & \ddots & \vdots \\ \rho_{k1} & \cdots & \rho_{kn} \\ \vdots & \ddots & \vdots \\ \rho_{n1} & \cdots & \rho_{nn} \end{pmatrix} \implies \vec{\rho} = \begin{bmatrix} \rho_{11} \\ \vdots \\ \rho_{1n} \\ \vdots \\ \rho_{k1} \\ \vdots \\ \rho_{kn} \\ \vdots \\ \rho_{n1} \\ \vdots \\ \rho_{nn} \end{bmatrix}. \tag{3.12}$$

In the general form of MME Eq. 2.62, there are three types of the (super)operations constructed from an operator $\hat{O}$ together with its Hermitian conjugate $\hat{O}^\dagger$ acting onto the density matrix $\hat{\rho}$: $\hat{O}$ and $\hat{O}^\dagger$ acts together on $\hat{\rho}$ from (i) left or (ii) right, or (iii) one

acts from right, the other from left. Such type of super-operators are shown below, and they are transformed into Liouville space operators acting on vector $\vec{\rho}$ as

$$\hat{O}\hat{\rho}\hat{O}^\dagger \implies ((\hat{O}^\dagger)^{\mathrm{T}} \otimes \hat{O})\vec{\rho}, \tag{3.13}$$

$$\hat{O}^\dagger\hat{O}\hat{\rho} \implies (\mathbb{1} \otimes (\hat{O}^\dagger\hat{O}))\vec{\rho}, \tag{3.14}$$

$$\hat{\rho}\hat{O}^\dagger\hat{O} \implies ((\hat{O}^\dagger\hat{O}) \otimes \mathbb{1})\vec{\rho}, \tag{3.15}$$

where superscript T means matrix transpose, and $\otimes$ is just the direct product. Then, we write MME in the Liouville space as

$$\frac{d}{dt}\vec{\rho} = \boldsymbol{L}\vec{\rho}, \tag{3.16}$$

where $\boldsymbol{L}$ is an $n^2 \times n^2$ matrix given as

$$\boldsymbol{L} = -i(\mathbb{1}\otimes\hat{H} - \hat{H}^\dagger\otimes\mathbb{1}) + \sum_{i=1}^{n^2-1} \kappa_i \left( \hat{F}_i^\dagger \otimes \hat{F}_i - \frac{1}{2}(\mathbb{1} \otimes \hat{F}_i^\dagger\hat{F}_i + (\hat{F}_i^\dagger\hat{F}_i)^{\mathrm{T}} \otimes \mathbb{1}) \right). \tag{3.17}$$

In Sec. 2.2.2, we show the general solution for this type of differential equations to be the exponentiation of $\boldsymbol{L}$ as

$$\vec{\rho} = e^{\boldsymbol{L}t}\vec{C}, \tag{3.18}$$

where $\vec{C}$ is included constants of integration determined by the initial conditions. After this point, numerical implementation is quite possible and easy. We either make an matrix exponentiation, which is easily done a power series expansion, or diagonalize $\boldsymbol{L}$, which corresponds to uncoupling of the equations.

Diagonalization can be carried by finding eigenvalues of the matrix. This approach has another use in MME. $\boldsymbol{L}$ is a trace preserving map, which makes its rows (or columns) linearly dependent and ensures $\det(\boldsymbol{L}) = 0$. Therefore, there exists at least one zero eigenvalue, and its eigenvector determines the steady state. In other words, we are now able to obtain steady state solution by obtaining the zero eigenvalue and its eigenvector.

Now, let us apply this technique to qubit example of this section. The matrix $\boldsymbol{L}$

of the qubit MME (without the dephasing term) reads

$$\begin{aligned}\boldsymbol{L} &= -i(\mathbb{1}\otimes\hat{H}_{\rm TLS}-\hat{H}_{\rm TLS}^{\dagger}\otimes\mathbb{1})+\kappa(1+\bar{n})(\hat{F}_i^{\dagger}\otimes\hat{F}_i-\frac{1}{2}(\mathbb{1}\otimes\hat{F}_i^{\dagger}\hat{F}_i+(\hat{F}_i^{\dagger}\hat{F}_i)^{\rm T}\otimes\mathbb{1}))\\ &= \begin{bmatrix}-\kappa(1+\bar{n}) & 0 & 0 & \kappa\bar{n}\\ 0 & i\omega-\frac{\kappa}{2}(1+\bar{n}) & 0 & 0\\ 0 & 0 & -i\omega-\frac{\kappa}{2}(1+2\bar{n}) & 0\\ \kappa(1+\bar{n}) & 0 & 0 & -\kappa\bar{n}\end{bmatrix}. \qquad (3.19)\end{aligned}$$

The eigenvalues with corresponding eigenvectors of $\boldsymbol{L}$ are respectively calculates as

$$\{0,-\kappa(1+2\bar{n}),i\omega-\tfrac{\kappa}{2}(1+2\bar{n}),-i\omega-\tfrac{\kappa}{2}(1+2\bar{n})\} \quad , \qquad (3.20)$$

$$\{\begin{bmatrix}\frac{\bar{n}}{1+\bar{n}}\\0\\0\\1\end{bmatrix},\begin{bmatrix}-1\\0\\0\\1\end{bmatrix},\begin{bmatrix}0\\1\\0\\0\end{bmatrix},\begin{bmatrix}0\\0\\1\\0\end{bmatrix}\} \quad . \qquad (3.21)$$

Then solution of the Eq. 3.16 is written in the form given in Eq. 2.11 as

$$\vec{\rho}(t)=\begin{bmatrix}\rho_{ee}\\\rho_{ge}\\\rho_{eg}\\\rho_{gg}\end{bmatrix}=c_1e^{0*t}\begin{bmatrix}\frac{\bar{n}}{1+\bar{n}}\\0\\0\\1\end{bmatrix}+c_2e^{-\kappa(1+2\bar{n})t}\begin{bmatrix}-1\\0\\0\\1\end{bmatrix}+c_3e^{(i\omega-\frac{\kappa}{2}(1+2\bar{n}))t}\begin{bmatrix}0\\1\\0\\0\end{bmatrix}+c_4e^{(-i\omega-\frac{\kappa}{2}(1+2\bar{n}))t}\begin{bmatrix}0\\0\\1\\0\end{bmatrix},$$

which obviously show that coefficients of all the other eigenvectors converges to zero as $t\to\infty$, and steady state is determined by the zero eigenvector. Only remaining calculation is to find $c_1$, which is easily be calculated from steady state solution by imposing the probability conservation $\rho_{ee}+\rho_{gg}=1$ as

$$\vec{\rho}(t) = \begin{bmatrix}\rho_{ee}\\\rho_{ge}\\\rho_{eg}\\\rho_{gg}\end{bmatrix}=\begin{bmatrix}\frac{c_1\bar{n}}{1+\bar{n}}-c_2e^{-\kappa(1+2\bar{n})t}\\c_3e^{i\omega-\frac{\kappa}{2}(1+2\bar{n})t}\\c_4e^{-i\omega-\frac{\kappa}{2}(1+2\bar{n})t}\\c_1+c_2e^{-\kappa(1+2\bar{n})t}\end{bmatrix}\implies\vec{\rho}_{\rm ss}=\begin{bmatrix}\rho_{ee}\\\rho_{ge}\\\rho_{eg}\\\rho_{gg}\end{bmatrix}=\begin{bmatrix}\frac{c_1\bar{n}}{1+\bar{n}}\\0\\0\\c_1\end{bmatrix}, \qquad (3.22)$$

$$\rho_{ee} + \rho_{gg}=\frac{c_1\bar{n}}{1+\bar{n}}+c_1=1\implies c_1=\frac{1+\bar{n}}{1+2\bar{n}}, \qquad (3.23)$$

which expectedly gives the detailed balance of the populations as $\rho_{ee} = \frac{\bar{n}}{1+2\bar{n}}$ and $\rho_{gg} = \frac{1+\bar{n}}{1+2\bar{n}}$. Also, density vector at any time $t$ is easily obtained from above by imposing the initial conditions, and its transformation to density matrix is quite straightforward. These techniques are implemented in a Python library called Qutip [113]. Qutip offers several ways to use these techniques and handles numerical error details, both of which are out of the scope of this thesis. Qutip is extensively used in this thesis, so it is reassuring to present some results calculated by the master equation solver of Qutip for qubit system and compare them with analytical solutions.

*Numerical vs Analytical Results*

We consider three different bath qubit configurations. In order to explain these cases, we first introduce an effective temperature definition by means of spin polarization, which is defined as the expectation value of $\hat{\sigma}_z$ operator, $\langle\hat{\sigma}_z\rangle = \rho_{ee} - \rho_{gg}$. In thermal equilibrium, populations satisfy the Gibbs ratio $\frac{\rho_{ee}}{\rho_{gg}} = e^{-\omega/T}$, then we define an effective (for non-equilibrium cases) temperature from the populations as

$$T = \frac{-\omega}{\ln \frac{\rho_{ee}}{\rho_{gg}}} = \frac{-\omega}{\ln \frac{1+\langle\hat{\sigma}_z\rangle}{1-\langle\hat{\sigma}_z\rangle}} \tag{3.24}$$

With this equation, we convert any polarization value to corresponding temperature and then to average excitation number. In below explanations, we indicate temperatures with the corresponding polarization values. In the calculations, we fix the bath temperature to $\langle\hat{\sigma}_z\rangle = -0.5$, and create three initial pure qubit states with $\langle\hat{\sigma}_z\rangle = -0.2$, $\langle\hat{\sigma}_z\rangle = -0.8$,$\langle\hat{\sigma}_z\rangle = -0.5$, which are respectively colder (green), hotter (red), and at equal temperature (blue) compared to bath. Other parameters are $\omega = 1$ and $\kappa = 0.2$

Fig. 3.2 shows the population evolution over time. In all there cases, populations converges to the Gibbs distribution imposed by the bath temperature,$\langle\hat{\sigma}_z\rangle \to -0.5$. In the analytical calculations, we see that the coherences die away, Fig. 3.3 and Fig. 3.4 show respectively that both imaginary and real parts of the coherences converge to zero. In all the plots, numerical results perfectly agrees the analytical calculations.

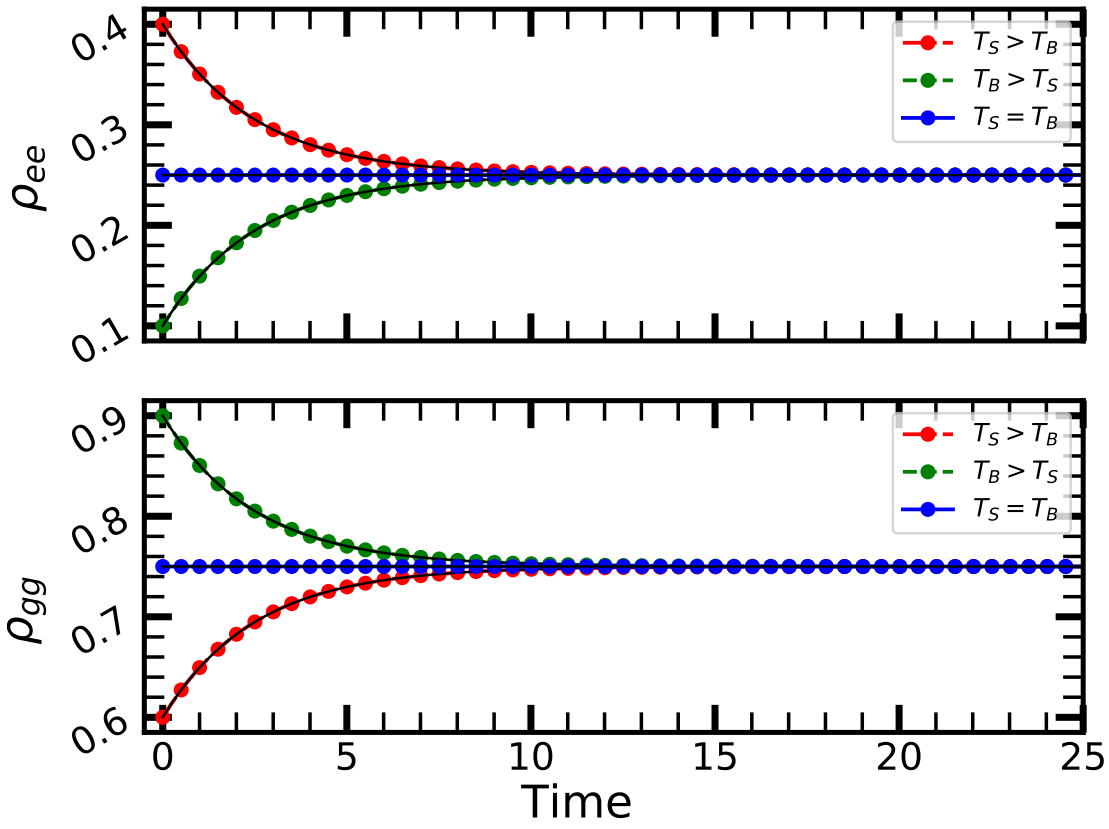


Figure 3.2: **Qubit Thermalization.** Populations converges to the Gibbs distribution of the bath temperature. Three different cases are as shown in the legends. Colored dots show analytical result, black solid lines are numerical.

### *3.1.5 Heat Current*

Now, we make use of the heat current definition Eq. 2.115 to show that the thermodynamical laws are satisfied. Heat current for the qubit is calculated by using the matrix form of its MME Eq. 3.11 as

$$\begin{aligned}\mathcal{J} &= \mathrm{Tr}\left[\dot{\hat{\rho}}\hat{H}\right] = \mathrm{Tr}\left[\begin{pmatrix} -\kappa(1+\bar{n})\rho_{ee} + \kappa\bar{n}\rho_{gg} & -\frac{1}{2}\kappa(1+2\bar{n})\rho_{eg} \\ -\frac{1}{2}\kappa(1+2\bar{n})\rho_{ge} & -\kappa(1+\bar{n})\rho_{ee} + \kappa\bar{n}\rho_{gg}\end{pmatrix}\begin{pmatrix}\frac{\omega}{2} & 0 \\ 0 & -\frac{\omega}{2}\end{pmatrix}\right] \\ &= \kappa(\bar{n}\rho_{gg} - (1+\bar{n})\rho_{ee}). \end{aligned} \tag{3.25}$$

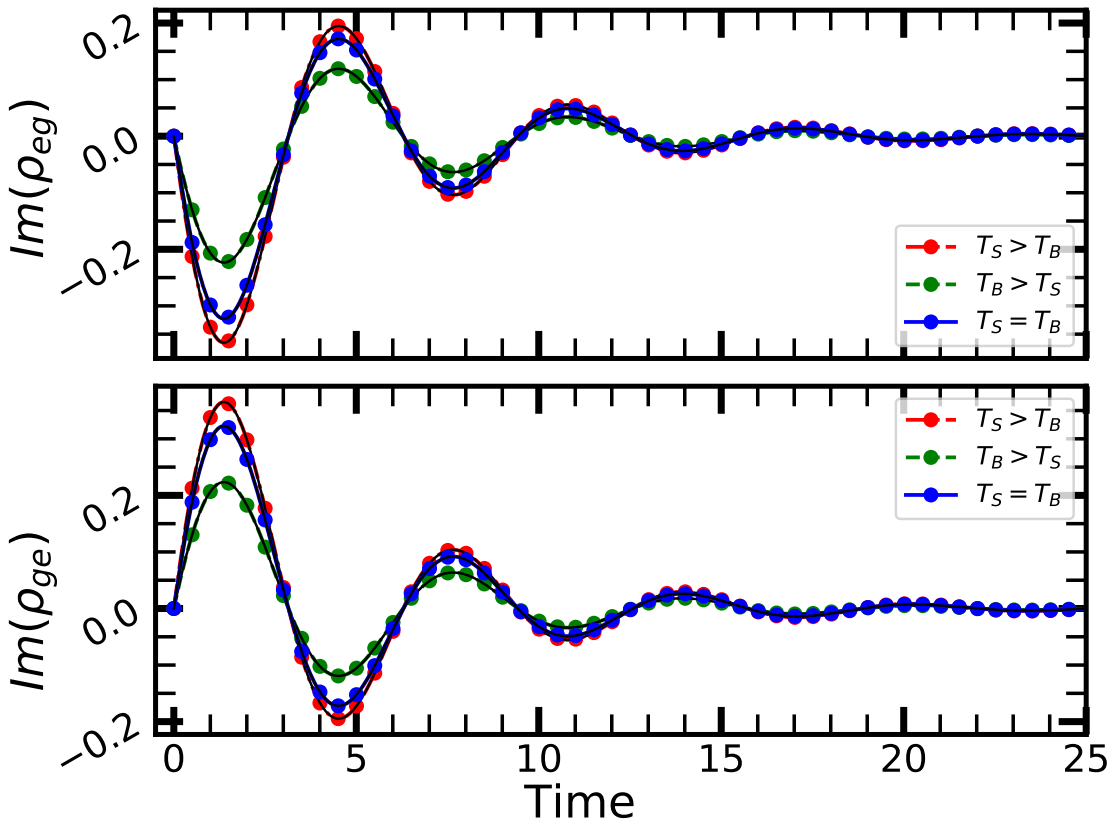


Figure 3.3: **Qubit Thermalization.** Coherences dies away in every case, and this plot shows the imaginary part. Three different cases are as shown in the legends. Colored dots show analytical result, black solid lines are numerical.

In the steady state, which is the thermal equilibrium by the zeroth law, there has to be zero heat current by first laws of thermodynamics. By substituting the detailed balance result of the populations into Eq. 3.25, we find $\mathcal{J}_{\rm ss} = 0$.

We also check the second law by the heat current directions. If $T_{\rm S} \geq T_{\rm B}$, then $\rho_{ee} \geq \frac{\bar{n}}{1+2\bar{n}}$. Therefore, let $\rho_{ee} = \frac{\bar{n}}{1+2\bar{n}} + \delta$ with some non-negative number $\delta \geq 0$, which of course should not violate probability requirements, then $\rho_{gg} = \frac{1+\bar{n}}{1+2\bar{n}} - \delta$. Substituting these into Eq. 3.25, we get $\mathcal{J} = -\kappa\delta(1+2\bar{n})$, which is a negative number. This means that heat flows out of the system. With the similar line of arguments, it is easy to show when $T_{\rm S} \leq T_{\rm B}$, $\mathcal{J}$ becomes positive, which means heat flows into the

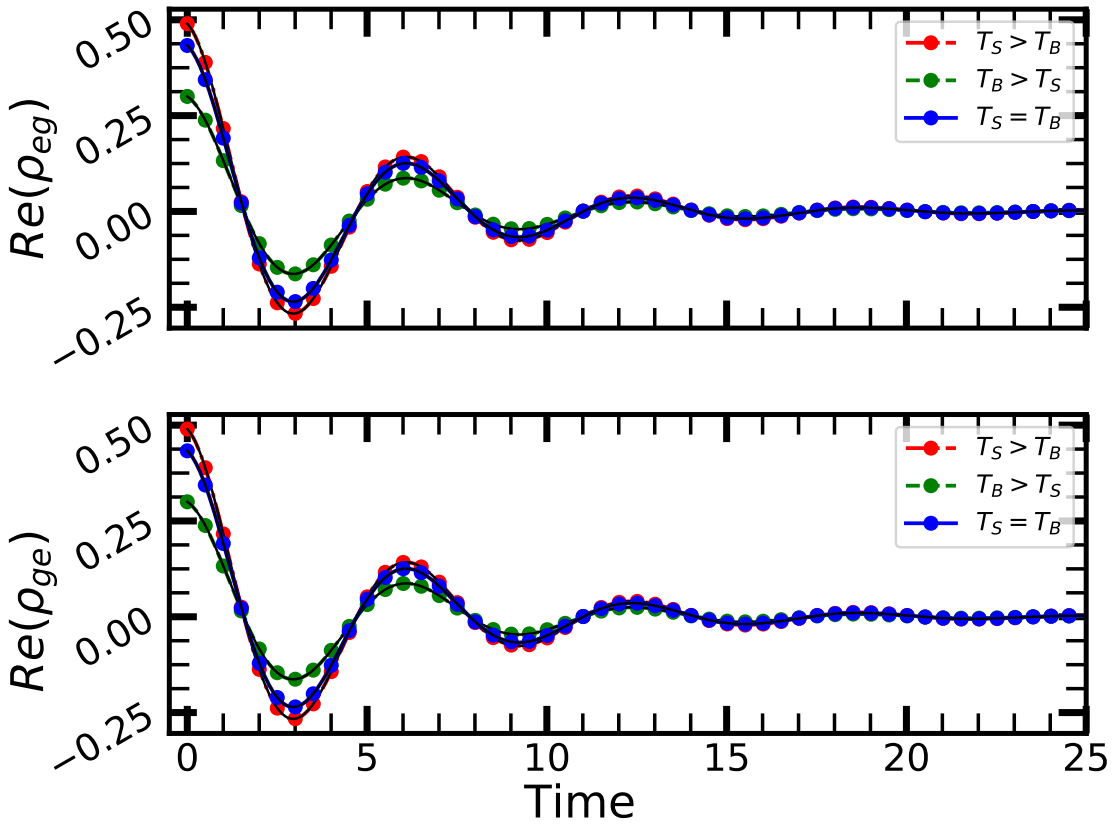


Figure 3.4: **Qubit Thermalization.** Coherences dies away in every case, and this plot shows the real part. Three different cases are as shown in the legends. Colored dots show analytical result, black solid lines are numerical.

system. These situations are shown in Fig. 3.5 for the three cases considered in the previous part.

Also, $\hat{\mathcal{D}}[\hat{\sigma}_-]$ and $\hat{\mathcal{D}}[\hat{\sigma}_+]$ terms of the MME, which shown to respectively de-exites and excites the system, can be analyzed with the heat current by them as

$$\mathcal{J}_- = \mathrm{Tr}\left[(1+\bar{n})\hat{\mathcal{D}}[\hat{\sigma}_-]\hat{H}\right] = -\kappa(1+\bar{n})\rho_{ee} \leq 0 \tag{3.26}$$

$$\mathcal{J}_+ = \mathrm{Tr}\left[\bar{n}\hat{\mathcal{D}}[\hat{\sigma}_+]\hat{H}\right] = \kappa\bar{n}\rho_{gg} \geq 0. \tag{3.27}$$

This mean that $\hat{\mathcal{D}}[\hat{\sigma}_-]$ and $\hat{\mathcal{D}}[\hat{\sigma}_+]$ terms respectively drains and pumps heat into the system, as expected. With a similar calculation, heat current for the unitary part and

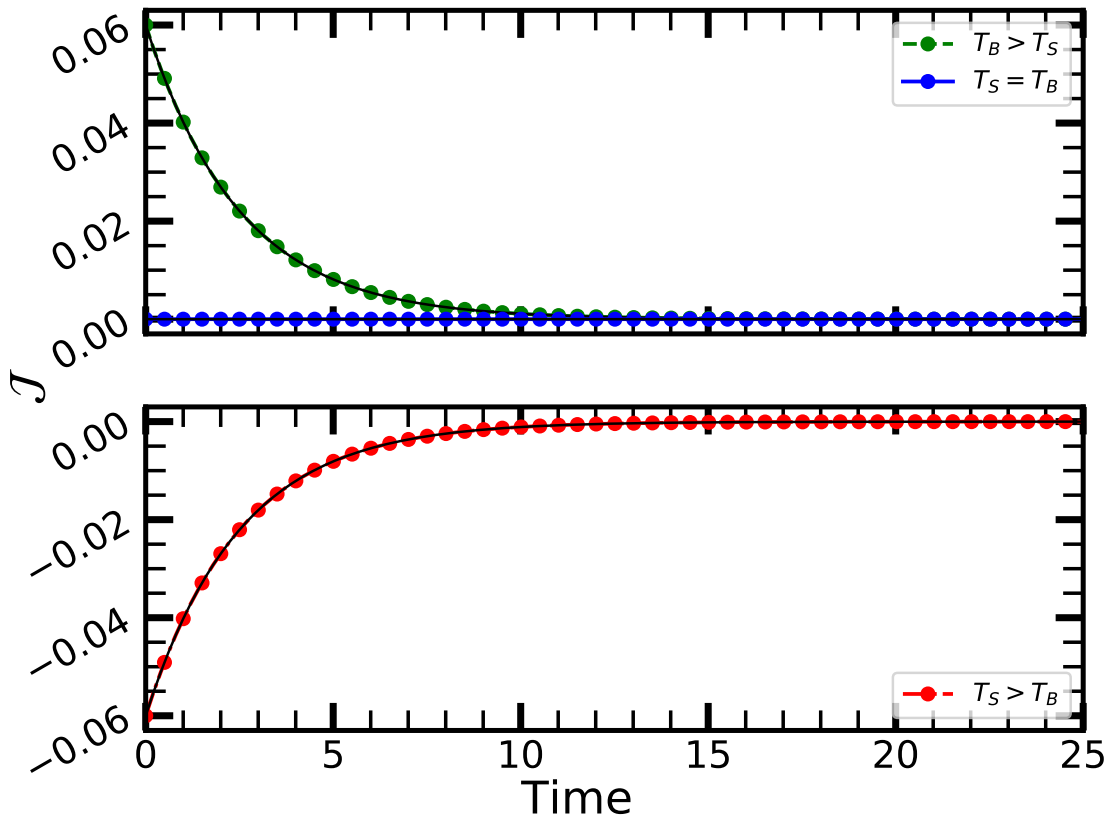


Figure 3.5: **Qubit Thermalization.** Heat flows from hot to cold. Three different cases are as shown in the legends. Colored dots show analytical result, black solid lines are numerical.

the pure-dephasing term, which are shown to be energy conserving, are shown to be zero.

### *3.2 Non-Equilibrium Two-Level System*

Two-level system (qubit) coupled to two thermal baths, shown in Fig. 3.1, does not reach to thermal equilibrium, unless of course $T_{\mathrm{R}} = T_{\mathrm{L}}$. Yet, it reaches to a steady state, and total steady state heat current into the system is zero, which means that it gets heat from the hot bath and dumps the same amount into the cold bath as required by the first and second laws of thermodynamics. First law requires the conservation of

energy, which is satisfied by total zero current, and the second law enforces that heat flows from hot to cold. In this section, we show that the dynamics under MME satisfies the second law, and we introduce another approach to calculate the heat current together with the expectation values of the system observables without explicitly calculating the density matrix elements. First, we present the MME and solve it with the differential equation approach of the previous section.

### *3.2.1 Master Equation*

In this scenario, MME in its closed form reads as

$$\dot{\hat{\rho}} = -i\left[\hat{H}, \hat{\rho}\right] + \hat{\mathcal{L}}_{\mathrm{L}}\hat{\rho} + \hat{\mathcal{L}}_{\mathrm{R}}\hat{\rho} \equiv \hat{\mathcal{L}}\hat{\rho}. \tag{3.28}$$

The second and third terms on the right hand side of the master equation are super-operators describing the effects of left (L) and right (R) baths, respectively. They are given in terms of Lindblad dissipators as

$$\hat{\mathcal{L}}_{\mathrm{B}} = \kappa_{\mathrm{B}}(1+\bar{n}_{\mathrm{B}})\left[\hat{\mathcal{D}}[\hat{\sigma}_{-}] \ + e^{-\beta_{\mathrm{B}}\omega}\hat{\mathcal{D}}[\hat{\sigma}_{+}]\right], \tag{3.29}$$

where B = L, R stand for the baths, and $\beta_{\mathrm{B}} = 1/T_B$ is the inverse temperature for bath B. Using the energy basis and the matrix approach of the previous section, equations of motion for the density matrix elements are written as

$$\dot{\hat{\rho}} = \begin{pmatrix} -(A+B)\rho_{ee} + (Ae^{-\beta_{\mathrm{L}}\omega} + Be^{-\beta_{\mathrm{R}}\omega})\rho_{gg} & -(\frac{A}{2}(1+e^{-\beta_{\mathrm{L}}\omega}) + \frac{B}{2}(1+e^{-\beta_{\mathrm{R}}\omega}) + i\omega)\rho_{eg} \\ -(\frac{A}{2}(1+e^{-\beta_{\mathrm{L}}\omega}) + \frac{B}{2}(1+e^{-\beta_{\mathrm{R}}\omega}) - i\omega)\rho_{ge} & (A+B)\rho_{ee} - (Ae^{-\beta_{\mathrm{L}}\omega} + Be^{-\beta_{\mathrm{R}}\omega})\rho_{gg} \end{pmatrix},$$

where the constants are defined as $A = \kappa_{\mathrm{L}}(1+\bar{n}_{\mathrm{L}})$ and $B = \kappa_{\mathrm{R}}(1+\bar{n}_{\mathrm{R}})$. Using the techniques introduced in the previous section, dynamics of the each element can be obtained. It is obvious that coherences again dies away, and the uncoupled equations of motion for the populations are given as

$$\begin{aligned} \dot{\rho}_{ee} &= \ - \ (A(1+e^{-\beta_{\mathrm{L}}\omega}) + B(1+e^{-\beta_{\mathrm{R}}\omega}))\rho_{ee} + Ae^{-\beta_{\mathrm{L}}\omega} + Be^{-\beta_{\mathrm{R}}\omega} \\ \dot{\rho}_{gg} &= \ - \ (A(1+e^{-\beta_{\mathrm{L}}\omega}) + B(1+e^{-\beta_{\mathrm{R}}\omega}))\rho_{gg} + A + B. \end{aligned} \tag{3.30}$$

Both of these equations are in the form: $af(t) + b = \dot{f}$, which has a solution of the form $f(t) = ce^{at} - \frac{a}{b}$. The constant $a$ is the same for both, and it is a negative number. Therefore, their steady state solution converges to the constant part $-\frac{a}{b}$. Then, we directly write steady state solution for the populations as

$$\rho_{ee}^{\mathrm{ss}} = \frac{Ae^{-\beta_{\mathrm{C}}\omega} + Be^{-\beta_{\mathrm{H}}\omega}}{A(1+e^{-\beta_C\omega}) + B(1+e^{-\beta_H\omega})}, \tag{3.31}$$

$$\rho_{gg}^{\mathrm{ss}} = \frac{A+B}{A(1+e^{-\beta_{\mathrm{C}}\omega}) + B(1+e^{-\beta_{\mathrm{H}}\omega})}. \tag{3.32}$$

Since $e^{-\beta_{\mathrm{B}}\omega} < 1$ for positive temperatures, $\rho_{gg}^{\mathrm{ss}} > \rho_{ee}^{\mathrm{ss}}$, which means that there occurs no population inversion, unless one of the temperature is negative. Also, it is easy to see that $\rho_{ee}^{\mathrm{ss}} + \rho_{gg}^{\mathrm{ss}} = 1$.

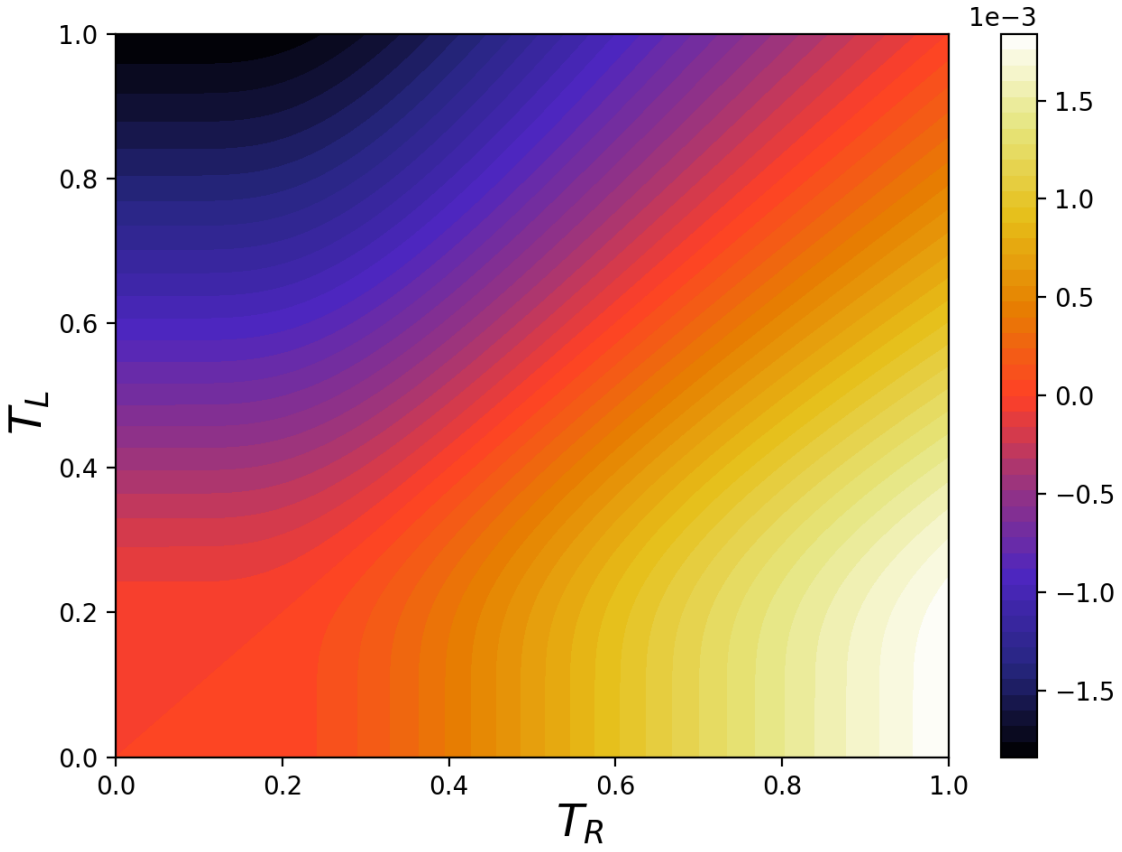


Figure 3.6: **Steady State Heat Current.** When $T_{\mathrm{R}} > T_{\mathrm{L}}$, $\mathcal{J}_{\mathrm{R}}^{\mathrm{ss}}$ is positive.

In order to check the consistency with first and second laws of thermodynamics,

we calculate the total heat current from both baths to the system as

$$\mathcal{J}_{\text{Total}} = \text{Tr}\left[((\hat{\mathcal{L}}_{\text{L}} + \hat{\mathcal{L}}_{\text{R}})\hat{\rho})\hat{H}\right] = \text{Tr}\left[\hat{\mathcal{L}}_{\text{L}}\hat{\rho}\hat{H}\right] + \text{Tr}\left[\hat{\mathcal{L}}_{\text{L}}\hat{\rho}\hat{H}\right] = \mathcal{J}_{\text{L}} + \mathcal{J}_{\text{R}}. \tag{3.33}$$

Then, substituting the steady state solutions of populations Eq. 3.31 and 3.32 in, we find the heat currents in the steady state as

$$\mathcal{J}_{\text{L}}^{\text{ss}} = \text{Tr}\left[\hat{\mathcal{L}}_{\text{L}}\hat{\rho}\hat{H}\right] = \omega A(e^{-\beta_{\text{L}}\omega}\rho_{gg} - \rho_{ee}) = \frac{\omega\kappa_{\text{L}}\kappa_{\text{R}}(\bar{n}_{\text{L}} - \bar{n}_{\text{R}})}{\kappa_{\text{R}}(1+2\bar{n}_{\text{R}}) + \kappa_{\text{L}}(1+2\bar{n}_{\text{L}})}, \tag{3.34}$$

$$\mathcal{J}_{\text{R}}^{\text{ss}} = \text{Tr}\left[\hat{\mathcal{L}}_{\text{R}}\hat{\rho}\hat{H}\right] = \omega B(\rho_{gg} - e^{-\beta_{\text{R}}\omega}\rho_{ee}) = \frac{\omega\kappa_{\text{L}}\kappa_{\text{R}}(\bar{n}_{\text{R}} - \bar{n}_{\text{L}})}{\kappa_{\text{R}}(1+2\bar{n}_{\text{R}}) + \kappa_{\text{L}}(1+2\bar{n}_{\text{L}})} \tag{3.35}$$

Sum of these two terms gives thermodynamically consistent total steady state heat current, that is $\mathcal{J}_{\text{Total}} = \mathcal{J}_{\text{L}}^{\text{ss}} + \mathcal{J}_{\text{R}}^{\text{ss}} = 0$ as required by the first law. Also, heat current direction enforced by the second law is from hot to cold bath, which is shown in Fig 3.6 by plotting $\mathcal{J}_{\text{R}}^{\text{ss}}$. Parameters of the Fig 3.6 are $\omega = 100\kappa_{\text{L}} = 100\kappa_{\text{R}} = 1$

Heat flow into system is positive by our convention, and Fig 3.6 shows that $\mathcal{J}_{\text{R}}^{\text{ss}}$ is positive when right bath is the hotter than left bath $T_{\text{R}} > T_{\text{L}}$. Since we show above that the total steady state heat current is zero, this means that heat flows into the system from the hotter bath (right one), and the same amount leaks into the cold one (left bath). When the temperature configuration is changed $T_{\text{R}} < T_{\text{L}}$, heat current becomes negative, which shows the consistency with second law. One other observation, which is detailedly discussed in the diode chapter 5, is that this heat current can be non-reciprocal.

### *3.2.2 Observable Dynamics*

One other approach of MME is to use it in Heisenberg picture to calculate expectation values of observables. They can be used to calculate heat currents, which is demonstrated below. This approach is especially useful in the infinite density matrix cases, like harmonic oscillators. Matrix approach is still useful and can be called as the last resort, if the observable dynamic approach is not possible [111], which requires a closed set of coupled differential equations of observable expectations.

MME in Heisenberg picture reads for an observable operator $\hat{O}$ (its expectation value to be precise) as [110, 111, 112]

$$\dot{\hat{O}} = \hat{\mathcal{L}}^{\dagger}\hat{O} = i\left[\hat{H}, \hat{O}\right] + \sum_{i,j=1}^{n^2-1} \kappa_{ij}\left(\hat{F}_i^{\dagger}\hat{O}\hat{F}_j - \frac{1}{2}\{\hat{F}_j^{\dagger}\hat{F}_i, \hat{O}\}\right). \tag{3.36}$$

We equivalently write the equation of motion for the expectation value of an observable $\hat{O}$ as

$$\frac{d}{dt}\langle\hat{O}\rangle = \frac{d}{dt}\,\mathrm{Tr}\left[\hat{\rho}\hat{O}\right]. \tag{3.37}$$

Now, we apply these techniques to obtain the heat current expression for the non-equilibrium qubit without explicitly calculating its density matrix. We start by writing the heat current due to one of the baths B as

$$\mathcal{J}_{\mathrm{B}} = \kappa_{\mathrm{B}}(1+\bar{n}_{\mathrm{B}})\,\mathrm{Tr}\left[\hat{\mathcal{D}}[\hat{\sigma}_-]\hat{H}\right] + \kappa_{\mathrm{B}}\bar{n}_{\mathrm{B}}\,\mathrm{Tr}\left[\hat{\mathcal{D}}[\hat{\sigma}_+]\hat{H}\right]. \tag{3.38}$$

An example calculation for the elements in this expression is given as

$$\begin{aligned}
\mathrm{Tr}\left[\hat{\mathcal{D}}[\hat{\sigma}_-]\hat{H}\right] &= \frac{\omega}{2}\,\mathrm{Tr}\left[(\hat{\sigma}_-\hat{\rho}\hat{\sigma}_+ - \frac{1}{2}\hat{\sigma}_+\hat{\sigma}_-\hat{\rho} - \frac{1}{2}\hat{\rho}\hat{\sigma}_+\hat{\sigma}_-)\hat{\sigma}_z\right] \\
&= \frac{\omega}{2}\,\mathrm{Tr}\left[\hat{\rho}(\hat{\sigma}_+\hat{\sigma}_z\hat{\sigma}_- - \frac{1}{2}\hat{\sigma}_+\hat{\sigma}_-\hat{\sigma}_z - \frac{1}{2}\hat{\sigma}_z\hat{\sigma}_+\hat{\sigma}_-)\right] \\
&= \frac{\omega}{2}\,\mathrm{Tr}\left[\hat{\rho}(\hat{\sigma}_+(\hat{\sigma}_+\hat{\sigma}_- - \hat{\sigma}_-\hat{\sigma}_+)\hat{\sigma}_- - \frac{1}{2}\hat{\sigma}_+\hat{\sigma}_-\hat{\sigma}_z - \frac{1}{2}\hat{\sigma}_z\hat{\sigma}_+\hat{\sigma}_-)\right] \\
&= \frac{\omega}{2}\,\mathrm{Tr}\left[\hat{\rho}(-\hat{\sigma}_+\hat{\sigma}_-\hat{\sigma}_+\hat{\sigma}_- - \frac{1}{2}\hat{\sigma}_+\hat{\sigma}_-\hat{\sigma}_+\hat{\sigma}_- - \frac{1}{2}\hat{\sigma}_+\hat{\sigma}_-\hat{\sigma}_+\hat{\sigma}_-)\right] \\
&= \frac{\omega}{2}\,\mathrm{Tr}\left[\hat{\rho}(-2\hat{\sigma}_+\hat{\sigma}_-\hat{\sigma}_+\hat{\sigma}_-)\right] = \frac{\omega}{2}\,\mathrm{Tr}\left[\hat{\rho}(-2\hat{\sigma}_+\hat{\sigma}_-)\right] = -\frac{\omega}{2}\,\mathrm{Tr}\left[\hat{\rho}(\hat{\sigma}_z + \mathbb{1})\right] \\
&= -\frac{\omega}{2}(\langle\hat{\sigma}_z\rangle + 1),
\end{aligned} \tag{3.39}$$

where we used the definitions and commutation relations of Pauli operators together with the cyclic property of trace. With very similar lines of calculations, other terms are calculated to give the total heat current expression for bath B as

$$\mathcal{J}_{\mathrm{B}} = -\frac{\omega}{2}\kappa_{\mathrm{B}}(1+2\bar{n}_{\mathrm{B}})\,\langle\hat{\sigma}_z\rangle - \frac{\omega}{2}\kappa_{\mathrm{B}}. \tag{3.40}$$

Then, all we need to calculate is $\langle\hat{\sigma}_z\rangle$ to find the heat current, so we calculate it using the approach in Eq.3.37 as

$$\begin{aligned}\frac{d}{dt}\langle\hat{\sigma}_z\rangle = \mathrm{Tr}\left[\dot{\hat{\rho}}\hat{\sigma}_z\right] &= \kappa_{\mathrm{L}}(1+\bar{n}_{\mathrm{L}})\,\mathrm{Tr}\left[\hat{\mathcal{D}}[\hat{\sigma}_-]\hat{\sigma}_z\right] + \kappa_{\mathrm{L}}\bar{n}_{\mathrm{L}}\,\mathrm{Tr}\left[\hat{\mathcal{D}}[\hat{\sigma}_+]\hat{\sigma}_z\right] \\ &\quad +\kappa_{\mathrm{R}}(1+\bar{n}_{\mathrm{R}})\,\mathrm{Tr}\left[\hat{\mathcal{D}}[\hat{\sigma}_-]\hat{\sigma}_z\right] + \kappa_{\mathrm{R}}\bar{n}_{\mathrm{R}}\,\mathrm{Tr}\left[\hat{\mathcal{D}}[\hat{\sigma}_+]\hat{\sigma}_z\right].\end{aligned}$$

Terms of this equation misses only the $\frac{\omega}{2}$ factor of the Hamiltonian. Therefore, by the same approach of Eq. 3.39, we write the equation of motion for $\hat{\sigma}_z$ as

$$\frac{d}{dt}\langle\hat{\sigma}_z\rangle = -\kappa_{\mathrm{R}}(1+2\bar{n}_{\mathrm{R}})\langle\hat{\sigma}_z\rangle - \kappa_{\mathrm{R}} - \kappa_{\mathrm{L}}(1+2\bar{n}_{\mathrm{L}})\langle\hat{\sigma}_z\rangle - \kappa_{\mathrm{L}}, \tag{3.41}$$

which has the solution given as

$$\langle\hat{\sigma}_z\rangle = Ce^{-(\kappa_{\mathrm{R}}(1+2\bar{n}_{\mathrm{R}})+\kappa_{\mathrm{L}}(1+2\bar{n}_{\mathrm{L}}))t} - \frac{\kappa_{\mathrm{L}}+\kappa_{\mathrm{R}}}{\kappa_{\mathrm{R}}(1+2\bar{n}_{\mathrm{R}})+\kappa_{\mathrm{L}}(1+2\bar{n}_{\mathrm{L}})}, \tag{3.42}$$

where C is the integration constant to be determined by the initial conditions. Steady state solution of this equation is the constant term at the end. Then, by substituting it into the Eq.3.40, we obtain the steady state heat currents as

$$\mathcal{J}_{\mathrm{L}}^{\mathrm{ss}} = = \frac{\omega\kappa_{\mathrm{L}}\kappa_{\mathrm{R}}(\bar{n}_{\mathrm{L}}-\bar{n}_{\mathrm{R}})}{\kappa_{\mathrm{R}}(1+2\bar{n}_{\mathrm{R}})+\kappa_{\mathrm{L}}(1+2\bar{n}_{\mathrm{L}})}, \tag{3.43}$$

$$\mathcal{J}_{\mathrm{R}}^{\mathrm{ss}} = = \frac{\omega\kappa_{\mathrm{L}}\kappa_{\mathrm{R}}(\bar{n}_{\mathrm{R}}-\bar{n}_{\mathrm{L}})}{\kappa_{\mathrm{R}}(1+2\bar{n}_{\mathrm{R}})+\kappa_{\mathrm{L}}(1+2\bar{n}_{\mathrm{L}})}, \tag{3.44}$$

which are the same as in Eq. 3.34. This method proves to be useful in the way that it does not require for us to explicitly calculate the density matrix. However, it requires a closed set of equations, which is obtained for other models in the subsequent chapters, and it may not always be possible.

Chapter 4

# LOCAL VS GLOBAL MARKOVIAN MASTER EQUATIONS

In this chapter, we present two different approaches of MME adopted for the multipartite quantum systems, namely local and global approaches [89, 114, 115, 116, 117]. In the previous chapter, we consider a single quantum system coupled to thermal baths and analyze its thermodynamical consistencies. Now, we turn our attention to composite systems and show that local approach may give thermodynamically inconsistent results [115, 116]. Then, we derive the global MME, which corrects the inconsistencies.

## *4.1 Local Approach*

Local (or phenomenological) MME relies on a weak coupling among the subsystems, and it is obtained by summing the individual MME of subsystems due to their local baths and including the interaction Hamiltonian of subsystems to unitary dynamics part. In this section, we exemplify this approach by writing the local MME for two and three interacting qubits systems shown in Fig. 4.1. Then, we show a parameter independent failure of the local approach, which also does not follow the Fourier law of thermal conduction.

### *4.1.1 Three Interacting Qubits*

We consider a system of three interacting qubits, with transition frequencies $\omega_{\mathrm{L}}$ and $\omega_{\mathrm{R}}$, as shown in Fig. 4.1 (a), described by a Hamiltonian with an opto-mechanical

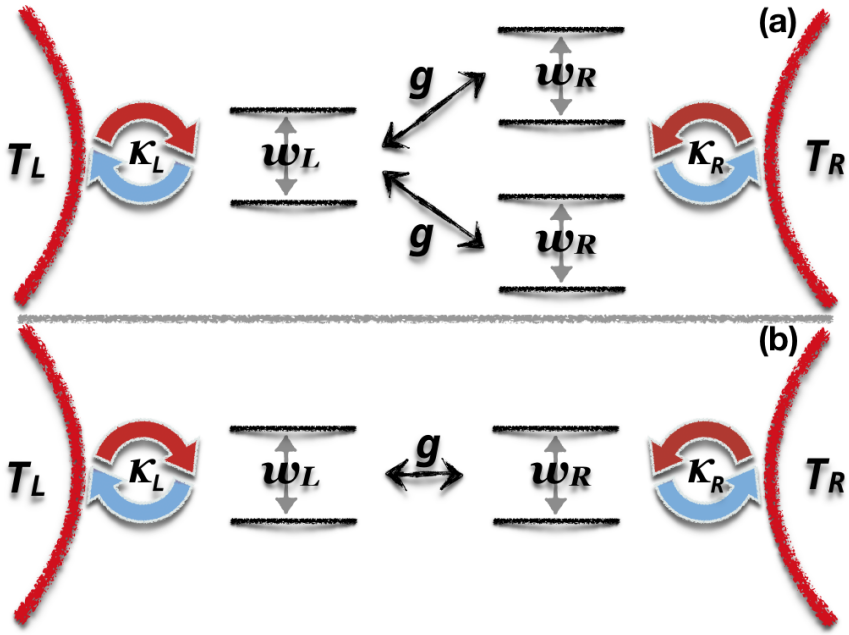


Figure 4.1: **Three and Two Interacting Qubits.** Left (L) and right (R) qubits are coupled to their local baths at temperature $T_{\rm L}$ and $T_{\rm R}$ with the rates $\kappa_{\rm L}$ and $\kappa_{\rm R}$, and right qubit interacts with left qubit/s with a coupling strength $g$.

like coupling of strength $g$ between the left (L) and two right (R) qubits,

$$\hat{H} = \frac{\omega_{\rm L}}{2}\hat{\sigma}_1^z + \frac{\omega_{\rm R}}{2}(\hat{\sigma}_2^z + \hat{\sigma}_3^z) - g\hat{\sigma}_1^z(\hat{\sigma}_2^x + \hat{\sigma}_3^x). \tag{4.1}$$

We take $\hbar = 1$ and $k_B = 1$. Also, $\hat{\sigma}_i^j$ reads as the Pauli j = x,y,z matrix of the $i^{th}$ qubit, and the tensor products, $\hat{\sigma}_1^j \otimes \mathbb{1} \otimes \mathbb{1}$, $\mathbb{1} \otimes \hat{\sigma}_2^j \otimes \mathbb{1}$,and $\mathbb{1} \otimes \mathbb{1} \otimes \hat{\sigma}_1^j$ are implicit above and rest of the thesis.

Left qubit is coupled to the left bath with the coupling constant $\kappa_{\rm L}$. The right qubits are connected to the right bath with the coupling constant $\kappa_{\rm R}$. Local GKLS Master equation [80, 81, 89, 114] then reads as

$$\begin{aligned}\dot{\hat{\rho}} = \hat{\mathcal{L}}\hat{\rho} \;\; = \;\; & -i[\hat{H}, \hat{\rho}] \\ & +\kappa_{\rm L}(1 + \bar{n}_{\rm L}(\omega_{\rm L}))\hat{\mathcal{D}}[\hat{\sigma}_1^-] + \kappa_{\rm L}(\bar{n}_{\rm L}(\omega_{\rm L}))\hat{\mathcal{D}}[\hat{\sigma}_1^+] \\ & +\kappa_{\rm R}(1 + \bar{n}_{\rm R}(\omega_{\rm R}))\hat{\mathcal{D}}[\hat{\sigma}_1^-] + \kappa_{\rm R}(\bar{n}_{\rm R}(\omega_{\rm R}))\hat{\mathcal{D}}[\hat{\sigma}_1^+] \\ & +\kappa_{\rm R}(1 + \bar{n}_{\rm R}(\omega_{\rm R}))\hat{\mathcal{D}}[\hat{\sigma}_1^-] + \kappa_{\rm R}(\bar{n}_{\rm R}(\omega_{\rm R}))\hat{\mathcal{D}}[\hat{\sigma}_1^+]\end{aligned} \tag{4.2}$$

The first term on the right hand side of Eq. 4.2 is unitary evolution of the system, and the local effects of the bath on their corresponding qubits are included to unitary dynamics by simply adding them. The Lindblad dissipator [80, 81] is given by

$$\hat{\mathcal{D}}[\hat{A}] = \hat{A}\hat{\rho}\hat{A}^{\dagger} - \frac{1}{2}\left(\hat{A}^{\dagger}\hat{A}\hat{\rho} + \hat{\rho}\hat{A}^{\dagger}\hat{A}\right). \tag{4.3}$$

As discussed in Ref. [118], for the subsystem whose free Hamiltonian commutes with the total Hamiltonian, steady state is invariant. In our model, left qubit satisfies this condition, and its invariant state is a thermal equilibrium state at temperature $T_{\mathrm{L}}$. Therefore, we can check the validity of numerical results by the steady state of left qubit.

We carry the further calculations of the model by considering the right bath at zero temperature, i.e. $\bar{n} = 0$, and we vary the left bath temperature. In this case, the master equation becomes

$$\dot{\hat{\rho}} = -i[\hat{H}, \hat{\rho}] + \kappa_{\mathrm{L}}(1 + \bar{n}_{\mathrm{L}}(\omega_{\mathrm{L}}))\hat{\mathcal{D}}[\hat{\sigma}_1^-] + \kappa_{\mathrm{L}}(\bar{n}_{\mathrm{L}}(\omega_{\mathrm{L}}))\hat{\mathcal{D}}[\hat{\sigma}_1^+] + \kappa_{\mathrm{R}}\hat{\mathcal{D}}[\hat{\sigma}_1^-] + \kappa_{\mathrm{R}}\hat{\mathcal{D}}[\hat{\sigma}_1^-]$$

We present the results obtained by the numerical solutions of the MME in Fig. 4.2. In the numerical calculations, we use a scaling with $\omega_{\mathrm{L}} = 1$. Then, we vary the inter-site coupling strength $g$ from 0.005 to 0.05, and we fix $\omega_{\mathrm{R}} = 0.05$. Environment couplings are $\kappa_{\mathrm{L}} = \kappa_{\mathrm{R}} = 0.01$. In our calculations, variation of the left temperature is carried as a function of spin polarization $\langle\hat{\sigma}_z\rangle$ approach presented in the Sec. 3.1.4.

Analytical heat current expressions are obtained in the Appendix 7.1 by using the operator expectation value method. A closed set of equations describing the dynamics governed by this MME and the steady state relations among them are also presented in the Appendix 7.1. This set of equations is easily solvable to obtain an expression for the heat current, which completely agrees with the numerical results. Analytic expressions for the heat currents are given as

$$\mathcal{J}_{\mathrm{L}}^{\mathrm{ss}} = \kappa_{\mathrm{L}}(1 + 2\bar{n}_{\mathrm{L}}(\omega_{\mathrm{L}}))g\,\langle\hat{\sigma}_1^z, \hat{S}^x\rangle_{\mathrm{ss}}\,, \tag{4.4}$$

$$\mathcal{J}_{\mathrm{R}}^{\mathrm{ss}} = -\kappa_{\mathrm{L}}(1 + 2\bar{n}_{\mathrm{L}}(\omega_{\mathrm{L}}))g\,\langle\hat{\sigma}_1^z, \hat{S}^x\rangle_{\mathrm{ss}}\,, \tag{4.5}$$

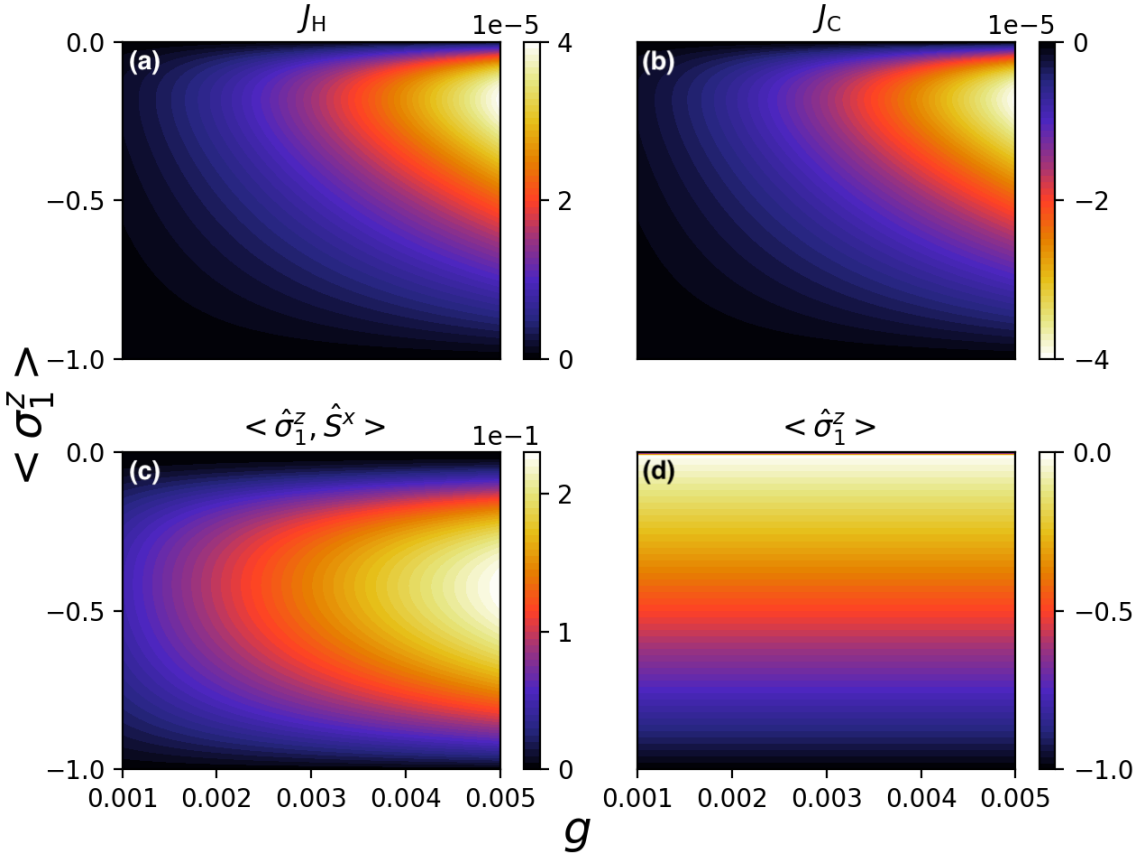


Figure 4.2: **Three Interacting Qubits.** Steady state heat currents from (a) hot and (b) cold baths sum to zero. Heat current maximizes at an optimized temperature as the (c) correlations, and (d) first qubit always thermalizes with its local bath.

where the sum of heat currents correctly gives zero, and the correlation is defined as

$$\langle \hat{\sigma}_1^z, \hat{S}^x \rangle \equiv \langle \hat{\sigma}_1^z \hat{S}^x \rangle - \langle \hat{\sigma}_1^z \rangle \langle \hat{S}^x \rangle \,. \tag{4.6}$$

Numerical calculations of the heat currents Eq. 4.4 - 4.5 are respectively shown in Fig. 4.2 (a) and (b) together with the correlation Eq. 4.6 in Fig. 4.2 (c). In our parameters, right bath is always colder (C) than the left bath (H), so steady state heat current from right($\mathcal{J}_C$)/left($\mathcal{J}_H$) bath to system have to be negative/positive. Fig. 4.2 (a) and (b) show that this is indeed the case, and their sum is zero. Also, Fig. 4.2 (d) shows that the left qubit always thermalizes to the temperature of its

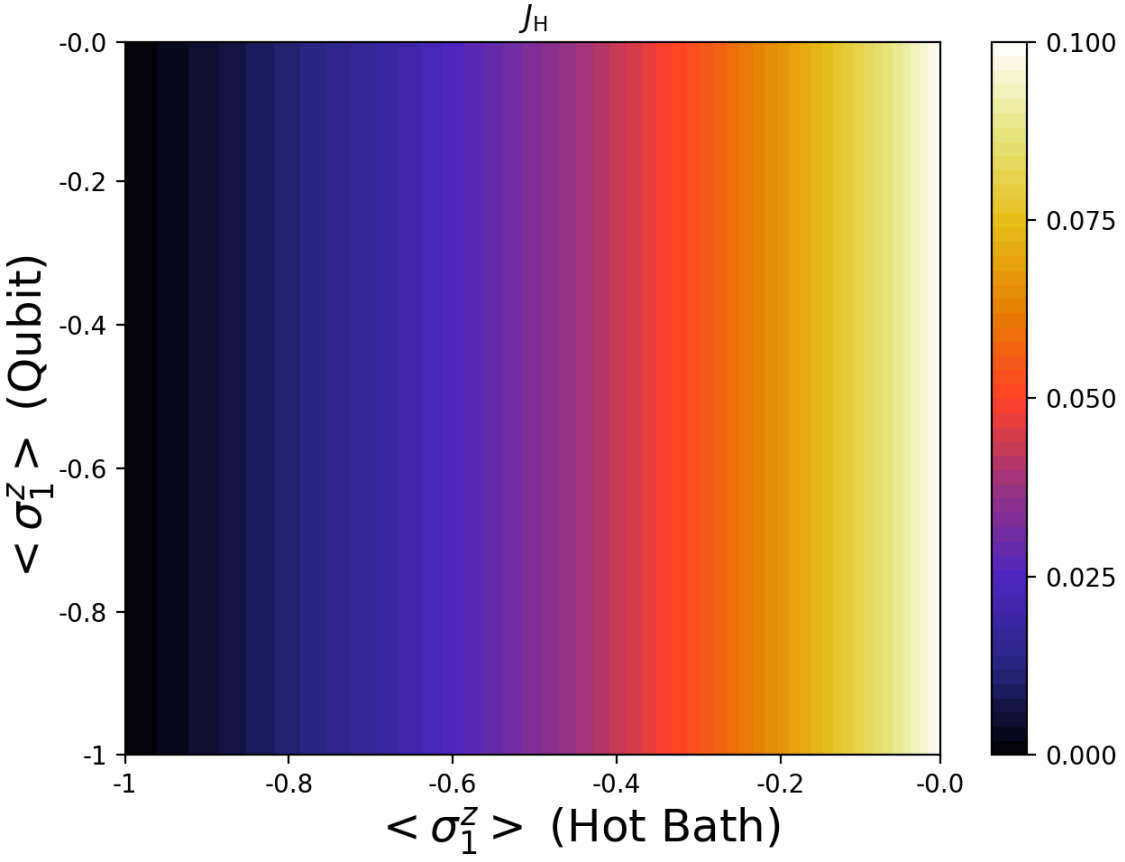


Figure 4.3: **Fourier Law of Thermal Conduction.** Steady state heat current through a single qubit increases as the temperature bias $T_{\text{Hot}} - T_{\text{Cold}}$ is increased.

local bath, so the numerics gives the expected results. Therefore, everything seems thermodynamically consistent expect that the heat currents do not follow Fourier's law of thermal conduction. However, as we explain below, local MME for this model actually completely fails.

Heat currents in Fig. 4.2 (a) and (b) does not always increases as temperature bias increases, but the bias has an optimum value. Steady state heat current of the non-equilibrium qubit, obtained in the previous chapter, obeys the Fourier's law, as shown in Fig. 4.3. Independent of the qubits initial state (y-axis), steady state heat current increases as the bias between hot and cold (at 0K) is increases (x-axis). In single qubit case, we use the same parameters $\omega = 1$, $\kappa_{\text{L}} = \kappa_{\text{R}} = 0.2$, and $T_{\text{Cold}} = 0\text{K}$.

However, this is not a strong violation compared to first or second law, which is also violated by the local MME of three interacting qubits case. In Fig. 4.2, right bath is at zero temperature and colder than left. If we make the right bath hotter of the two and use MME in Eq. 4.2, heat current direction does not change, independent of $g$ or any other parameter. We do present it graphically here, and we show this violation by only numerical means for two interacting qubits, which is the model for quantum thermal diode, in the next part.

### *4.1.2 Two Interacting Qubits*

We consider the two interacting quibts model shown in Fig. 4.1 (b) with two different interaction Hamiltonians between the qubits, dipole-dipole and opto-mechanical like coupling. The Hamiltonians for these two cases are given as

$$\hat{H}_1 = \frac{\omega_{\rm L}}{2}\hat{\sigma}_1^z + \frac{\omega_{\rm R}}{2}\hat{\sigma}_2^z + g(\hat{\sigma}_1^z\hat{\sigma}_2^x), \tag{4.7}$$

$$\hat{H}_2 = \frac{\omega_{\rm L}}{2}\hat{\sigma}_1^z + \frac{\omega_{\rm R}}{2}\hat{\sigma}_2^z + g(\hat{\sigma}_1^+\hat{\sigma}_2^- + \hat{\sigma}_1^-\hat{\sigma}_2^+), \tag{4.8}$$

and the master equations read as

$$\dot{\hat{\rho}} = -i\left[\hat{H}_i, \hat{\rho}\right] + \hat{\mathcal{L}}_{\rm L}\hat{\rho} + \hat{\mathcal{L}}_{\rm R}\hat{\rho}, \tag{4.9}$$

with

$$\hat{\mathcal{L}}_{\rm L}\hat{\rho} = \kappa_{\rm L}(1+\bar{n}_{\rm L})\left[\hat{\mathcal{D}}[\hat{\sigma}_1^-] + e^{-\beta_{\rm L}\omega}\hat{\mathcal{D}}[\hat{\sigma}_1^+]\right], \tag{4.10}$$

and

$$\hat{\mathcal{L}}_{\rm R}\hat{\rho} = \kappa_{\rm R}(1+\bar{n}_{\rm R})\left[\hat{\mathcal{D}}[\hat{\sigma}_2^-] + e^{-\beta_{\rm R}\omega}\hat{\mathcal{D}}[\hat{\sigma}_2^+]\right], \tag{4.11}$$

where $\hat{\sigma}_1^i = \hat{\sigma}^i \otimes \hat{\mathbb{I}}$ and $\hat{\sigma}_2^i = \hat{\mathbb{I}} \otimes \hat{\sigma}^i$ are the Pauli operators for the first and second qubit, respectively.

Numerical results for the heat currents of the two cases are presented in Fig. 4.4 with correlations $\langle\sigma_1^z, \sigma_2^x\rangle$ and $\langle\sigma_1^z, \sigma_2^z\rangle$, relevant to the interaction Hamiltonians. Our parameters for the calculation are $\omega_{\rm L} = \omega_{\rm R} = 1$ and $\kappa_{\rm H} = \kappa_{\rm C} = 0.1$. We see that heat current, unlike the single qubit case, again has an optimal temperature in every case.

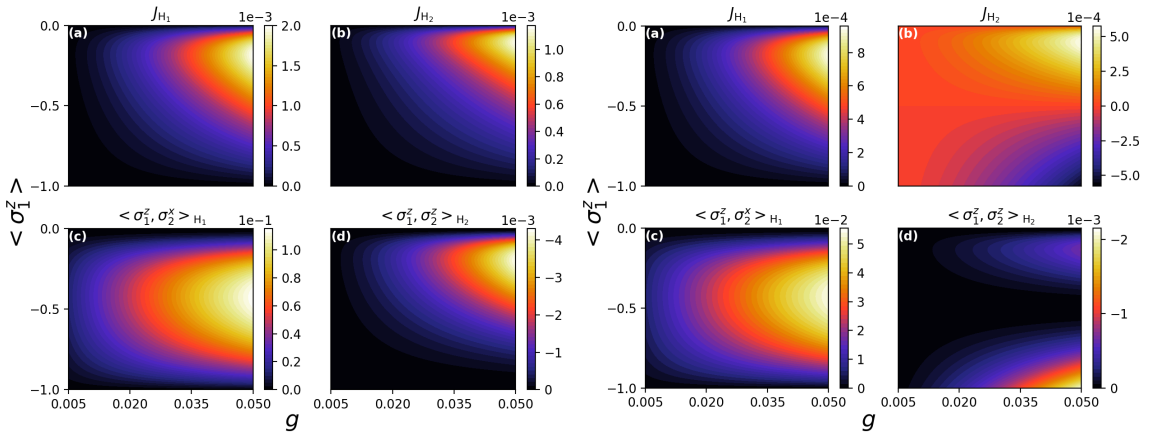


a: $\langle \hat{\sigma}_z \rangle_{T_R} = -1$ b: $\langle \hat{\sigma}_z \rangle_{T_R} = -0.5$

Figure 4.4: **Local MME Comparison.** a: When, left bath is always hotter than the right bath, which is at temperature $\langle \hat{\sigma}_z \rangle_{T_R} = -1$ (0 K), everything, deceivingly, seem consistent. b: When right bath has a finite temperature, that is $\langle \hat{\sigma}_z \rangle_{T_R} = -0.5$, heat current direction of (b) dipole-dipole coupling is always from hot to cold, which is violated in the (a) opto-mechanical like coupling case.

In the first case, shown in Fig. 4.4a, temperature of the right bath is fixed to $\langle \hat{\sigma}_z \rangle = -1$, and temperature of the left bath is varied. As in the three interacting qubits case of the previous part, everything seems consistent for both opto-mechanical like and dipole-dipole coupling of the qubits, respectively shown in Fig. 4.4a (a) and (b). However, in this case, right bath is always colder than left, and if we make the temperature of right bath $\langle \hat{\sigma}_z \rangle = -0.5$, we expect a change in the heat current sign (direction) before and after left bath reaches the temperature $\langle \hat{\sigma}_z \rangle = -0.5$.

As seen from Fig. 4.4b (b), local MME of the dipole-dipole coupling give a negative steady state heat from left bath to system for the case $T_L \leq -0.5$, which is zero at equal temperature point, and it becomes positive for the range $T_L > -0.5$. We do not present here but the sum of currents give zero. Therefore, it is consistent with thermodynamical laws. On the other hand, as seen from Fig. 4.4b (a), local MME of the opto-mechanical like coupling do not change, only the magnitude of heat current

changes but the direction is from left to right. In the next section, we derive global MME for the two qubits with opto-mechanical like interaction and show that it fixes the inconsistencies.

### *4.2 Global Approach*

In the previous section, we show that, independently of coupling strength $g$ between the qubits, local MME approach to the opto-mechanically like interacting qubits violate the second law of thermodynamics. Local MME for dipole-dipole coupling of the qubits, on the other hand, does not violate the second law, yet it is limited to the weakly interacting qubits. Global MME for dipole-dipole or $\hat{\sigma}_z\hat{\sigma}_z$ interaction between two qubits are derived and used in many works [119, 120, 121, 122, 123], including quantum thermal diode proposals [54, 55, 56].

In this section, we consider a system of two interacting qubits, with transition frequencies $\omega_{\rm L}$ and $\omega_{\rm R}$, described by a Hamiltonian with an opto-mechanical like coupling of strength $g$ between the left (L) and right (R) qubits,

$$\hat{H} = \frac{\omega_{\rm L}}{2}\hat{\sigma}^z_{\rm L} + \frac{\omega_{\rm R}}{2}\hat{\sigma}^z_{\rm R} + g\hat{\sigma}^z_{\rm L}\hat{\sigma}^x_{\rm R}, \tag{4.12}$$

which is called as the bare Hamiltonian. We derive the global MME for this system by dressing it. The first step of obtaining GME is to diagonalize (dress) the system Hamiltonian, which done by using the unitary transformation

$$U := \exp\Big(-i\frac{\theta}{2}\hat{\sigma}^z_{\rm L}\hat{\sigma}^y_{\rm R}\Big), \tag{4.13}$$

where the angle $\theta$ is defined as

$$\sin\theta := \frac{2g}{\Omega}; \qquad \cos\theta := \frac{\omega_{\rm R}}{\Omega}; \qquad \tan\theta := \frac{2g}{\omega_{\rm R}}, \tag{4.14}$$

such that $\Omega := \sqrt{\omega_{\rm R}^2 + 4g^2}$. The transformed (or dressed) operators then read

$$\hat{\tilde{\sigma}}^x_{\rm L} = U\hat{\sigma}^x_{\rm L}U^\dagger = \cos\theta\hat{\sigma}^x_{\rm L} + \sin\theta\hat{\sigma}^y_{\rm L}\hat{\sigma}^y_{\rm R}, \tag{4.15}$$

$$\hat{\tilde{\sigma}}^y_{\rm L} = U\hat{\sigma}^y_{\rm L}U^\dagger = \cos\theta\hat{\sigma}^y_{\rm L} - \sin\theta\hat{\sigma}^x_{\rm L}\hat{\sigma}^y_{\rm R}, \tag{4.16}$$

$$\hat{\tilde{\sigma}}^z_{\rm L} = U\hat{\sigma}^z_{\rm L}U^\dagger = \sigma^z_{\rm L}, \tag{4.17}$$

and

$$\hat{\tilde{\sigma}}^x_{\rm R} = U\hat{\sigma}^x_{\rm R}U^\dagger = \cos\theta\hat{\sigma}^x_{\rm R} - \sin\theta\hat{\sigma}^z_{\rm L}\hat{\sigma}^z_{\rm R}, \tag{4.18}$$

$$\hat{\tilde{\sigma}}^y_{\rm R} = U\hat{\sigma}^y_{\rm R}U^\dagger = \sigma^y_{\rm R}, \tag{4.19}$$

$$\hat{\tilde{\sigma}}^z_{\rm R} = U\hat{\sigma}^z_{\rm R}U^\dagger = \cos\theta\hat{\sigma}^z_{\rm R} - \sin\theta\hat{\sigma}^z_{\rm L}\hat{\sigma}^x_{\rm R}. \tag{4.20}$$

The back transformations from dressed operators to bare operators reads from the Eqs. (4.15)-(4.20) by switching dressed operators to bare operators and vice versa with $\theta$ replaced by $-\theta$. Then, with the transformation Eq. (4.13), the diagonalized (dressed) Hamiltonian is given as

$$\hat{\tilde{H}} = \frac{\omega_{\rm L}}{2}\hat{\tilde{\sigma}}^z_{\rm L} + \frac{\Omega}{2}\hat{\tilde{\sigma}}^z_{\rm R}, \tag{4.21}$$

Exemplary calculations regarding this diagonalization process and operator transformations are given in the Appendix 7.2. Eigenstates of the dressed Hamiltonian are given by the individual eigenstates of the qubits as

$$|1\rangle = \cos\frac{\theta}{2}|{+}{+}\rangle - \sin\frac{\theta}{2}|{+}{-}\rangle, \tag{4.22}$$

$$|2\rangle = \sin\frac{\theta}{2}|{+}{+}\rangle + \cos\frac{\theta}{2}|{+}{-}\rangle, \tag{4.23}$$

$$|3\rangle = \cos\frac{\theta}{2}|{-}{+}\rangle + \sin\frac{\theta}{2}|{-}{-}\rangle, \tag{4.24}$$

$$|4\rangle = \cos\frac{\theta}{2}|{-}{-}\rangle - \sin\frac{\theta}{2}|{-}{+}\rangle, \tag{4.25}$$

with their corresponding eigenvalues $\omega_1 = \frac{1}{2}(\omega_{\rm L}+\Omega)$, $\omega_2 = \frac{1}{2}(\omega_{\rm L}-\Omega)$, $\omega_3 = \frac{1}{2}(-\omega_{\rm L}+\Omega)$, and $\omega_4 = \frac{1}{2}(-\omega_{\rm L}-\Omega)$, respectively.

Now, we try to write the global MME by identifying the coupling operators in the interaction picture. After deriving the MME for a harmonic oscillator Eq. 2.113, we make a claim on how to directly write the MME from interaction picture couplings and, in Sec. 3.1, we show that it works. We here use the same argument to write global MME.

Qubits are coupled to two baths of temperature $T_{\rm R}$ and $T_{\rm L}$ via the the Hamiltonian $\hat{H}^i_{SB} = \sigma^x_i \otimes \sum_k g^i_k(\hat{a}^i_k + \hat{a}^{i\dagger}_k)$, where $g^i_k$ are the coupling strengths to baths, and $\hat{a}^i_k$ ($\hat{a}^{i\dagger}_k$)

are the creation (annihilation) operator of the $k$ mode of the bath $i$ = L,R, whose Hamiltonian is $\hat{H}_i = \sum_k \omega_k \hat{a}_k^{i\dagger} \hat{a}_k^i$. To calculate the master equation, we move to the interaction picture, and the coupling terms to baths evaluate to

$$\begin{aligned} \hat{\sigma}_{\rm L}^x(t) &= \cos\theta \hat{\tilde{\sigma}}_{\rm L}^- e^{-i\omega_{\rm L} t} - \sin\theta \hat{\tilde{\sigma}}_{\rm L}^+ \hat{\tilde{\sigma}}_{\rm R}^- e^{-i(\Omega-\omega_{\rm L})t} \\ &\quad + \sin\theta \hat{\tilde{\sigma}}_{\rm L}^- \hat{\tilde{\sigma}}_{\rm R}^- e^{-i(\Omega+\omega_{\rm L})t} + \text{H.c.} \end{aligned} \tag{4.26}$$

$$\hat{\sigma}_{\rm R}^x(t) = \cos\theta \hat{\tilde{\sigma}}_{\rm R}^- e^{-i\Omega t} + \frac{1}{2}\sin\theta \hat{\tilde{\sigma}}_{\rm L}^z \hat{\tilde{\sigma}}_{\rm R}^z + \text{H.c.} \tag{4.27}$$

Hence, the GME in interaction picture straightforwardly evaluates to

$$\dot{\hat{\rho}} = \hat{\mathcal{L}}_{\rm L} + \hat{\mathcal{L}}_{\rm R} + \hat{\mathcal{L}}_{\rm R}^{deph},$$

where three Liouville super-operators are explicitly given in terms of Lindblad dissipators [80, 81] as follows: the dissipative one due to left bath,

$$\begin{aligned} \hat{\mathcal{L}}_{\rm L} &= G_{\rm L}(\omega_{\rm L})\cos^2\theta \hat{\mathcal{D}}[\hat{\tilde{\sigma}}_{\rm L}^-] + G_{\rm L}(-\omega_{\rm L})\cos^2\theta \hat{\mathcal{D}}[\hat{\tilde{\sigma}}_{\rm L}^+] \\ &+ G_{\rm L}(-\omega_{2,3})\sin^2\theta \hat{\mathcal{D}}[\hat{\tilde{\sigma}}_{\rm L}^- \hat{\tilde{\sigma}}_{\rm R}^+] + G_{\rm L}(\omega_{2,3})\sin^2\theta \hat{\mathcal{D}}[\hat{\tilde{\sigma}}_{\rm L}^+ \hat{\tilde{\sigma}}_{\rm R}^-] \\ &+ G_{\rm L}(\omega_{1,4})\sin^2\theta \hat{\mathcal{D}}[\hat{\tilde{\sigma}}_{\rm L}^- \hat{\tilde{\sigma}}_{\rm R}^-] + G_{\rm L}(-\omega_{1,4})\sin^2\theta \hat{\mathcal{D}}[\hat{\tilde{\sigma}}_{\rm L}^+ \hat{\tilde{\sigma}}_{\rm R}^+], \end{aligned} \tag{4.28}$$

the dissipative one due to right bath,

$$\hat{\mathcal{L}}_{\rm R} = G_{\rm R}(\Omega)\cos^2\theta \hat{\mathcal{D}}[\hat{\tilde{\sigma}}_{\rm R}^-] + G_{\rm R}(-\Omega)\cos^2\theta \hat{\mathcal{D}}[\hat{\tilde{\sigma}}_{\rm R}^+], \tag{4.29}$$

and the pure-dephasing due to right bath

$$\hat{\mathcal{L}}_{\rm R}^{deph} = \frac{1}{2} G_{\rm R}(0)\sin^2\theta \hat{\mathcal{D}}[\hat{\tilde{\sigma}}_{\rm L}^z \hat{\tilde{\sigma}}_{\rm R}^z], \tag{4.30}$$

where $\theta = \arctan(2g/\omega_{\rm R})$. In other words, the first two terms in $\hat{\mathcal{L}}_{\rm L}$, respectively, dissipate and drive the system through dressed-left qubit, while the two terms in $\hat{\mathcal{L}}_{\rm R}$ dissipate and drive the system through dressed-right qubit, respectively. The remaining four terms of $\hat{\mathcal{L}}_{\rm L}$ are the global channels of the left bath interacting simultaneously with the two dressed qubits. The coefficients $G_i(\omega)$ are given as

$$G_i(\omega) = \begin{cases} \kappa_i(\omega)[1+\bar{n}_i(\omega)], & \omega > 0 \\ \kappa_i(|\omega|)\bar{n}_i(|\omega|), & \omega < 0 \\ 0, & \omega = 0 \end{cases}, \tag{4.31}$$

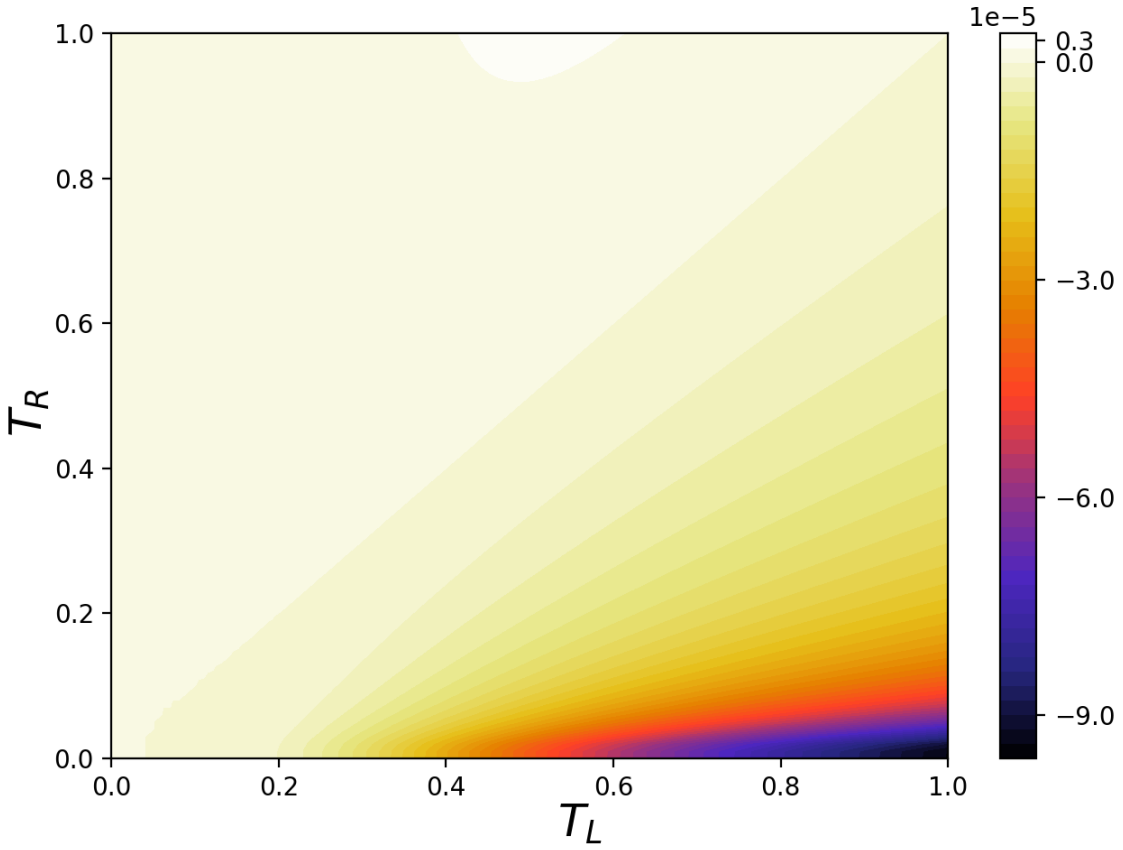


Figure 4.5: **Global MME for Two Interacting Qubits.** Steady state heat currents have the correct direction, and its non-reciprocal.

where $\bar{n}_i(\omega) := \frac{1}{e^{\omega/T_i}-1}$ is the average excitation number and $i =$ L,R.

This model is the main diode model of the next chapter 5, and we further explain and analyze it in there. For the moment, we just present the heat current from right bath to system and show that it now satisfy thermodynamical laws, including Fourier's law, as shown in Fig. 4.5. Yet, it is non-reciprocal and we explain its basis in the next chapter 5. Fig. 4.5 is plotted using the off-resonant parameters, which are given in the next chapter, with the coupling strength between qubits $g = 0.02$.

Chapter 5

# QUANTUM THERMAL DIODES

In the previous chapters, we present the MME tool from the theory of open quantum systems and apply it to different cases with its two approaches, local and global. We show that the local approach gives thermodynamically inconsistent results, and they are fixed by adopting the global approach. Additionally, we find an asymmetry in the heat currents under switching of bath temperatures, a diode behavior. In other words, when two thermal baths are connected via a lead, heat flows from hot to cold bath. However, switching the bath temperatures changes just not the direction of steady state heat current but also the amount, if the lead behaves as a diode, a non-reciprocal device.

In this chapter, we explain the mechanism leading to quantum thermal diodes [54, 55, 56] by considering three different models, a single qubit, a three level atom, and two qubits interacting with an opto-mechanical like qubits. First two models are presented to gain intuition about the involved mechanism, which is the interplay between coupling of energy levels to baths and qubit-bath coupling strengths. In other words, as in the case of heat valve in Ref. [59], the tunable diode behavior depends on the interplay between with qubit-bath and qubit-qubit couplings. We analyze such an interplay to demonstrate working mechanism of the quantum thermal diodes, and the absence of rectification at resonance in Ref. [56] is understood from the mechanism. We show that there are three separate places in which an asymmetry can be introduced to enable diode behavior namely, free Hamiltonians of subsystems, interaction among subsystems, and bath couplings. Therefore, in our analysis, we consider an asymmetric coupling between the two qubits and two other toy models, a single qubit and a three-level atom.

### *5.1 A Single Qubit as the Smallest Diode*

We start by demonstrating the effects of qubit-bath coupling strengths. We already give the MME and calculate the heat current for a single qubit coupled to two baths in Sec. 3.2.1. Analytical expressions for the steady state heat currents are given Eq. 3.43 as

$$\mathcal{J}^{\mathrm{ss}}_{\mathrm{L/R}} \quad = \quad = \frac{\omega\kappa_{\mathrm{L}}\kappa_{\mathrm{R}}(\bar{n}_{\mathrm{L/R}} - \bar{n}_{\mathrm{L/R}})}{\kappa_{\mathrm{R}}(1+2\bar{n}_{\mathrm{R}}) + \kappa_{\mathrm{L}}(1+2\bar{n}_{\mathrm{L}})}. \tag{5.1}$$

Sign of this heat current depends on the average excitation numbers, and it give a

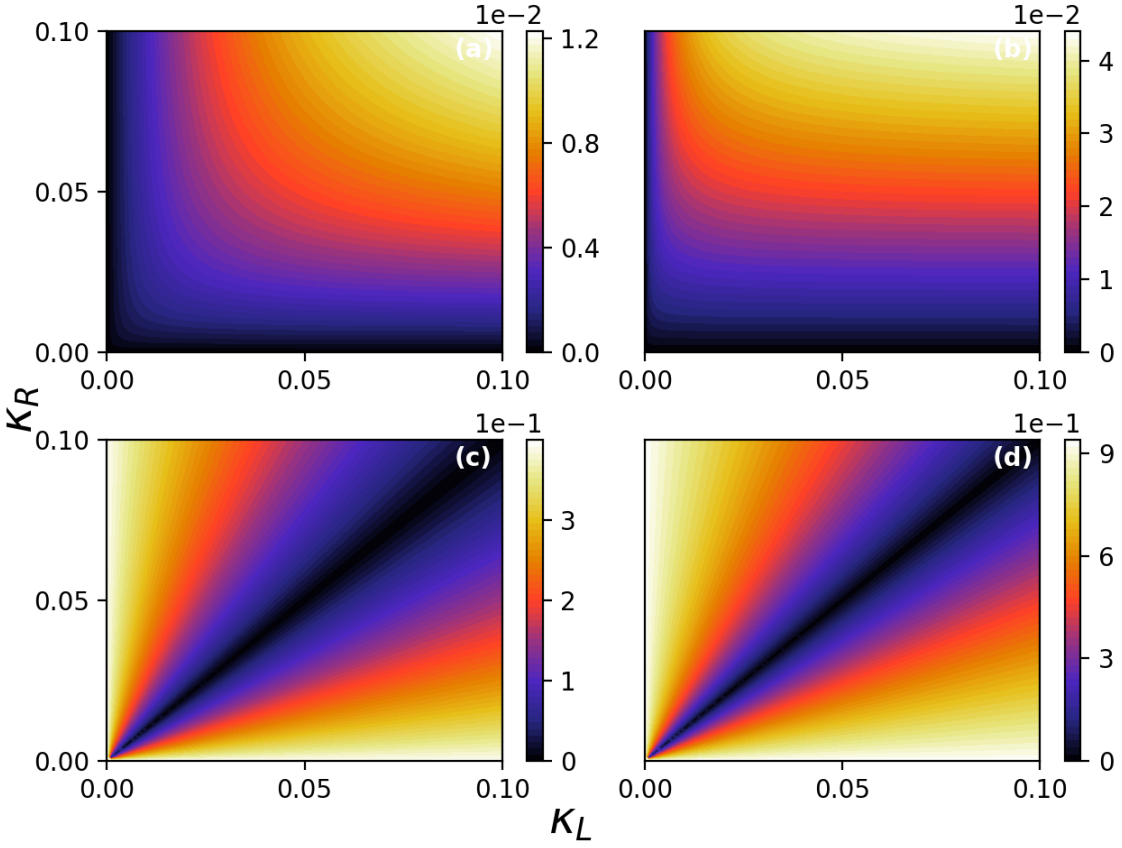


Figure 5.1: **Asymmetric coupling of a single qubit.** (a) Magnitude of the heat currents for low temperature, $T_{\mathrm{L}} = 2T_{\mathrm{R}} = \omega$ is asymmetric if environmental couplings are not symmetric. (b) Asymmetry in heat current gets stronger in high temperatures $T_{\mathrm{L}} = 20T_{\mathrm{R}} = 10\omega$, as also seen in their respective rectification factors (c) and (d).

direction from hot to cold, as expected. However, we can already be seen that it is an asymmetric function of environmental coupling strengths, $\kappa_{\mathrm{R}}$ and $\kappa_{\mathrm{L}}$. Fig. 5.1 shows that the heat current amount is asymmetric under the exchange of temperatures, unless $\kappa_{\mathrm{L}} \approx \kappa_{\mathrm{R}}$. We plot the amplitude of heat currents, and Figs. 5.1 (a) and (c) show the asymmetry at $T_{\mathrm{L}} = 2T_{\mathrm{R}} = \omega$. Figs. 5.1 (b) and (d) present the asymmetry at $T_{\mathrm{L}} = 20T_{\mathrm{R}} = 10\omega$, and exhibit that better rectification values are obtained at high temperatures.

This sort of an asymmetric environmental coupling is obtained for the two interacting qubits by different number of local environments with the same couplings strengths in Ref. [55], and they have a diode behavior with the resonant qubits, even though at resonance their system Hamiltonian become completely symmetric. This observation on the asymmetric bath-qubits coupling strengths explains one side of the interplay. The other side, namely asymmetric coupling of energy levels to baths is demonstrated in the next section with the artificial three level atom scenario shown in Fig. 5.2.

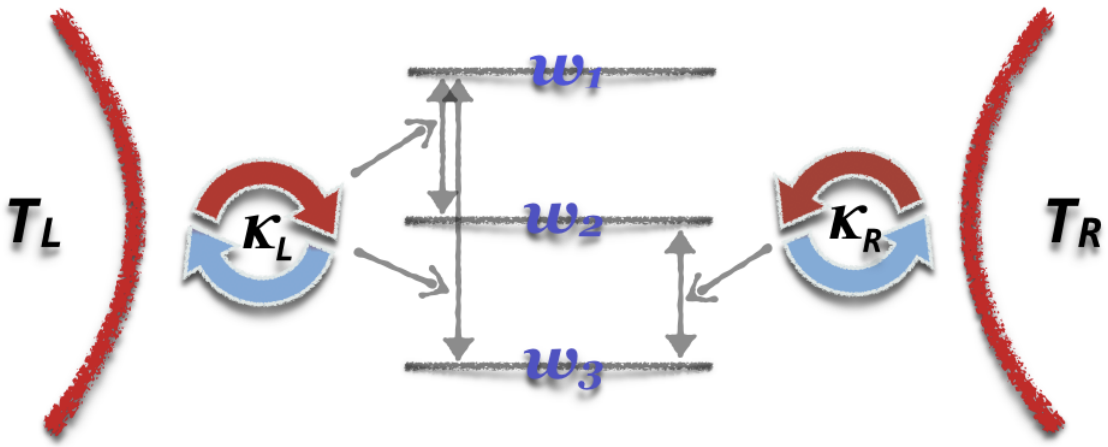


Figure 5.2: **Elements of the models.** For a symmetrically coupled system $\kappa_{\mathrm{L}} = \kappa_{\mathrm{R}}$, asymmetric coupling of energy levels to baths enables the diode behavior.

## 5.2 Diode Behavior form a Three Level Atom

In order to clearly demonstrate that the asymmetric coupling of energy levels to baths leads to the rectification even when the bath coupling strengths are symmetric, we consider the simplest, yet artificial, case of a three-level atom depicted in Fig. 5.2.

Hamiltonian and master equation of such configuration are given [124, 125] respectively as

$$\hat{H} = \omega_1 |1\rangle\langle 1| + \omega_2 |2\rangle\langle 2| + \omega_3 |3\rangle\langle 3| \tag{5.2}$$

and,

$$\dot{\hat{\rho}} = -i\left[\hat{H}, \hat{\rho}\right] + \hat{\mathcal{L}}_{\mathrm{L}}[\hat{\rho}] + \hat{\mathcal{L}}_{\mathrm{R}}[\hat{\rho}]. \tag{5.3}$$

The second and third terms on the left hand side of the master equation are super-operators describing the effects of left and right baths, respectively. They are given as

$$\begin{aligned}\hat{\mathcal{L}}_{\mathrm{L}}[\hat{\rho}] &= \kappa_{21}^{-}\left(\rho_{11}|2\rangle\langle 2| - \frac{1}{2}\{|1\rangle\langle 1|, \rho\}\right) + \kappa_{21}^{+}\left(\rho_{22}|1\rangle\langle 1| - \frac{1}{2}\{|2\rangle\langle 2|, \rho\}\right) \\ &+ \kappa_{31}^{-}\left(\rho_{11}|3\rangle\langle 3| - \frac{1}{2}\{|1\rangle\langle 1|, \rho\}\right) + \kappa_{31}^{+}\left(\rho_{33}|1\rangle\langle 1| - \frac{1}{2}\{|3\rangle\langle 3|, \rho\}\right),\end{aligned}$$

and,

$$\hat{\mathcal{L}}_{\mathrm{R}}[\hat{\rho}] = \kappa_{32}^{-}\left(\rho_{22}|3\rangle\langle 3| - \frac{1}{2}\{|2\rangle\langle 2|, \rho\}\right) + \kappa_{32}^{+}\left(\rho_{33}|2\rangle\langle 2| - \frac{1}{2}\{|3\rangle\langle 3|, \rho\}\right) \tag{5.4}$$

where $\kappa_{ji}^{-} = \kappa_{\mathrm{B}}(1 + \bar{n}(\omega_{j,i}))$ and $\kappa_{ji}^{+} = \kappa_{\mathrm{B}}\bar{n}(\omega_{ij})$ with $\omega_{ji} = \omega_i - \omega_j$ and B = R, L. Then, by explicitly writing the matrix representations, the heat current expressions in terms of the populations calculate to

$$\begin{aligned}\mathcal{J}_{\mathrm{L}} &= \kappa_{21}^{-}\rho_{11}\omega_{12} + \kappa_{21}^{+}\rho_{22}\omega_{21} + \kappa_{31}^{-}\rho_{11}\omega_{13} + \kappa_{31}^{+}\rho_{33}\omega_{31} \\ \mathcal{J}_{\mathrm{R}} &= \kappa_{32}^{-}\rho_{22}\omega_{23} + \kappa_{32}^{+}\rho_{33}\omega_{32}.\end{aligned} \tag{5.5}$$

By calculating the steady state solution for the populations with symmetric environmental couplings, that is $\kappa_{\mathrm{L}} = \kappa_{\mathrm{R}} = \kappa$, we write the heat current Eq. 5.5 as,

$$\mathcal{J}_{\mathrm{R}} = \frac{\kappa\omega_{32}\mathfrak{K}}{-\mathfrak{K} - f(T_{\mathrm{L},3}, T_{\mathrm{R},3})(1 + 2f(T_{\mathrm{L},-1}, T_{\mathrm{L},2})) + 2f(T_{\mathrm{L},1}, T_{\mathrm{R},2}) + 2f(T_{\mathrm{L},1}, T_{\mathrm{R},3})}, \tag{5.6}$$

where $\mathfrak{K} = f(T_{\mathrm{L},2}, T_{\mathrm{R},3}) - f(T_{\mathrm{L},3}, T_{\mathrm{R},2})$ and $f(T_{\mathrm{B},\pm j}, T_{\mathrm{B}',\pm j}) = \exp\left(\frac{\pm\omega_j}{\mathrm{B}} + \frac{\pm\omega_j}{\mathrm{B}'}\right)$.

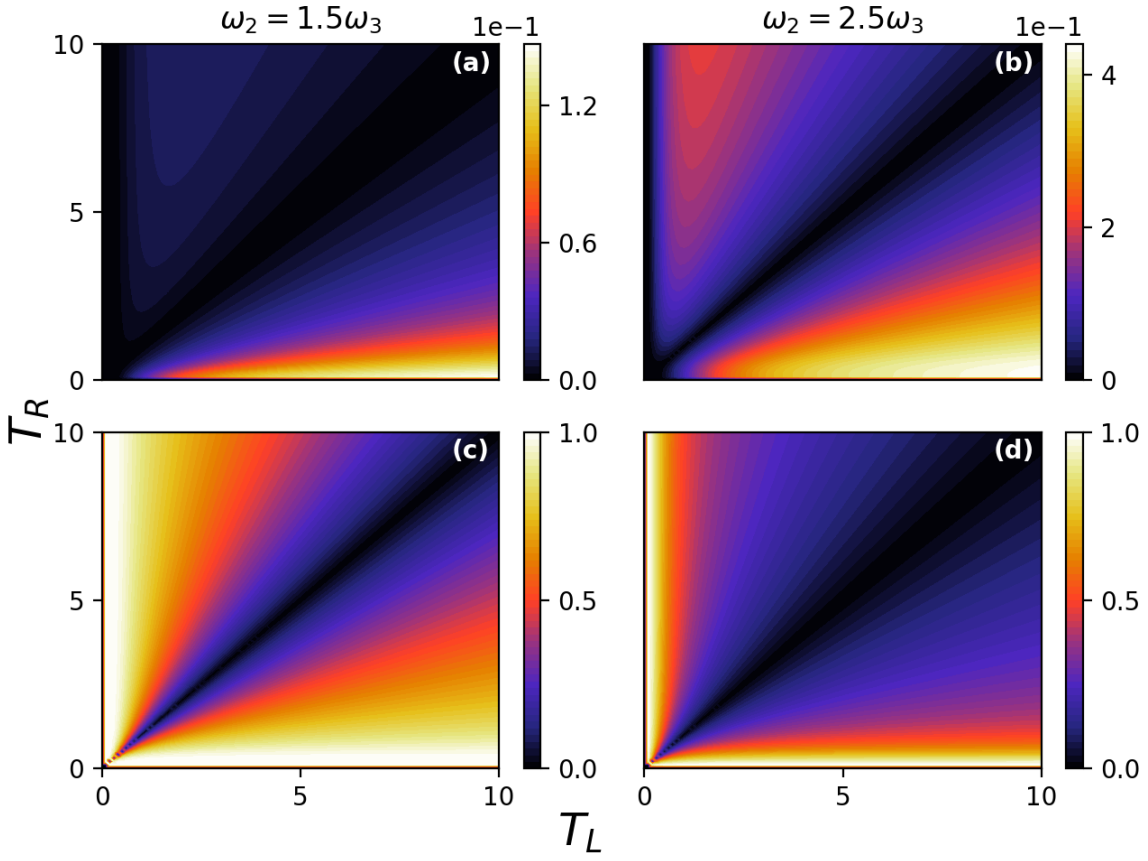


Figure 5.3: **Asymmetric heat current of a three-level atom.** Rectification is stronger, if the asymmetry in energy levels is strong (a) $\omega_2 = 1.5\omega_3$. Asymmetry in heat current and the rectification value weakens as the asymmetry in energy levels decreases (b) $\omega_2 = 1.5\omega_3$. This comparison is also seen in the respective rectification factors (c) and (d).

We plot magnitude of the heat current Eq. 5.6 together with the rectification values in Fig. 5.3 for high temperature limit using $\omega_3 = 1$ as the scaling parameter, and we use two different values for $\omega_2$ while fixing $\omega_1 = 3\kappa = 3\omega_3$. In this configuration, baths are energetic enough to properly support all the transitions, so being coupled to a big transition determines the rectification. Since the left bath is coupled to the transition $|1\rangle \leftrightarrows |3\rangle$, which is the biggest one, rectification is always from left to right,

as seen in Figs. 5.3 (a) and (b). We first consider $\omega_2 = 1.5\omega_3$ in Fig. 5.3 (a), and show that, when $|\omega_{23}|$, the transition supported by right bath, is small compared to both the other transitions and $T_{\max}$, right bath is not able to give its energy away due to the transitions supported by it being small. This lead to high rectification values for a bigger range of temperatures compared to the second case in which $\omega_2 = 2.5\omega_3$, as seen in Figs. 5.3 (c) and (d). In the second case, $|\omega_{23}| \approx |\omega_{13}| \gg |\omega_{12}|$, both baths have big enough transitions coupled to them, and the one with bigger transition (left bath), also with small but the additional $|\omega_{12}|$ is still able give more heat than the other bath. As a result, rectification direction does not change, but diode quality decreases, as shown in Fig. 5.3 (d).

Asymmetric coupling of the energy levels is the main cause of the rectification in Ref. [56], and such asymmetry vanishes for resonant qubits in their model. Therefore, their model do not show diode behavior when qubits are resonant to each other. In our model of two interacting qubits, the energy levels are coupled to baths as shown in Fig. 5.4, and the asymmetric coupling does not vanish with resonant qubits because its mainly due to the asymmetric qubit-qubit interaction term in the bare Hamiltonian 4.12. Reason for the choosing above three level configuration is that it resembles dressed transitions of our two qubit model, shown in Fig. 5.4.

## *5.3 Two-Qubit Quantum Thermal Diode*

We derive the global MME for two qubits interacting with each other by an opto-mechanical like coupling in Sec. 4.2, and we give an example of the asymmetry in steady state heat currents of this model in Fig. 4.5. In this chapter, we start by explaining the dressed system with its global MME, and then we demonstrate that behavior of our model agrees with the above explained interplay mechanism.

### *5.3.1 Dressed System Description*

The dressed system Hamiltonian and the global MME are respectively given as

$$\hat{\tilde{H}} = \frac{\omega_{\rm L}}{2}\hat{\tilde{\sigma}}_{\rm L}^{z} + \frac{\Omega}{2}\hat{\tilde{\sigma}}_{\rm R}^{z}, \tag{5.7}$$

and

$$\dot{\hat{\rho}} \;\; = \hat{\mathcal{L}}_{\rm L} + \hat{\mathcal{L}}_{\rm R} + \hat{\mathcal{L}}_{\rm R}^{deph},$$

where three Liouville super-operators are explicitly given in terms of Lindblad dissipators [80, 81] as follows: the dissipative one due to left bath,

$$\begin{aligned}
\hat{\mathcal{L}}_{\rm L} &= G_{\rm L}(\omega_{\rm L})\cos^2\theta\hat{\mathcal{D}}[\hat{\tilde{\sigma}}_{\rm L}^{-}] + G_{\rm L}(-\omega_{\rm L})\cos^2\theta\hat{\mathcal{D}}[\hat{\tilde{\sigma}}_{\rm L}^{+}] \\
&+ G_{\rm L}(-\omega_{2,3})\sin^2\theta\hat{\mathcal{D}}[\hat{\tilde{\sigma}}_{\rm L}^{-}\hat{\tilde{\sigma}}_{\rm R}^{+}] + G_{\rm L}(\omega_{2,3})\sin^2\theta\hat{\mathcal{D}}[\hat{\tilde{\sigma}}_{\rm L}^{+}\hat{\tilde{\sigma}}_{\rm R}^{-}] \\
&+ G_{\rm L}(\omega_{1,4})\sin^2\theta\hat{\mathcal{D}}[\hat{\tilde{\sigma}}_{\rm L}^{-}\hat{\tilde{\sigma}}_{\rm R}^{-}] + G_{\rm L}(-\omega_{1,4})\sin^2\theta\hat{\mathcal{D}}[\hat{\tilde{\sigma}}_{\rm L}^{+}\hat{\tilde{\sigma}}_{\rm R}^{+}],
\end{aligned} \tag{5.8}$$

the dissipative one due to right bath,

$$\hat{\mathcal{L}}_{\rm R} = G_{\rm R}(\Omega)\cos^2\theta\hat{\mathcal{D}}[\hat{\tilde{\sigma}}_{\rm R}^{-}] + G_{\rm L}(-\Omega)\cos^2\theta\hat{\mathcal{D}}[\hat{\tilde{\sigma}}_{\rm R}^{+}], \tag{5.9}$$

and the pure-dephasing due to right bath

$$\hat{\mathcal{L}}_{\rm R}^{deph} = \frac{1}{2}G_{\rm R}(0)\sin^2\theta\hat{\mathcal{D}}[\hat{\tilde{\sigma}}_{\rm R}^{z}\hat{\tilde{\sigma}}_{\rm R}^{z}], \tag{5.10}$$

where $\theta = \arctan(2g/\omega_{\rm R})$.

Dressed system can be though in two way: (i) an effective four level system and (ii) two uncoupled qubits communicating through global channels derived by the baths.

Fig. 5.4 illustrates the four level system case and shows the couplings between baths and the allowed transitions. Colored lines with two arrowheads show the allowed transitions, colored wavy lines indicate the baths that they are coupled to. Eigenkets of the dressed-system, $|1\rangle$, $|2\rangle$, $|3\rangle$, and $|4\rangle$, and the corresponding eigenvalues are given in the Sec. 4.2. The transitions, $|1\rangle \leftrightarrows |4\rangle$, $|1\rangle \leftrightarrows |3\rangle$, $|2\rangle \leftrightarrows |4\rangle$, and $|3\rangle \leftrightarrows |4\rangle$ are coupled to left bath, and the corresponding transition frequencies are $\omega_1 - \omega_4 \equiv \omega_{14} = \omega_{\rm L} + \Omega$, $\omega_{13} = \omega_{24} = \omega_{\rm L}$, and $\omega_{23} = \omega_{\rm L} - \Omega$. The remaining two transitions

are coupled to right bath, and their transition frequencies are $\omega_{12} = \omega_{34} = \Omega$. This asymmetric coupling of energy levels to the baths play a key role in the diode behavior, and it is due to the asymmetry in the system Hamiltonian, specifically in our case in the interaction part.

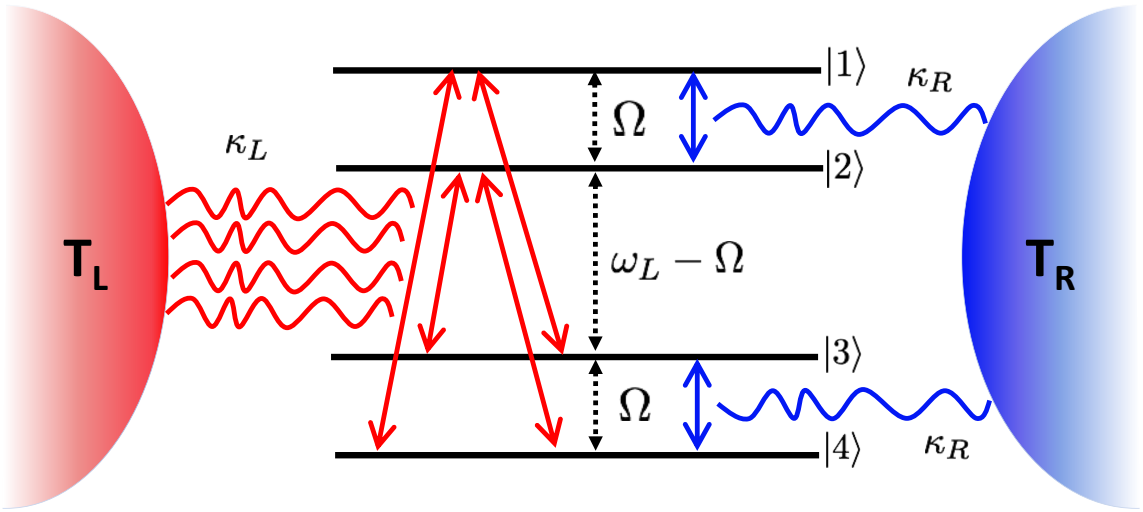


Figure 5.4: **Dressed Levels.** Allowed transitions between the dressed states $|i\rangle$ with $i = 1, 2, 3, 4$, coupled to the baths with the dissipation rates $\kappa_L, \kappa_R$.

Uncoupled qubits case and the global dissipation, derive, and dephasing channels are depicted in Fig. 5.5. The first two terms in $\hat{\mathcal{L}}_{\mathrm{L}}$, respectively, dissipate and drive the system through dressed-left qubit, while the two terms in $\hat{\mathcal{L}}_{\mathrm{R}}$ dissipate and drive the system through dressed-right qubit, respectively. The term in Eq. 5.10 is pure dephasing by the right bath. The remaining four terms of $\hat{\mathcal{L}}_{\mathrm{L}}$ are the global channels of the left bath interacting simultaneously with the two dressed qubits.

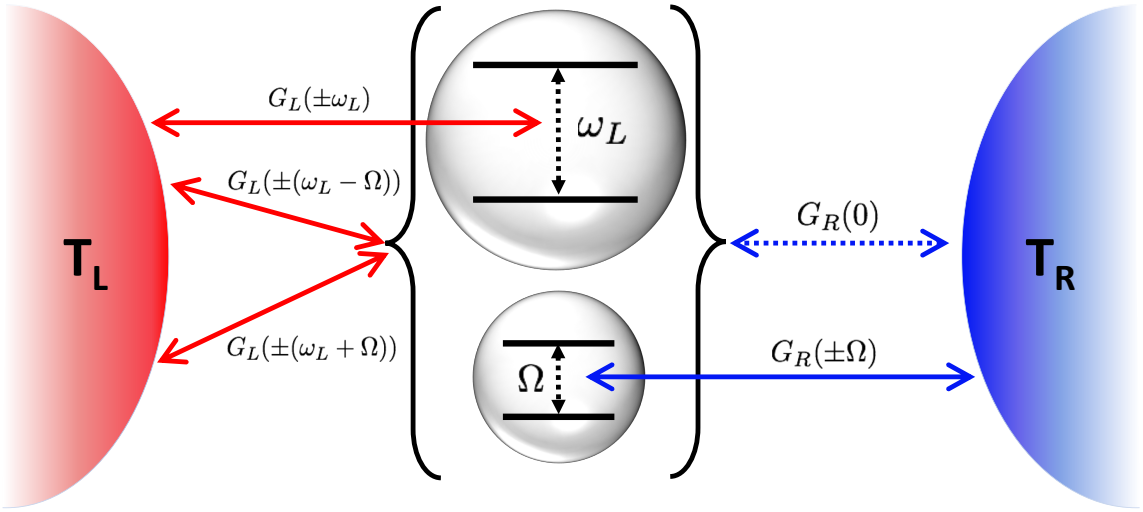


Figure 5.5: **Dressed Qubits.** Dressed qubits, with frequencies $\omega_{\rm L}$ and $\Omega$, are uncoupled but heat transfer occurs via global dissipation channels with spectral response functions $G(\pm(\omega_{\rm L}-\Omega))$ and $G(\pm(\omega_{\rm L}+\Omega))$. The channels with $G(\pm\omega_{\rm L}$ and $G(\pm\Omega$ are local dissipation channels.

### *5.3.2 Model Realizations, Comparisons, and Explanations*

The quantum thermal diode of two qubits interacting with an opto-mechanical like coupling is similar to single bosonic excitation limit of an opto-mechanical system [126], off-resonant Raman transition [127], and quantum walk on a cycle [128, 129], which suggest that the diode behavior will we apparent in opto-mechanical system close to its ground state and can be realized in these platforms. Therefore, we consider a parameter set, named off-resonant qubits (ORQ) with one qubit frequency (Right) much smaller than the other (Left), similar to opto-mechanical systems.

In the Ref. [56], rectification optimization is considered for a system of two qubits interacting with each other by the symmetric coupling $\hat{\sigma}_{\mathrm{L}}^{z}\hat{\sigma}_{\mathrm{R}}^{z}$. In the proposed model of Ref. [56], diode behavior is absent when qubits have the same transition frequencies. Thus, by using a parameter set named resonant qubtis (RQ), we show that almost unit rectification is realizable with an asymmetric coupling (opto-mechanical like) at resonant case.

This difference is related to THE involved mechanism. Environmental couplings determine the baths ability to support any transition induced by them, meaning that higher the environmental coupling strength for a bath the more heat will flow away from it. First toy model, a single qubit, constitute the smallest possible diode, if the environmental coupling strengths are asymmetric. When the environmental coupling strengths are symmetric, asymmetric coupling of the energy levels to baths enables the diode. In order to exhibit this case, we use the artificial scenario of a three-level atom as in Fig. 5.2, which has a similarity to the dressed-system couplings shown in Fig. 5.4. Even though these two constitute the smallest quantum diode examples, they offer very little control over the rectification direction and the heat current amount. On the other hand, system of two interacting qubits offer various control schemes, so it might be considered as the smallest useful diode.

Above explanations mean that, in the case of two interacting qubits, an asymmetry in the Hamiltonian and/or environmental coupling strengths enables the diode. For example, our coupling, which does not include $\hat{\sigma}_{\mathrm{L}}^{x}\hat{\sigma}_{\mathrm{R}}^{z}$, is asymmetric, and the coupling part of the Hamiltonian in Ref. [56] is symmetric, as well as the environmental couplings. Therefore, only remaining asymmetry source, which is the free Hamiltonians of subsystems, is lost, unless the transition frequencies of qubits are non-resonant. This explains why there is no rectification at resonance in Ref. [56]. Since we consider an asymmetric coupling, it allows us to have symmetry in both the free Hamiltonians and environmental couplings yet still have rectification. Finally, if we have a totally symmetric Hamiltonian, asymmetric environmental coupling strengths are required, which can also be achieved by introducing a third thermal bath as in Ref. [55].

### *5.3.3 Heat Currents and Thermal Diode Quality Measure*

In this part, we first present the analytical expression of the heat current [40], which is given by

$$\mathcal{J}_{\mathrm{R(L)}} = \mathrm{Tr}[\hat{\mathcal{L}}_{\mathrm{R(L)}}\hat{\tilde{H}}], \tag{5.11}$$

from right (left) bath to system. We calculate the heat current expression by the observable dynamics technique introduced in Sec. 3.2.2. Heat current from the right bath to two interacting qubits is given in terms of bare picture operators as,

$$\mathcal{J}_{\mathrm{R}} = -\frac{1}{2}\kappa_{\mathrm{R}}\Omega\cos^2\theta[1 + (2\bar{n}_{\mathrm{R}} + 1)(\cos\theta\langle\hat{\sigma}^z_{\mathrm{R}}\rangle + \sin\theta\langle\hat{\sigma}^z_{\mathrm{L}}\hat{\sigma}^x_{\mathrm{R}}\rangle)], \tag{5.12}$$

Relation for $\mathcal{J}_{\mathrm{L}}$ and closed set of equation for the relevant expectation values are given in Appendix 7.3. The Eq.(5.12) also shows that $g$ and transition frequencies play roles on the diode behavior, and we examine those roles.

To characterize diode behavior, we use a measure, namely the rectification factor [43], defined by,

$$\mathcal{R} = \frac{|\mathcal{J}_{\mathrm{R}}(T_{\mathrm{R}}, T_{\mathrm{L}}) + \mathcal{J}_{\mathrm{R}}(T_{\mathrm{L}}, T_{\mathrm{R}})|}{\mathrm{Max}(|\mathcal{J}_{\mathrm{R}}(T_{\mathrm{R}}, T_{\mathrm{L}})|, |\mathcal{J}_{\mathrm{R}}(T_{\mathrm{L}}, T_{\mathrm{R}}))|}, \tag{5.13}$$

where the $\mathcal{J}_{\mathrm{R}}(T_{\mathrm{R}}, T_{\mathrm{L}})$ is the heat current from right bath to the system when $T_{\mathrm{R}} > T_{\mathrm{L}}$, and Max function picks the biggest of its arguments. Thus, its value is between 0 and 1 describing from a symmetric heat current to a perfect diode, respectively.

### *5.3.4 Asymmetry in the Heat Current*

In this part, we illustrate the quantum thermal diode behavior by showing that switching the bath temperatures changes the magnitude of steady state heat current.

In order to demonstrate and explain how the interplay explained above leads to the diode behavior, we vary bath temperatures and calculate the magnitude of heat current Eq.(5.12) along with the rectification factors Eq.(5.13). The analytical solution to heat current Eq.(5.12) is easy to obtain, but the solution is complicated to make any deduction. Thus, we analyze the model numerically to show the asymmetry

in heat current and to explain the control schemes of the rectification direction. We report the results of extensive numerical calculations for both flat and Ohmic spectral densities and present only some key results graphically. We plot magnitudes (absolute values) of the heat currents from right to the system for consistent comparison of the heat current amounts with the color scales. We also present all the heat current calculation with the correct signs in Appendix 7.4.

We run our simulations by using scientific python packages and some key libraries of QuTiP python [113]. We chose $\omega_{\rm L} = 1$ as the scaling in both off-resonant (ORQ) and resonant-qubit (RQ) parameters. Unless the otherwise is stated in the text or on the plots, ORQ parameters are $\omega_{\rm R} = 0.05$, $g = 0.005$. We define $\kappa_i(\omega)$ as rates, which are independent of frequency for the flat spectrum, and $\kappa_{\rm R/L}(\omega) = \kappa_{\rm R/L}\omega$ for the Ohmic spectral density, and we fix the rates $\kappa_{\rm R} = 0.005$ and $\kappa_{\rm L} = 0.2$. RQ parameters are $\omega_{\rm R} = 1$, $\kappa_{\rm R} = \kappa_{\rm L} = 0.01$, and $g = 0.005$. In the text, we describe behavior of the diode with these parameter, but the Appendix 7.4 present the results for $\kappa_{\rm R} = \kappa_{\rm L} = 0.01$ even in the ORQ case. Reason for this is to prevent an objection to consider a high rate, $\kappa_{\rm L} = 0.2$, in ORQ parameters. Plots in the Appendix 7.4 show the same behavior described in the text but at different $g$ values.

*Flat Spectral Density*

We divide the analysis into two temperature ranges, high and low. Former means that $T_{\rm max}$ is one order of magnitude bigger than $\mathrm{Max}(\omega_{\rm L}, \omega_{\rm R}, g)$, and the latter is when $T_{\rm max}$ is in the order of $\mathrm{Max}(\omega_{\rm L}, \omega_{\rm R}, g)$. Fig. 5.6 shows the asymmetry in heat current for ORQ parameters in both temperature ranges for two different values of $g$.

In the low temperature range, diode behavior is dominant when $g$ is weak for ORQ parameters, and rectification direction is left to right, as shown in Fig. 5.6 (a). Rectification direction is reversed when $g$ is increased, as seen in Fig. 5.6 (b).

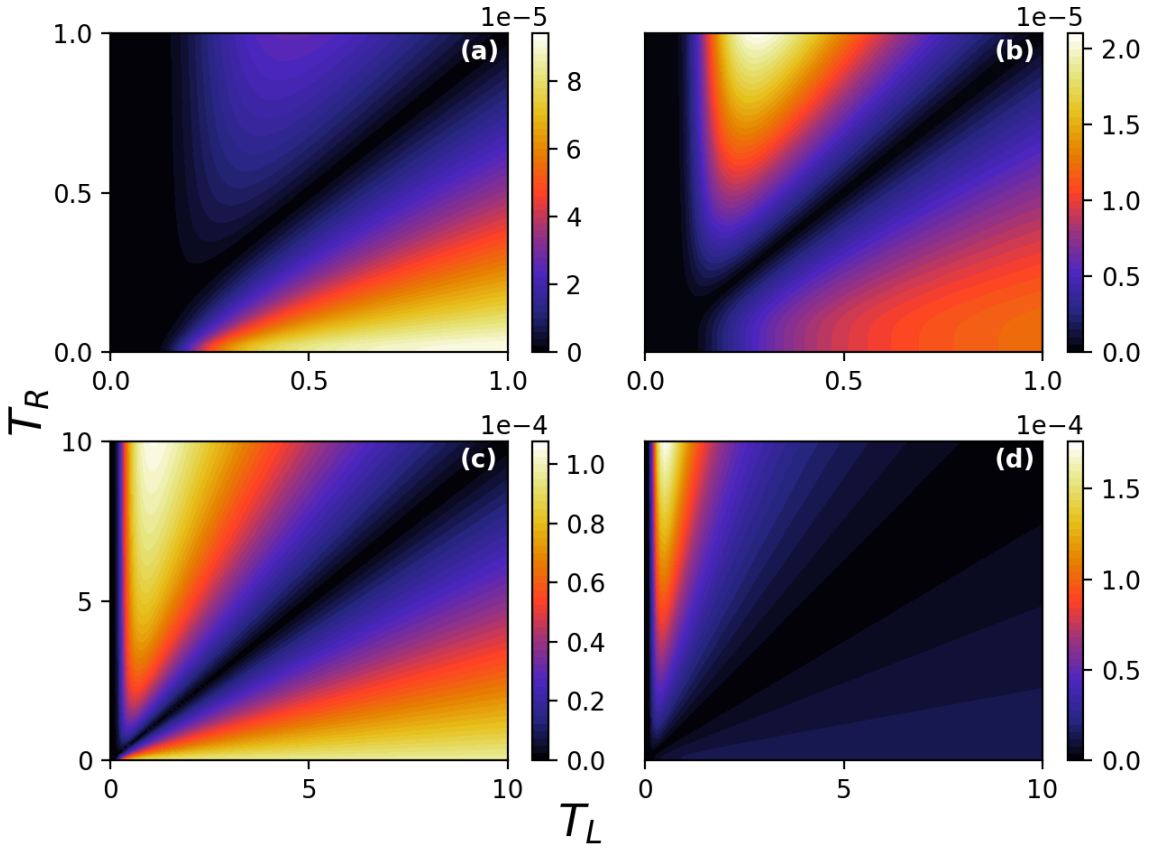


Figure 5.6: **ORQ parameters with flat spectral density.** Magnitude of the steady state heat current from right bath to the system $\mathcal{J}_{\mathrm{R}}$ is asymmetric under the switching of bath temperatures. Magnitude plot is suited for the ease it brings into the visualization of asymmetry by use of color scales. In the low temperature range (a) and (b), rectification direction is reversed by changing $g$ from $0.4\omega_{\mathrm{R}}$ to $4\omega_{\mathrm{R}}$. High temperature ranges for the same parameters are shown in (c) and (d).

This change in the rectification direction is understood from its cause, which is the asymmetric coupling of energy levels to thermal baths (originating from the asymmetry of third term in the Eq.(4.12)) and abilities of baths to support the transitions. ORQ parameters ($\omega_{\mathrm{R}} = 0.05\omega_{\mathrm{L}}$) with an even smaller $g = 0.4\omega_{\mathrm{R}}$ cause the transitions induced by right bath, which are $\omega_{12} = \omega_{34} = \Omega$, to become too small (almost negligible) compared to other transitions. Also, the transition frequencies,

$\omega_{14} \approx \omega_{23} \approx \omega_{13} = \omega_{24} = \omega_{\mathrm{L}}$, supported by the left bath are in the order of $T_{\max}$. These mean that the transitions supported by right bath are too small to adequately receive and transfer the available energy at any temperature, resulting in almost zero heat current. On the other hand, left bath supports its transitions as the temperature is increased. By increasing $g$, $\Omega$ increases, and the two transitions due to left bath, $\omega_{14}$, $\omega_{23}$, become respectively bigger and smaller than the $T_{\max}$. As a result, right bath starts to properly transmit its energy, while ability of left bath to support $\omega_{14}$ and capability of the transition $\omega_{23}$ to transmit the available energy are decreased. Thus, the asymmetry first weakens, and the further increase in $g$ brings back the asymmetry with a change in rectification direction.

Since bath-spin coupling strengths of ORQ parameters are not symmetric, clear connection of rectification direction change to transition energies and baths abilities to support them is not obvious here. Therefore, we present an artificial scenario of a three level system with symmetric coupling strength to baths and asymmetric coupling of energy levels to baths, and we make the clear connection in the previous section.

Finally, asymmetry becomes negligible at very strong $g$, because the transitions become so big ($|\omega_{\mathrm{L}} - \Omega| \approx \omega_{\mathrm{L}} + \Omega \approx \Omega \gg \omega_{\mathrm{L}}$) compared to temperatures, so both the amount of heat current and rectification are decreased. The reduction of asymmetry at very strong $g$ is common in both parameters (ORQ and RQ), spectral densities, and temperatures.

Rectification values corresponding to Figs. 5.6 (a) and (b) are given in Figs. 5.7 (a) and (b) and are closer to unity over a bigger range of temperatures in the weak coupling.

Results for the RQ parameters in the low temperature are presented graphically in the Appendix 7.4, and they are listed as follows. Rectification is left to right at any $g$ and do not reverses direction when $g$ is increased. The fixed rectification direction of RQ parameters is due to $\Omega > \omega_{\mathrm{L}}$ for any $g$. Rectification of ORQ parameters is from higher dressed frequency side to lower. However, even though the right dressed

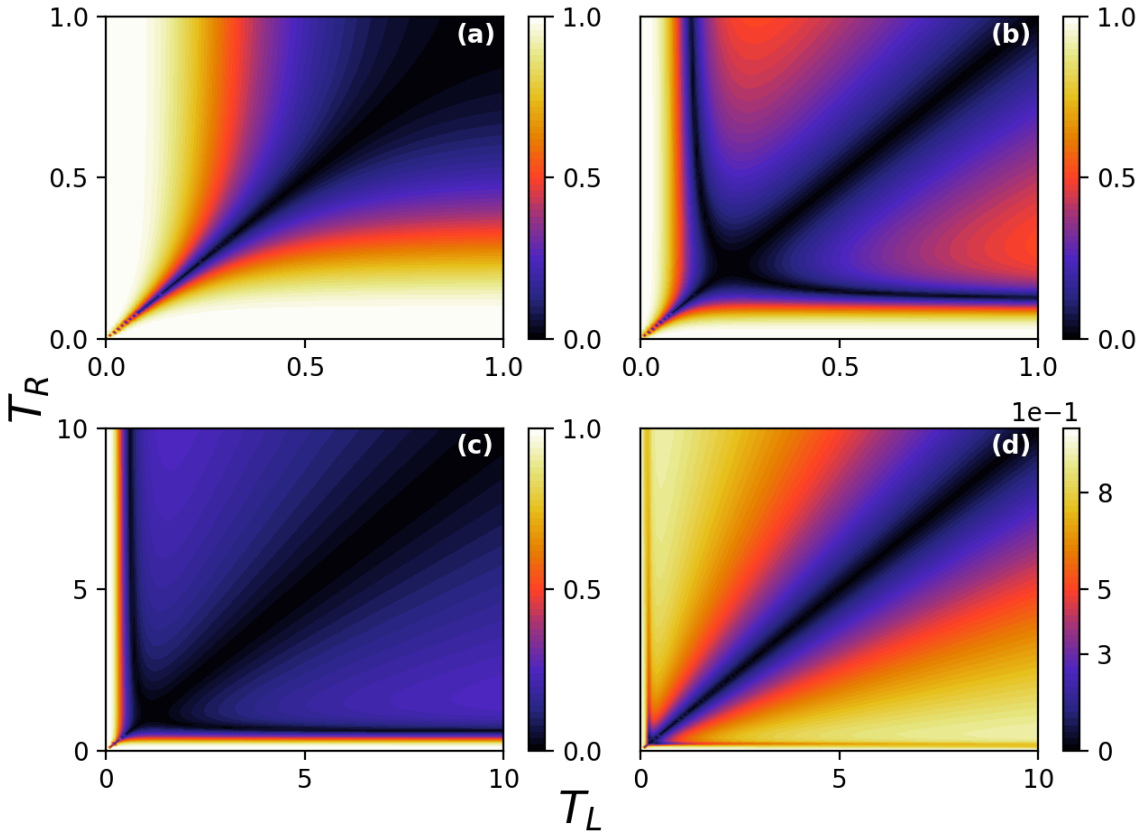


Figure 5.7: **Rectification values for flat spectral density.** Parameters are the same as in Fig. 5.6.

frequency of RQ parameters is bigger than the left to begin with, rectification is left to right. As discussed above, this is because the rectification direction is not only related to the transition frequencies but also how good are the baths to support them. ORQ parameters includes a transition ($\Omega$) much smaller than $T_{\max}$ for the right bath and one other transition ($\omega_{\mathrm{L}}$) comparable to $T_{\max}$ for the left bath. Thus, both transitions are supported easily by the baths. However, when both frequencies are comparable to $T_{\max}$, the smaller transition is better supported. Another way to understand this effect is to change the rates $\kappa_i(\omega)$. For example, the small $g$ regime rectification of RQ parameters (left to right) is reversed by increasing $\kappa_{\mathrm{R}}$, which enables right bath to better support its transitions $\Omega > \omega_{\mathrm{L}}$.

Figs. 5.6 (c) and (d) show the high temperature range for the ORQ parameters. In this case, there is little asymmetry at low $g$, because, as discussed above, baths become energetic enough to make the asymmetry induced by eigenvalues negligible. In other words, all the transitions, not just $\Omega$, are now order of magnitude smaller than $T_{\max}$. Diode behavior is realized back by increasing $g$, because it increases the required energy for the transitions. Rectification gets better as $g$ increases, but asymmetry again starts to weaken after a threshold is reached and eventually fades away at strong couplings. Rectification values for Figs. 5.6 (c) and (d) are presented in Figs. 5.7 (c) and (d).

Again we present the results for RQ parameters graphically in Appendix 7.4, and list them as follows. For the resonant case, asymmetry is apparent even at weak $g$ in high temperature range, and the rectification direction is left to right at low $g$, i.e. from lower frequency to higher. Since we relate the low temperature behavior of RQ parameters to energetic requirements of the transitions and baths abilities to support them, this might seem contradicting. Because, baths are energetic enough to easily support the transition at small $g$. However, left bath also has another transition, that is $\omega_{14} = \Omega + \omega_{\mathrm{L}}$, which is not supported properly at low temperatures, and left bath is now energetic enough. If we increase $g$, $\Omega$ increases, making left bath insufficient to support $\omega_{14}$, while $\Omega > \omega_{\mathrm{L}}$ is still in the order of $T_{\max}$, and rectification switches direction. In other words, transitions induced by right bath were bigger than $T_{\max}$ in low temperature regime, so the bath was unable to properly support it. However, high temperatures made the right bath more energetic, and it is now able to give the more energies to already available big transition. Again, further increase in $g$ results fading away of asymmetry in heat current, because it increases $\Omega$ excessively to the levels where both bath again becomes insufficient to support the transitions depending on it.

These results suggest that ORQ parameters provide a better control of the diode at low temperature range, and RQ or near resonant parameters are better at high range. This is simply because ORQ parameters has a really small transition which

is the only transition supported by right bath and is modified by changing either the qubit-qubit coupling strength or transition frequency of bare right qubit.

*Ohmic Spectral Density*

In this part, we follow the same division of temperature ranges, and Figs. (5.8) and (5.9) show the asymmetries and rectification values for both ORQ and RQ parameters. The numerical investigations give the following results.

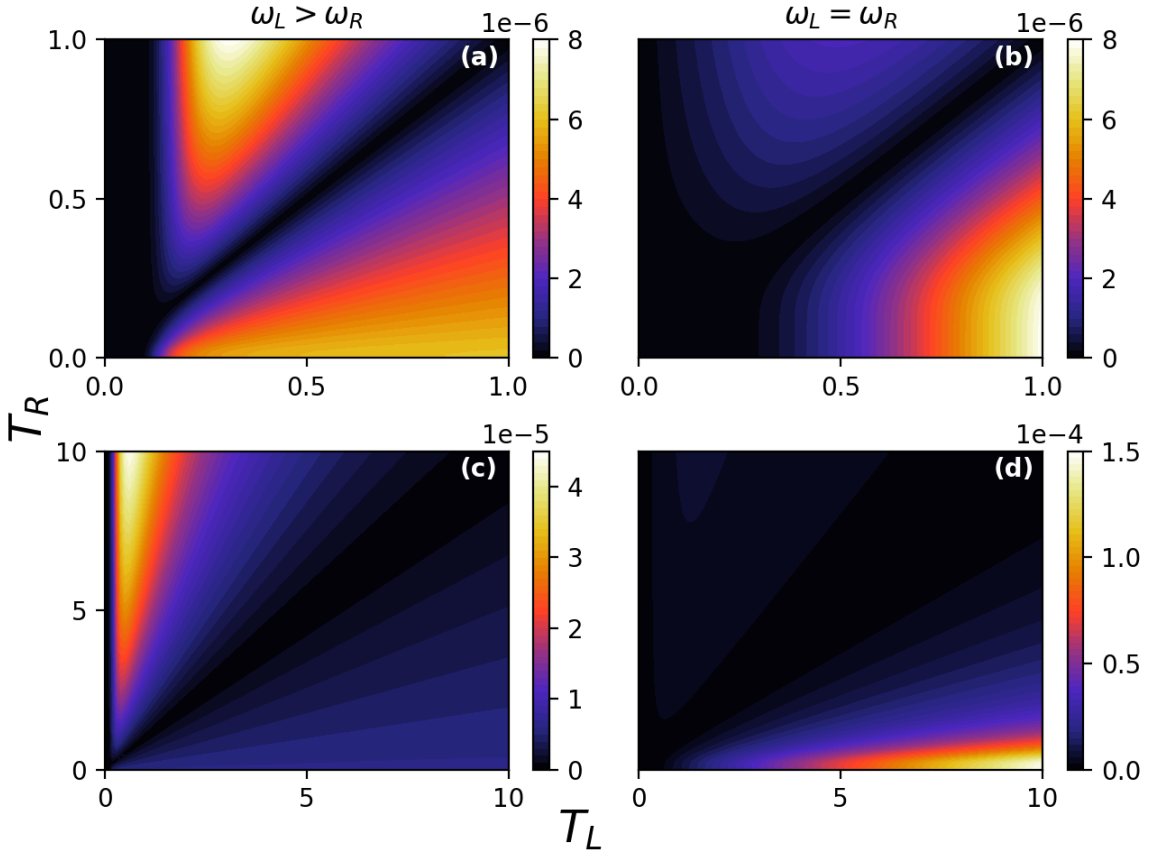


Figure 5.8: **Asymmetry in heat current for Ohmic spectral density.** In the low temperature range (a) and (b), magnitudes of the steady state heat currents from right bath to the system show asymmetries in both ORQ (titled $\omega_{\mathrm{L}} > \omega_{\mathrm{R}}$) and RQ (titled $\omega_{\mathrm{L}} = \omega_{\mathrm{R}}$) parameters, for $g = 0.02\omega_{\mathrm{L}}$. High temperature ranges for the same parameters are shown in (c) and (d).

In the Ohmic spectrum case, behavior of the rectification direction is the same as above for ORQ parameters, but the parametric regimes of $g$ are different. For example, at low temperatures, asymmetry is not strong at the same value of $g$ for which there is strong asymmetry in the flat spectrum case, shown in Fig. 5.8 (a). This difference is due to the frequency dependence of $\kappa_i(\omega)$, because now it is not just the transitions that are changing with $g$ but also the rates $\kappa_i(\omega)$. In other words, abilities of baths to support the transitions has dependence not only to their temperature but also to the transitions. Numerical investigations show that rectification direction is left to right at smaller coupling constants such that $g < 0.02\omega_{\mathrm{L}}$, and it is reversed when $g > 0.02\omega_{\mathrm{L}}$.

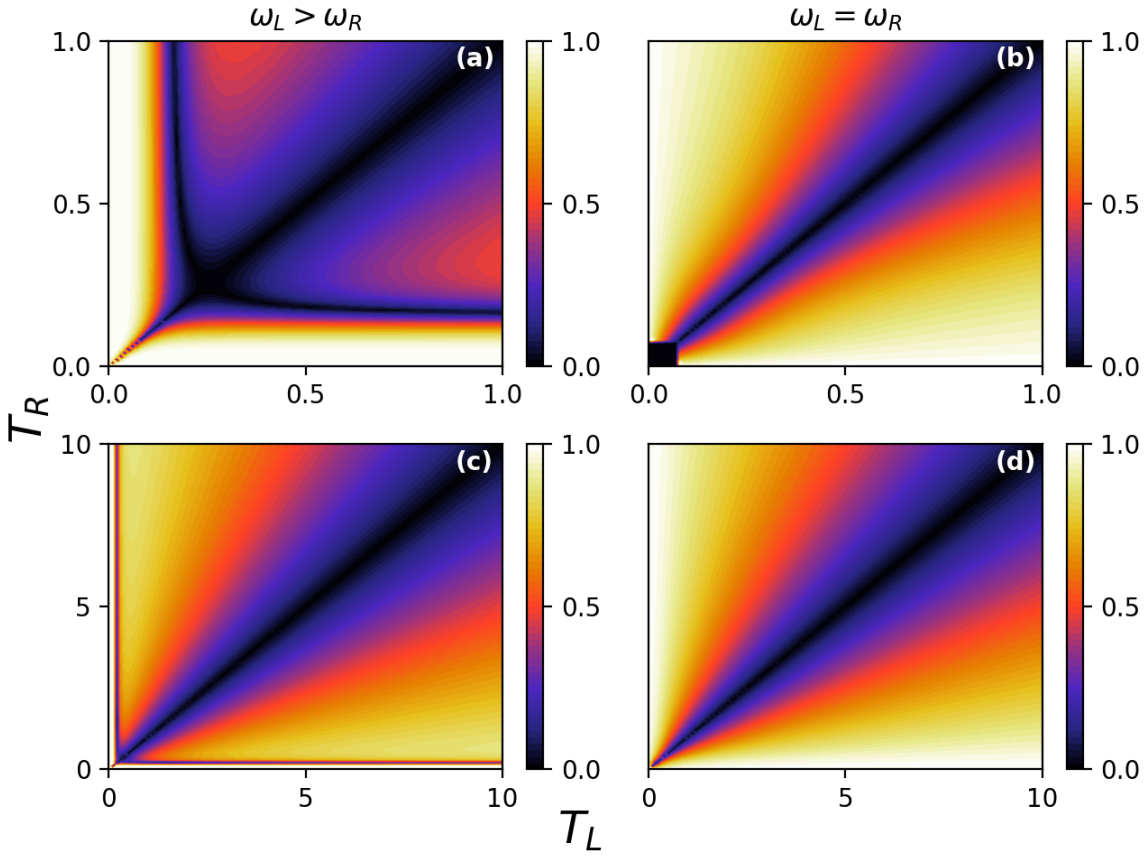


Figure 5.9: **Rectification values for Ohmic spectral density.** Parameters are the same as in Fig. 5.8

For the resonant case, behavior at low temperatures is the same with flat case in the way that rectification direction is always from left to right for any value of $g$. In other words, it shows a rectification from left to right as shown in Fig. 5.8 (b), and it does not change direction with changing $g$. Comparison of the low temperature results shown in Figs. 5.8 (a) and (b) suggest that the diode can be controlled by changing the transition frequencies.

Above behaviors of ORQ parameters for low the temperature range become more dominant at high temperature range as shown in Fig. 5.8 (c). Rectification values for high and low temperature ranges of the ORQ parameters are shown in Figs. 5.9 (a) and (c). In the case of resonant transitions, rectification direction is unidirectional for the low temperature range. However, numerical analysis shows that it becomes controllable at the high temperatures. This is explained by the same argument above on dependence of the rates to transition frequencies and the bath temperatures. In the low temperature case, numerical analysis shows that bath temperatures have a minor effect on supporting the transitions compared to the rates $\kappa_i(\omega)$. This is because both transition frequencies are in the order of $T_{\max}$. However, high temperatures are effective, and the rectification direction is now controllable by changing $g$. Also, even though Figs. 5.9 (c) and (d) (or (a) and (b)) have different rates $\kappa_i(\omega)$, their comparison suggests that by changing the transition frequencies rectification direction is controllable.

All these numerical observations for both spectral densities suggests that the control scheme for the diode to switch rectification direction or turn on/off the heat current is quite versatile and depends on the considered spectral density, and any optimization of rectification need to the interplay between transition energies and bath coupling strengths.

### *5.3.5 Asymmetry due to Transition Frequencies*

In the previous part, we show that the heat current is not symmetric by varying temperatures, and the qubit-environment couplings play role in the diode behavior.

In this section, we focus on the effects of transition frequencies on the rectification. We first present the analysis of our main model to demonstrate that it does not have the previously reported drawback [56], then we used an artificial case for a three-level system in Sec. 5.2 to clarify the physical mechanism.

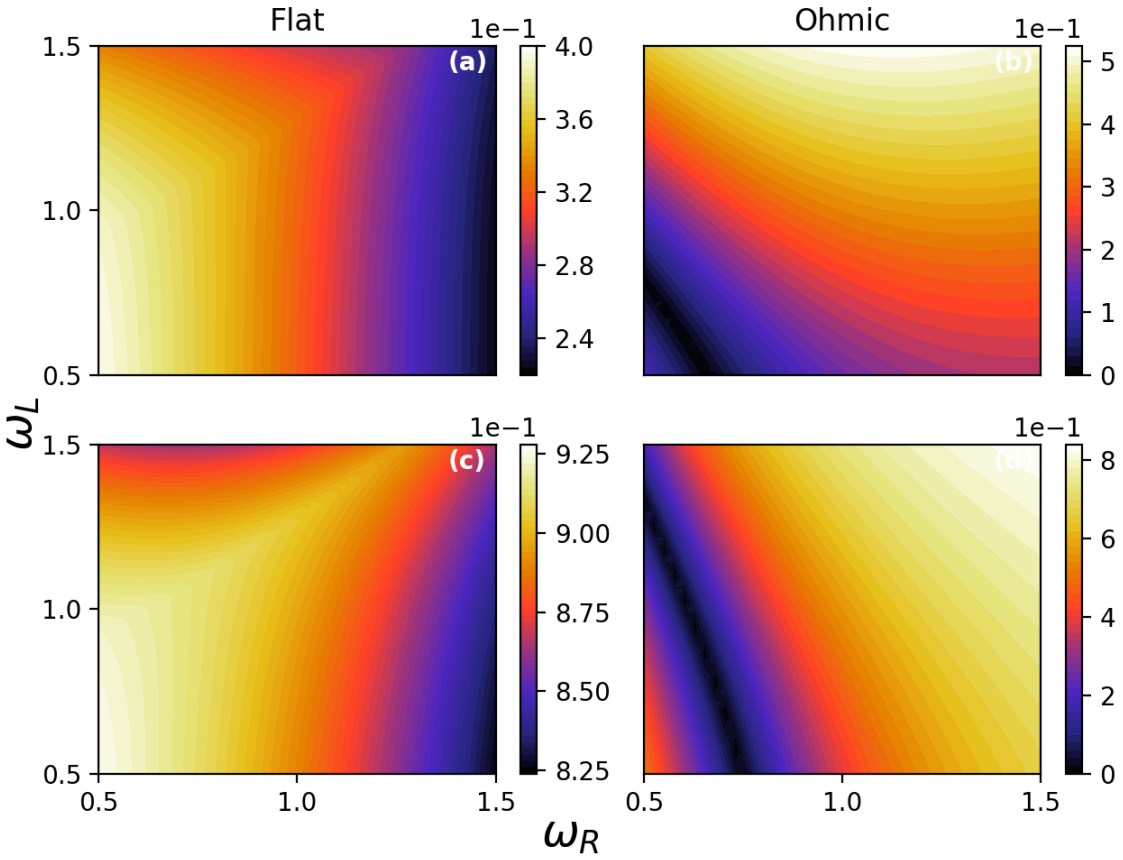


Figure 5.10: **Variations of transition frequencies.** Rectification values for flat (a) and (c) and Ohmic spectral densities (b) and (d) at low ($T_{\text{hot}} = 1$) (a) and (b) and high ($T_{\text{hot}} = 10$) (c) and (d) temperatures (with a cold bath at $T_{\text{cold}} = 0.5$.)

In the previous part, we show that the rectification of two interacting qubits system is controllable by changing $g$ and/or transition frequencies. In this part, we explicitly examine the effect of these parameters on diode behavior by fixing the temperatures. We again consider two temperature regimes. In the cases here, temperature of the colder bath is fixed to the value $0.5\omega_{\text{L}}$, and temperature of the hotter bath is $\omega_{\text{L}}$ for

low and $10\omega_{\mathrm{L}}$ for high temperature ranges. Unless $\omega_{\mathrm{L}}$ is varied, we consider its default value given in Sec. 5.3.4, and the scaling of the parameters is again in terms of the $\omega_{\mathrm{L}}$ in Sec. 5.3.4.

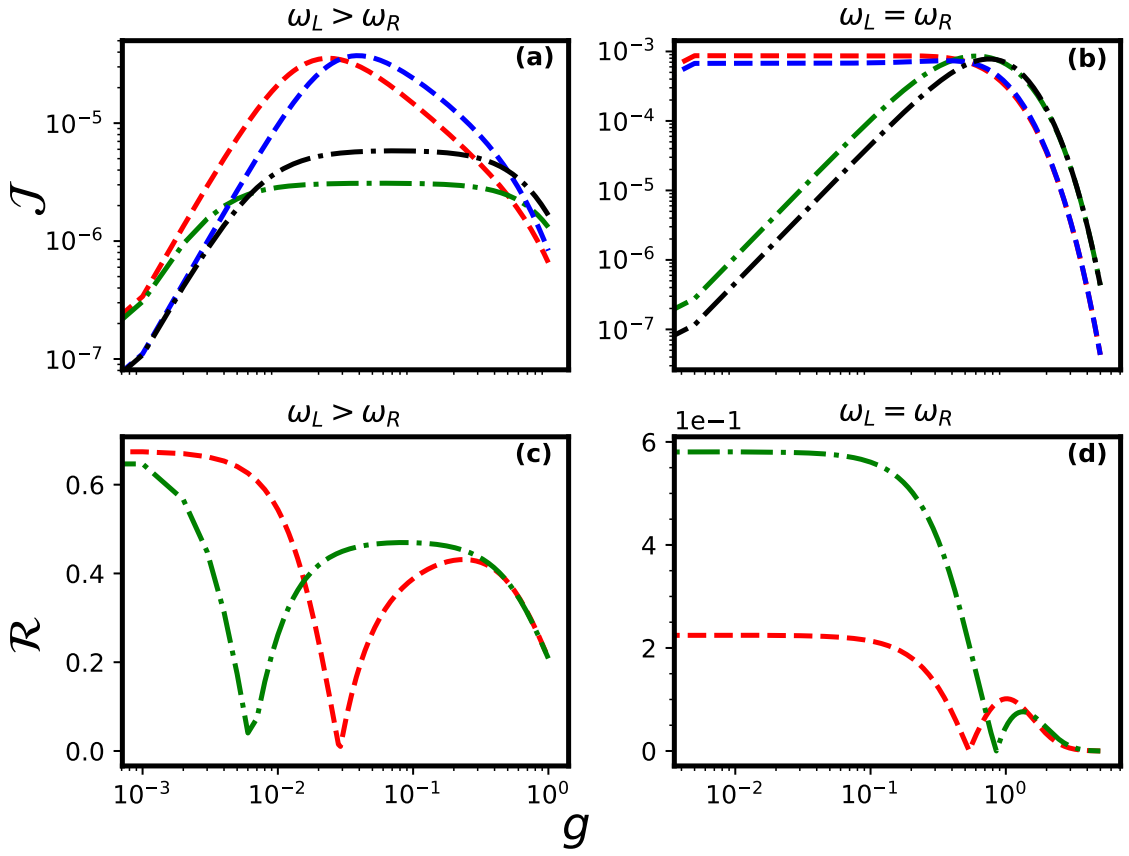


Figure 5.11: **Variations of g at low temperature regime.** Heat currents for flat (dash) and Ohmic (dash-dot) spectrum for both cases of $T_{\mathrm{R}} = 1 > T_{\mathrm{L}} = 0.5$ (red and green) and $T_{\mathrm{L}} = 1 > T_{\mathrm{R}} = 0.5$ (black and blue) are given in (a) and (b) for off-resonant and resonant parameters, respectively. The corresponding rectifications are given in (c) and (d).

The low temperature heat currents and the corresponding rectifications are presented in Fig. 5.11 for both ORQ and RQ parameters. In Fig. 5.11 (a), we see that there exist optimal values for $g$ in flat and a range of $g$ for the Ohmic spectrum with ORQ parameters that maximize the heat current. In the flat spectrum, the

optimal value for maximum current is close to the point where asymmetry switches (also vanishes). Thus, the rectification and heat current seems to have a trade-off in the flat spectrum. However, this observation is misleading since it is calculated for a particular temperature configuration.

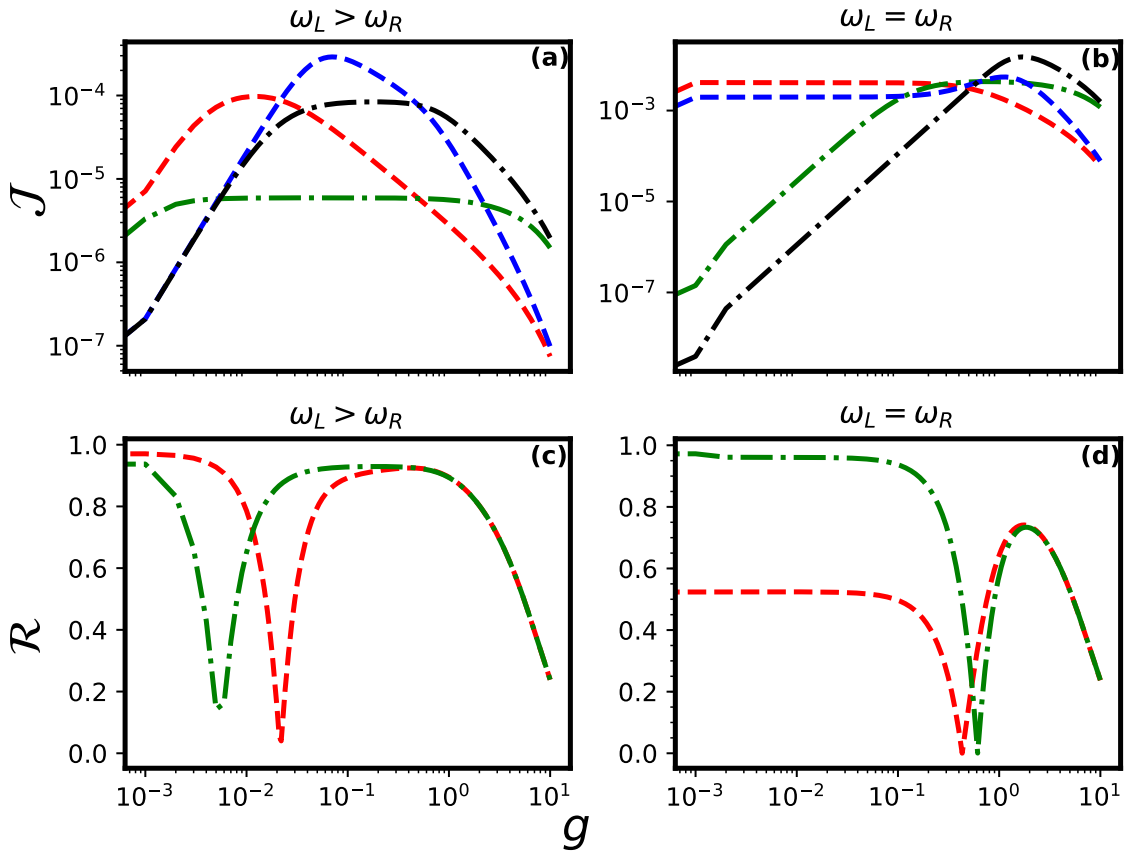


Figure 5.12: **Variations of g at high temperature regime.** Plot styles, colors and parameters are the same as in 5.11. Only difference is in the temperatures, here $T_{\mathrm{R}} = 10 > T_{\mathrm{L}} = 0.5$ (red and green) and $T_{\mathrm{L}} = 10 > T_{\mathrm{R}} = 0.5$

In the high temperature range, almost unit rectifications are obtainable at the optimum values of $g$ for the flat spectrum, as shown in Fig. 5.12 (a). Also, the dependence on transition frequencies affects the rectification values drastically. Fig. 5.11 (b) and Fig. 5.12 (b), suggests that RQ parameters with flat spectrum has higher heat currents, yet they give very weak rectifications in both temperature ranges. Again,

this is an inaccurate deduction because it is obtained for particular values of transition frequencies. In Figs. 5.10 (a) and (c), it is shown that better rectification values are realizable with different resonant transition frequencies at both low and high temperatures, respectively. Yet, this time, $g$ is fixed to $0.4\omega_{\mathrm{L}}$, and even higher rectification values are obtainable by changing it. In short, comprehensive numerical analysis shows that almost unit rectification factors can be obtained around the optimal $g$ at which the current is maximized, and rectification direction can be reversed by changing the transition frequencies.

As presented by all the discussions so far and especially in Fig. 5.10, results of the flat spectrum are different from the Ohmic case. Without any further discussions on results, we emphasize the difference of our model from previously proposed diode [56]. Figs. 5.11 (a) and (b) and Figs. 5.12 (a) and (b) show that heat current for the Ohmic spectral density is larger for RQ parameters than ORQ for both temperature ranges, and the rectification factors can be for high heat currents. In other words, there is no trade-off between heat current and rectification value when higher heat current values are obtained by changing the ratio between transition frequencies. Also, the resonant transition frequencies show almost unit rectification factors especially at high temperature range, as also shown in Figs. 5.10 (b) and (d). The reason behind these differences is that the asymmetry introduced to the Hamiltonian is in the interaction term, which lead to asymmetric coupling of energy levels to baths, so rectification is obtained even when qubits are resonant, and their coupling to environments is symmetric.

# Chapter 6

# CONCLUSION AND OUTLOOK

We analyzed a quantum thermal diode composed of two interacting qubits together with two other toy models. We analyzed the interacting qubits model by deriving the global master equation. We have calculated an analytical expression for the heat current and carried numerical examinations of it for various cases of variable variations. We have used the rectification factor to quantify the diode quality and carried our calculations for both flat and Ohmic spectral densities.

We found that the rectification direction is controllable by changing the coupling strength between qubits and/or their transition frequencies, and we described the ways to control the diode for different parameters and ranges of temperatures. We identified the mechanism behind our results as the interplay between transition frequencies and bath coupling strengths, and we demonstrate it by using two toy models. We connect the mechanism to an asymmetry either in system Hamiltonian or bath couplings. The main result of our paper is the establishment of the mechanism, which suggests that the same results will be apparent in corresponding bosonic models, which include harmonic oscillators instead of qubits. It is trivial to calculate and see that a single harmonic oscillator has rectified heat, if it has asymmetric environmental coupling.

To sum up, we conclude that the physical mechanism enabling the diode behavior is the transitions between dressed eigenstates and abilities of the baths to support these transitions. Thus, an asymmetric coupling, either to bath or among the subsystems, empower the two interacting resonant qubits to behave as a diode, and allow more control on the parameters to optimize the diode quality without any trade-off.

## *6.1 Outlook*

The interplay leading to rectification is analyzed by using Markovian master equations, which relies on weak environmental couplings, but environmental couplings comprise an important part of the involved mechanism. Thus, non-Markovian approach is required to properly analyze the mechanism, and we plan to carry these analyses using two interacting qubits. Also, we are going to analyze the smallest possible diode, which is a single qubit.

For the two interacting qubits with the Hamiltonian,

$$H = \frac{\omega_1}{2}\sigma_1^z + \frac{\omega_2}{2}\sigma_2^z + g(\sigma_1^+\sigma_2^- + \sigma_1^-\sigma_2^+), \tag{6.1}$$

the non-Markovian master equation is present in the literature for zero temperature baths [103] and for single-excitation limit [104]. Thus, we will modify these derivations for finite temperature baths. The reason for choosing this symmetric Hamiltonian (Eq. 6.1) is to better understand the effect of bath asymmetry on diode behavior in non-Markovian case. Also, the non-Markovian master equation for a single qubit is present in Ref. [105].

Finally, quantum thermal diode models lead to design of quantum thermal transistors [51, 52, 53], and advantages of our opto-mechanically interacting qubits diode model motivates an analysis on diode models with such coupling.

# Chapter 7

# APPENDIX

## *7.1 Quantum Dynamics of Three Interacting Qubits*

Total heat current to the system is sum of the heat currents from the left and right baths, and they are calculated and given respectively as

$$\mathcal{J}_{\rm Total} = {\rm Tr}\left[\hat{\mathcal{L}}[\hat{\rho}]\hat{H}\right] = \overbrace{{\rm Tr}\left[\hat{\mathcal{L}}_{\rm L}[\hat{\rho}]\hat{H}\right]}^{\mathcal{J}_{\rm L}} + \overbrace{{\rm Tr}\left[\hat{\mathcal{L}}_{\rm R}[\hat{\rho}]\hat{H}\right]}^{\mathcal{J}_{\rm R}}, \tag{7.1}$$

$$\mathcal{J}_{\rm L} = {\rm Tr}\left[\hat{\mathcal{L}}_{\rm L}[\hat{\rho}]\hat{H}\right] = -\frac{A}{2}\omega_{\rm L} - \frac{B}{2}\omega_{\rm L}\left\langle\hat{\sigma}_1^z\right\rangle + \frac{AD}{2}\left\langle\hat{S}^x\right\rangle + \frac{BD}{2}\left\langle\hat{\sigma}_1^z\hat{S}^x\right\rangle, \tag{7.2}$$

$$\mathcal{J}_{\rm R} = {\rm Tr}\left[\hat{\mathcal{L}}_{\rm R}[\hat{\rho}]\hat{H}\right] = -C\omega_{\rm R} - \frac{C}{2}\omega_{\rm R}\left\langle\hat{S}^z\right\rangle + \frac{CD}{4}\left\langle\hat{\sigma}_1^z\hat{S}^x\right\rangle, \tag{7.3}$$

where $A = \kappa_{\rm L}$, $B = \kappa_{\rm L}(1 + 2\bar{n}_{\rm L}(\omega_{\rm L}))$, $C = \kappa_{\rm R}$, and $D = 2g$. Also, equations of motions for the operators needed to calculate these heat currents form a closed set of equations and they are given as

$$\frac{d}{dt}\left\langle\hat{\sigma}_1^z\right\rangle = -A - B\left\langle\hat{\sigma}_1^z\right\rangle, \tag{7.4}$$

$$\frac{d}{dt}\left\langle\hat{S}^z\right\rangle = -C\left(2 + \left\langle\hat{S}^z\right\rangle\right) - D\left(\left\langle\hat{\sigma}_1^z, \hat{S}^y\right\rangle + \left\langle\hat{\sigma}_1^z\right\rangle\left\langle\hat{S}^y\right\rangle\right), \tag{7.5}$$

$$\frac{d}{dt}\left\langle\hat{S}^y\right\rangle = D\left(\left\langle\hat{\sigma}_1^z\hat{S}^z\right\rangle + \left\langle\hat{\sigma}_1^z\right\rangle\left\langle\hat{S}^z\right\rangle\right) - \frac{C}{2}\left\langle\hat{S}^y\right\rangle + \omega_{\rm R}\left\langle\hat{S}^x\right\rangle, \tag{7.6}$$

$$\frac{d}{dt}\left\langle\hat{S}^x\right\rangle = -\frac{C}{2}\left\langle\hat{S}^x\right\rangle - \omega_{\rm R}\left\langle\hat{S}^y\right\rangle, \tag{7.7}$$

$$\frac{d}{dt}\left\langle\hat{\sigma}_1^z, \hat{S}^z\right\rangle = -(B + C)\left\langle\hat{\sigma}_1^z, \hat{S}^z\right\rangle + D\left\langle\hat{\sigma}_1^z\right\rangle\left\langle\hat{\sigma}_1^z, \hat{S}^y\right\rangle - D(1 - \left\langle\hat{\sigma}_1^z\right\rangle^2)\left\langle\hat{S}^y\right\rangle, \tag{7.8}$$

$$\frac{d}{dt}\left\langle\hat{\sigma}_1^z, \hat{S}^y\right\rangle = -(B + \frac{C}{2})\left\langle\hat{\sigma}_1^z, \hat{S}^y\right\rangle + \omega_{\rm R}\left\langle\hat{\sigma}_1^z, \hat{S}^x\right\rangle + D(1 - \left\langle\hat{\sigma}_1^z\right\rangle^2)\left\langle\hat{S}^z\right\rangle - D\left\langle\hat{\sigma}_1^z\right\rangle\left\langle\hat{\sigma}_1^z, \hat{S}^z\right\rangle, \tag{7.9}$$

$$\frac{d}{dt}\left\langle\hat{\sigma}_1^z, \hat{S}^x\right\rangle = -(B + \frac{C}{2})\left\langle\hat{\sigma}_1^z, \hat{S}^x\right\rangle - \omega_{\rm R}\left\langle\hat{\sigma}_1^z, \hat{S}^y\right\rangle, \tag{7.10}$$

where we have used the collective operators $\hat{S}^i = \hat{\sigma}_2^i + \hat{\sigma}_3^i$ and the correlations $\langle\hat{\sigma}_1^z, \hat{S}^i\rangle = \langle\hat{\sigma}_1^z\hat{S}^i\rangle - \langle\hat{\sigma}_1^z\rangle\langle\hat{\sigma}_1^z\rangle$.

Steady state relations among the operators and correlations are

$$\begin{aligned}
\langle\hat{\sigma}_1^z\rangle_{\rm ss} &= -\frac{1}{1+2\bar{n}_H} \equiv A_0 && (7.11)\\
\langle\hat{S}^z\rangle_{\rm ss} &= -2 - A_1(\langle\hat{\sigma}_1^z,\hat{S}^y\rangle_{\rm ss} + A_0\langle\hat{S}^y\rangle_{\rm ss}), && (7.12)\\
\langle\hat{S}^y\rangle_{\rm ss} &= 2A_2\langle\hat{S}^x\rangle_{\rm ss} + 2A_1\langle\hat{\sigma}_1^z,\hat{S}^z\rangle_{\rm ss} + 4A_1A_0\langle\hat{S}^z\rangle_{\rm ss}\,,\\
\langle\hat{S}^x\rangle_{\rm ss} &= -2A_2\langle\hat{S}^y\rangle_{\rm ss}\,, && (7.13)\\
\langle\hat{\sigma}_1^z,\hat{S}^z\rangle_{\rm ss} &= A_3((1-A_0^2)\langle\hat{S}^y\rangle_{\rm ss} - A_0\langle\hat{\sigma}_1^z,\hat{S}^y\rangle_{\rm ss}), && (7.14)\\
\langle\hat{\sigma}_1^z,\hat{S}^y\rangle_{\rm ss} &= A_4\langle\hat{\sigma}_1^z,\hat{S}^x\rangle_{\rm ss} + A_5(1-A_0^2)\langle\hat{S}^z\rangle_{\rm ss} - A_5A_0\langle\hat{\sigma}_1^z,\hat{S}^z\rangle_{\rm ss}\,,\\
\langle\hat{\sigma}_1^z,\hat{S}^x\rangle_{\rm ss} &= -A_4\langle\hat{\sigma}_1^z,\hat{S}^y\rangle_{\rm ss} + A_5(1-A_0^2)\langle\hat{S}^z\rangle_{\rm ss} - A_5A_0\langle\hat{\sigma}_1^z,\hat{S}^z\rangle_{\rm ss}\,, && (7.15)
\end{aligned}$$

where we have defined $A_1 = \frac{D}{C}$, $A_2 = \frac{\omega_{\rm R}}{C}$, $A_3 = \frac{D}{C+B}$, $A_4 = \frac{2\omega_{\rm R}}{C+2B}$ and, $A_5 = \frac{2D}{C+2B}$. Then, using these relations, steady state heat currents from hot and cold baths to the system is obtained respectively as

$$\begin{aligned}
\mathcal{J}_{\rm L}^{\rm ss} &= \kappa_{\rm L}(1+2\bar{n}_{\rm L}(\omega_{\rm L}))g\langle\hat{\sigma}_1^z,\hat{S}^x\rangle_{\rm ss}\,, && (7.16)\\
\mathcal{J}_{\rm R}^{\rm ss} &= -\kappa_{\rm L}(1+2\bar{n}_{\rm L}(\omega_{\rm L}))g\langle\hat{\sigma}_1^z,\hat{S}^x\rangle_{\rm ss}\,, && (7.17)
\end{aligned}$$

which checks that the total heat current is zero.

## *7.2 Dressing Two Interacting Qubits*

We dress the Hamiltonian in Eq. 4.12 using the unitary transformation given in Eq. 4.13. We write this transformation in terms of rotation operations around the related axis by $\frac{\theta}{2}$ degrees, so let us first give the definition rotation operator [65] by an angle $\phi$ around the $\alpha = x, y, z$ axis as

$$\mathfrak{D}_\alpha(\phi) = e^{-i\phi\hat{\sigma}_\alpha}. \tag{7.18}$$

We put this into another form, which is more useful for our purpose here, as

$$\begin{aligned}
\mathfrak{D}_\alpha(\frac{\theta}{2}) = e^{-i\frac{\theta}{2}\hat{\sigma}_\alpha} = \sum_{k=0}^{\infty}\left(\frac{-i\theta}{2}\right)^k\hat{\sigma}_\alpha &= \left(\mathbb{1} - \frac{1}{2!}\left(\frac{\theta}{2}\right)^2(\hat{\sigma}_\alpha)^2 + \cdots\right)\\
&\quad -i\left(\frac{\theta}{2}\hat{\sigma}_\alpha - \frac{1}{3!}\left(\frac{\theta}{2}\right)^3(\hat{\sigma}_\alpha)^3 + \cdots\right),
\end{aligned}$$

which is rewritten, by using the fact that $\hat{\sigma}_\alpha^n = \begin{cases} \mathbb{1}, & \text{for even } n \\ \hat{\sigma}_\alpha, & \text{for odd } n \end{cases}$ for the Pauli x,y,z, operators, as

$$\begin{aligned} \mathfrak{D}_\alpha(\frac{\theta}{2}) &= \overbrace{\left(1 - \frac{1}{2!}\left(\frac{\theta}{2}\right)^2 + \cdots\right)}^{\cos\frac{\theta}{2}} \mathbb{1} - i \overbrace{\left(\frac{\theta}{2} - \frac{1}{3!}\left(\frac{\theta}{2}\right)^3 + \cdots\right)}^{\sin\frac{\theta}{2}} \hat{\sigma}_\alpha \\ &= (\cos\frac{\theta}{2})\mathbb{1} - i(\sin\frac{\theta}{2})\hat{\sigma}_\alpha. \end{aligned} \tag{7.19}$$

Other two useful identities that we use below are given as

$$\cos(\phi\hat{\sigma}_\alpha) = \mathbb{1} - \frac{1}{2!}(\phi)^2(\hat{\sigma}_\alpha)^2 + \cdots = \left(1 - \frac{1}{2!}(\phi)^2 + \cdots\right)\mathbb{1} = (\cos\phi)\mathbb{1} \tag{7.20}$$

$$\sin(\phi\hat{\sigma}_\alpha) = \phi\hat{\sigma}_\alpha - \frac{1}{3!}(\phi)^3(\hat{\sigma}_\alpha)^3 + \cdots = \left(\phi - \frac{1}{3!}(\phi)^3 + \cdots\right)\mathbb{1} = (\sin\phi)\hat{\sigma}_\alpha \tag{7.21}$$

Then, using these identities together with the expression for rotation operator in Eqn 7.19, we transform any Pauli spin operator $\hat{\sigma}^\alpha_{\mathrm{L/R}}$ of left (L) or right (R) qubits as the below $\hat{\sigma}^x_{\mathrm{L}}$ transformation.

$$\begin{aligned} \hat{\tilde{\sigma}}^x_{\mathrm{L}} &= U\hat{\sigma}^x_{\mathrm{L}}U^\dagger = \mathfrak{D}^{\mathrm{L}}_z(\frac{\theta}{2}\hat{\sigma}^y_{\mathrm{R}})\hat{\sigma}^x_{\mathrm{L}}((\mathfrak{D}^{\mathrm{L}}_z)^\dagger(\frac{\theta}{2}\hat{\sigma}^y_{\mathrm{R}})) \\ &= ((\cos\frac{\theta}{2})\mathbb{1} - i(\sin\frac{\theta}{2})\hat{\sigma}^y_{\mathrm{R}})\hat{\sigma}^x_{\mathrm{L}}((\cos\frac{\theta}{2})\mathbb{1} + i(\sin\frac{\theta}{2})\hat{\sigma}^y_{\mathrm{R}}) \\ &= \overbrace{(\cos^2\frac{\theta}{2} - \sin^2\frac{\theta}{2})}^{\cos\theta}\hat{\sigma}^x_{\mathrm{L}} + i\overbrace{\sin\frac{\theta}{2}\cos\frac{\theta}{2}}^{\frac{1}{2}\sin\theta}\underbrace{(\hat{\sigma}^x_{\mathrm{L}}\hat{\sigma}^z_{\mathrm{L}} - \hat{\sigma}^z_{\mathrm{L}}\hat{\sigma}^x_{\mathrm{L}})}_{[\hat{\sigma}^x_{\mathrm{L}},\hat{\sigma}^z_{\mathrm{L}}]=-2i\hat{\sigma}^y_{\mathrm{L}}}\hat{\sigma}^y_{\mathrm{R}} \\ &= (\cos\theta)\hat{\sigma}^x_{\mathrm{L}} + (\sin\theta)\hat{\sigma}^y_{\mathrm{R}}\hat{\sigma}^y_{\mathrm{L}}, \end{aligned} \tag{7.22}$$

where we also use the fact that the operators of left and right qubits commute. Rest of the operators are transformed similarly. Then, we write the dressed Hamiltonian with the same transformation as

$$\hat{\tilde{H}} = U\hat{H}U^\dagger = \frac{\omega_{\mathrm{L}}}{2}\hat{\sigma}^z_{\mathrm{L}} + (\frac{\omega_{\mathrm{R}}}{2}\cos\theta - g\sin\theta)\hat{\sigma}^z_{\mathrm{R}} + (\frac{\omega_{\mathrm{R}}}{2}\sin + g\cos\theta)\hat{\sigma}^z_{\mathrm{L}}\hat{\sigma}^x_{\mathrm{R}}, \tag{7.23}$$

which is given in terms of the dressed operator as

$$\hat{\tilde{H}} = \frac{\omega_{\mathrm{L}}}{2}\hat{\tilde{\sigma}}^z_{\mathrm{L}} + (\frac{\omega_{\mathrm{R}}}{2}\cos\theta + g\sin\theta)\hat{\tilde{\sigma}}^z_{\mathrm{R}} + (-\frac{\omega_{\mathrm{R}}}{2}\sin + g\sin\theta)\hat{\tilde{\sigma}}^z_{\mathrm{L}}\hat{\tilde{\sigma}}^x_{\mathrm{R}}. \tag{7.24}$$

We want this Hamiltonian to be diagonal, which means that the last term should has a zero coefficient. Therefore, we choose a $\theta$ such that $g\cos\theta = \frac{\omega_{\rm R}}{2}\sin\theta$, which gives the angle given in Eq.4.14, and we obtain the diagonalized Hamiltonian given in Eq. 4.21.

### *7.3 Dynamics of the Dressed Two Qubits*

Equations of motions for the relevant dynamical observables of our system are determined from the master equation, Eq. (4.28), and given by

$$\begin{aligned}
\frac{d}{dt}\langle\hat{\tilde{\sigma}}^z_{\rm L}\rangle &= \cos^2\theta[G_{\rm L}(-\omega_{\rm L})\langle\mathbb{A}\rangle - G_{\rm L}(\omega_{\rm L})\langle\mathbb{B}\rangle] + \frac{1}{2}\sin^2\theta[G_{\rm L}(\omega_1)\langle\mathbb{AD}\rangle - G_{\rm L}(-\omega_1)\langle\mathbb{BC}\rangle \\
&\quad + G_{\rm L}(-\omega_2)\langle\mathbb{AC}\rangle - G_{\rm L}(\omega_2)\langle\mathbb{BD}\rangle] \\
\frac{d}{dt}\langle\hat{\tilde{\sigma}}^z_{\rm R}\rangle &= \cos^2\theta[G_{\rm R}(-\Omega)\langle\mathbb{C}\rangle - G_{\rm R}(\Omega)\langle\mathbb{D}\rangle] + \frac{1}{2}\sin^2\theta[-G_{\rm L}(\omega_1)\langle\mathbb{AD}\rangle + G_{\rm L}(-\omega_1)\langle\mathbb{BC}\rangle \\
&\quad + G_{\rm L}(-\omega_2)\langle\mathbb{AC}\rangle - G_{\rm L}(\omega_2)\langle\mathbb{BD}\rangle] \\
\frac{d}{dt}\langle\hat{\tilde{\sigma}}^z_{\rm L}\hat{\tilde{\sigma}}^z_{\rm R}\rangle &= \cos^2\theta[G_{\rm L}(-\omega)\langle\mathbb{A}\hat{\tilde{\sigma}}^z_{\rm R}\rangle - G_{\rm L}(\omega)\langle\mathbb{B}\hat{\tilde{\sigma}}^z_{\rm R}\rangle + G_{\rm R}(-\Omega)\langle\mathbb{D}\hat{\tilde{\sigma}}^z_{\rm L}\rangle - G_{\rm R}(\Omega)\langle\mathbb{C}\hat{\tilde{\sigma}}^z_{\rm L}\rangle],
\end{aligned}$$

where we use the operators $\mathbb{A} = (\mathbb{1} - \hat{\tilde{\sigma}}^z_{\rm L})$, $\mathbb{B} = (\mathbb{1} + \hat{\tilde{\sigma}}^z_{\rm L})$, $\mathbb{C} = (\mathbb{1} - \hat{\tilde{\sigma}}^z_{\rm R})$, and $\mathbb{D} = (\mathbb{1} + \hat{\tilde{\sigma}}^z_{\rm R})$.

The heat currents evaluate to

$$\begin{aligned}
\mathcal{J}_{\rm L} = &\quad \frac{1}{2}\omega_{\rm L}\cos^2\theta[G_{\rm L}(-\omega_{\rm L})\langle\mathbb{A}\rangle - G_{\rm L}(\omega_{\rm L})\langle\mathbb{B}\rangle] + \frac{1}{4}\sin^2\theta[\omega_1 G_{\rm L}(-\omega_1)\langle\mathbb{BC}\rangle - \omega_1 G_{\rm L}(\omega_1)\langle\mathbb{AD}\rangle \\
&- \omega_2 G_{\rm L}(\omega_2)\langle\mathbb{BD}\rangle + \omega_2 G_{\rm L}(-\omega_2)\langle\mathbb{AC}\rangle], \qquad (7.25) \\
\mathcal{J}_{\rm R} &= \frac{1}{2}\Omega\cos^2\theta[G_{\rm R}(-\Omega)\langle\mathbb{C}\rangle - G_{\rm R}(\Omega)\langle\mathbb{D}\rangle]. \qquad (7.26)
\end{aligned}$$

Substation of transformed operator relation Eq. (4.20) to Eq. (7.26) gives the heat current relation in terms of bare operators, Eq. (5.12). Even though, the Eqs. (7.25)-(7.26) are easy to solve, the analytical expressions are too bulky to present. We do not provide them here, but we just state that $\mathcal{J}_{\rm L} + \mathcal{J}_{\rm R} = 0$ at the steady state.

## *7.4 Heat Currents of the Dressed Two Qubits*

Here, we present numerical results for the steady heat current from right bath to system $\mathcal{J}_{\mathrm{R}}$ for both ORQ and RQ parameter. Only difference is that we consider the rates $\kappa_{\mathrm{R}} = \kappa_{\mathrm{L}} = 0.001$ for both parameters, and we state qubit-qubit coupling strengths $g$ at the title of each plot. We present the flat and ohmic spectrum separately, and we divide each of them into two parts, which give the ORQ and RQ results.

### *7.4.1 Flat Spectrum*

*off-Resonant Qubits*

The low temperature regime heat currents for the ORQ parameters are given as

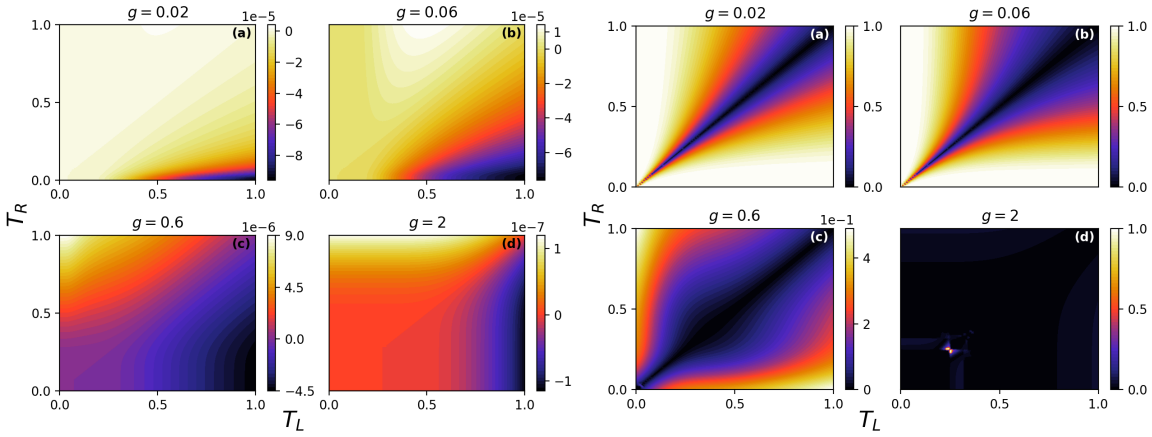


a: Heat Current $\mathcal{J}_{\mathrm{R}}$ b: Rectification $\mathcal{R}$

Figure 7.1: **ORQ Flat Spectrum Low temperature.**

The high temperature regime heat currents for the ORQ parameters are given as

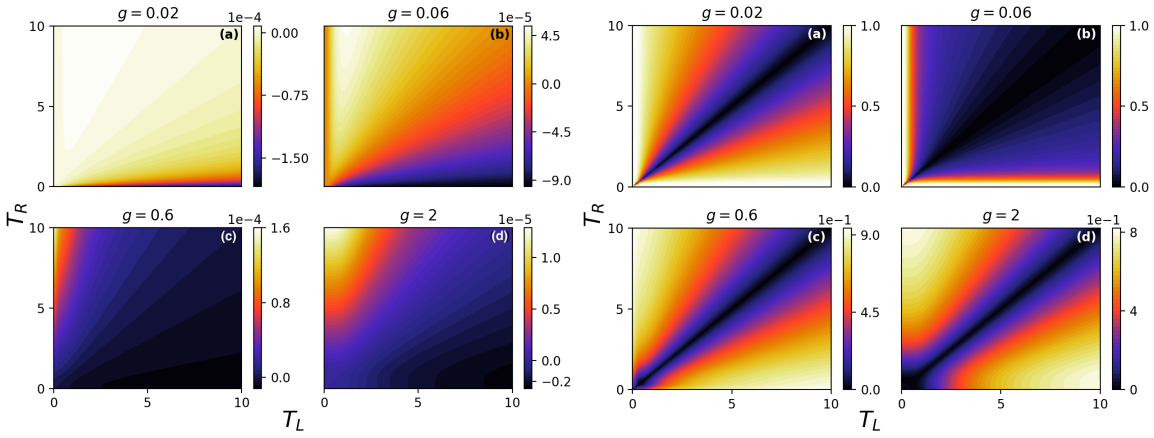


a: Heat Current $\mathcal{J}_{\mathrm{R}}$ b: Rectification $\mathcal{R}$

Figure 7.2: **ORQ Flat Spectrum High temperature.**

*Resonant Qubits*

The low temperature regime heat currents for the RQ parameters are given as

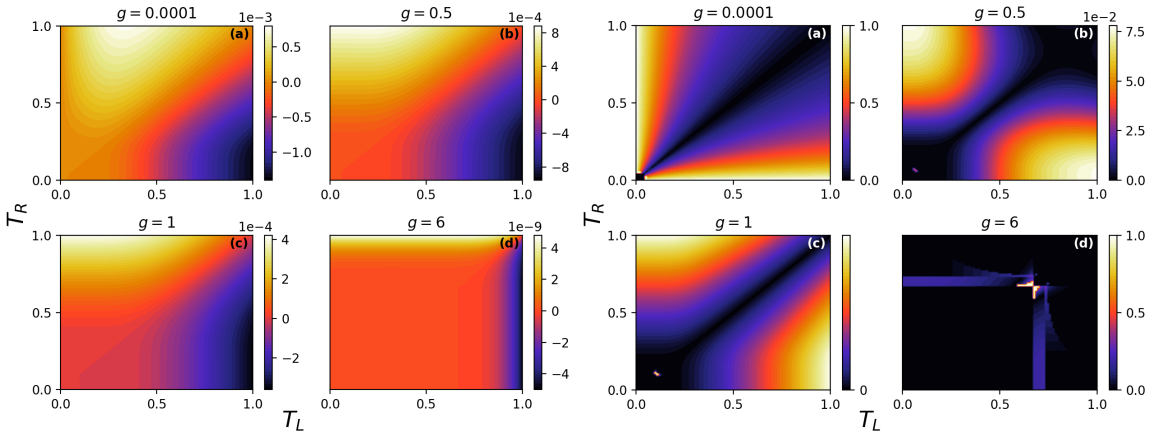


a: Heat Current $\mathcal{J}_{\mathrm{R}}$ b: Rectification $\mathcal{R}$

Figure 7.3: **RQ Flat Spectrum Low temperature.**

The high temperature regime heat currents for the RQ parameters are given as

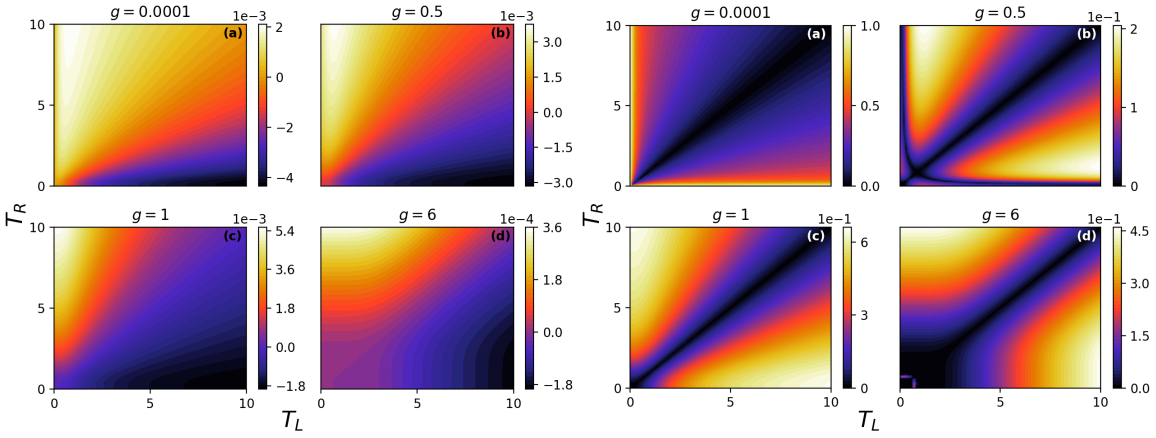


a: Heat Current $\mathcal{J}_{\mathrm{R}}$ b: Rectification $\mathcal{R}$

Figure 7.4: **RQ Flat Spectrum High temperature.**

### *7.4.2 Ohmic Spectrum*

*off-Resonant Qubits*

The low temperature regime heat currents for the ORQ parameters are given as

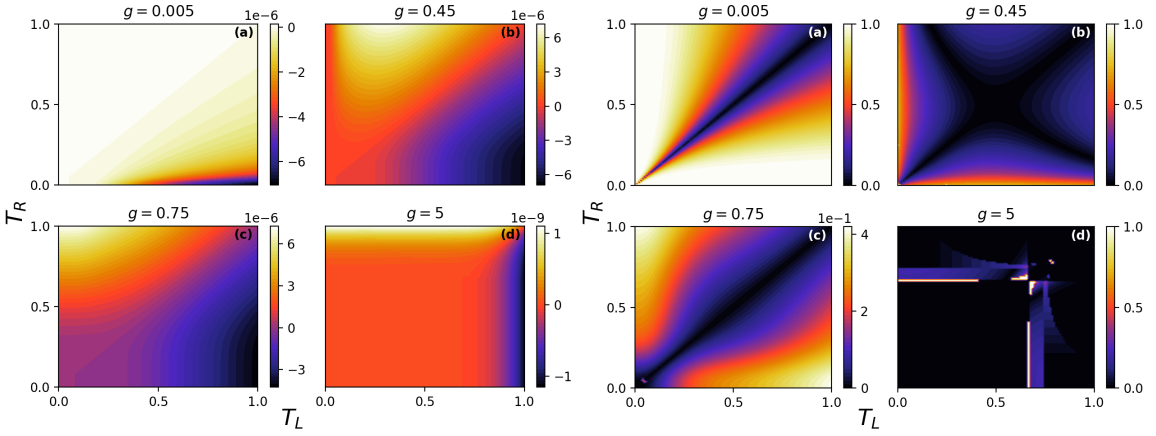


a: Heat Current $\mathcal{J}_{\mathrm{R}}$ b: Rectification $\mathcal{R}$

Figure 7.5: **ORQ Ohmic Spectrum Low temperature.**

The high temperature regime heat currents for the ORQ parameters are given as

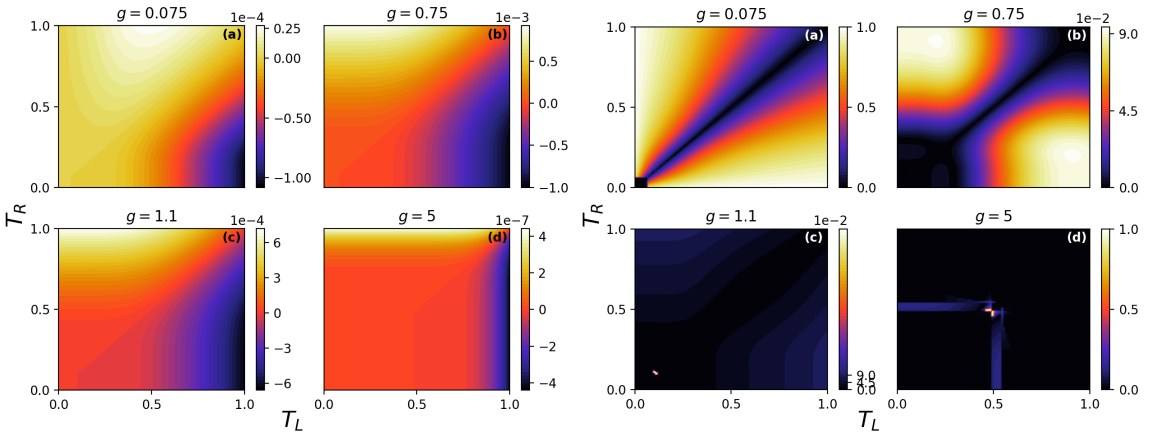


a: Heat Current $\mathcal{J}_{\mathrm{R}}$ b: Rectification $\mathcal{R}$

Figure 7.6: **ORQ Ohmic Spectrum High temperature.**

*Resonant Qubits*

The low temperature regime heat currents for the RQ parameters are given as

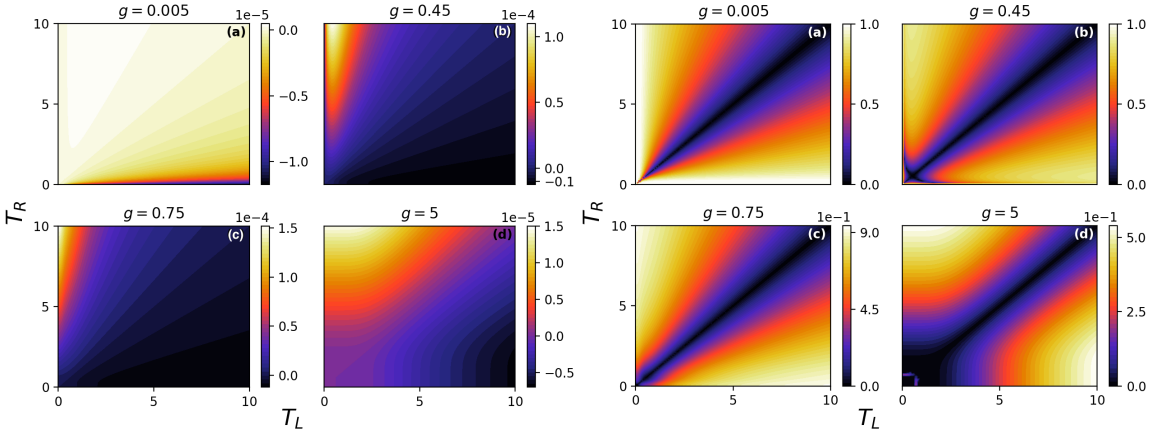


a: Heat Current $\mathcal{J}_{\mathrm{R}}$ b: Rectification $\mathcal{R}$

Figure 7.7: **RQ Ohmic Spectrum Low temperature.**

The high temperature regime heat currents for the RQ parameters are given as

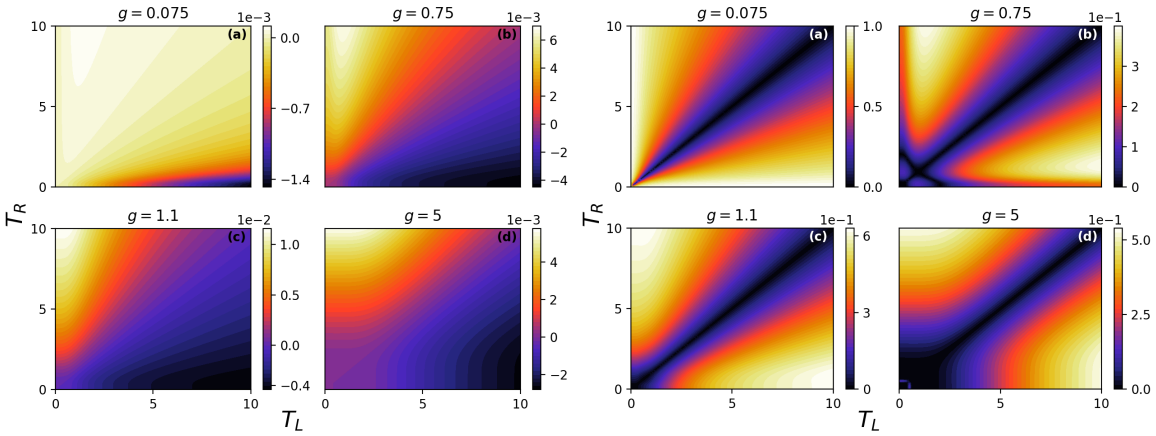


a: Heat Current $\mathcal{J}_{\mathrm{R}}$ b: Rectification $\mathcal{R}$

Figure 7.8: **RQ Ohmic Spectrum High temperature.**

# BIBLIOGRAPHY


[1] S.F. Huelga and M.B. Plenio. Vibrations, quanta and biology. *Contemporary Physics*, 54(4):181–207, 2013.

[2] N. Lambert, Y.-N. Chen, Y.-C. Cheng, C.-M. Li, G.-Y. Chen, and F. Nori. Quantum biology. *Nature Physics*, 9:10–18, 2013.

[3] M. Mohseni, Y. Omar, G.S. Engel, and M.B. Plenio. *Quantum Effects in Biology*. Cambridge University Press, Cambridge, 2014.

[4] Hohjai Lee, Yuan-Chung Cheng, and Graham R. Fleming. Coherence dynamics in photosynthesis: Protein protection of excitonic coherence. *Science*, 316(5830):1462–1465, 2007.

[5] G. S. Engel, T. R. Calhoun, E. L. Read, T.-K. Ahn, T. Mancal, Y.-C. Cheng, R. E. Blankenship, and G. R. Fleming. Evidence for wavelike energy transfer through quantum coherence in photosynthetic systems. *Nature*, 446:782, 2007.

[6] E. Collini, C. Y. Wong, K. E. Wilk, P. M. G. Curmi, P. B. Brumer, and G. D. Scholes. Coherently wired light-harvesting in photosynthetic marine algae at ambient temperature. *Nature*, 463:644, 2010.

[7] G.Panitchayangkoon, D. Hayes, K. A. Fransted, J. R. Caram, E. Harel, J. Wen, R. E. Blankenship, and G. S. Engel. Direct evidence of quantum transport in photosynthetic light-harvesting complexes. *Proceedings of the National Academy of Sciences*, 107, 2010.

[8] G.Panitchayangkoon, D.V. Voronine, D. Abramavicius, J. R. Caram, N. H. C. Lewis, S. Mukamel, and G. S. Engel. Long-lived quantum coherence in photo-

synthetic complexes at physiological temperature. *Proceedings of the National Academy of Sciences*, 108, 2011.

[9] E. B. Davies. *Quantum Theory of Open Systems*. Academic Press, London, 2007.

[10] H.-P. Breuer and F. Petruccioneo. *The Theory of Open Quantum Systems*. Oxford University Press, Oxford, 2007.

[11] Robert Alicki and Karl Lendi. *Quantum Dynamical Semigroups and Applications*. Lecture Notes in Physics 717. Springer-Verlag Berlin Heidelberg, 1 edition, 2007.

[12] Á. Rivas and S. F. Huelga. *Open Quantum Systems, An Intorduction*. Springer, Heidelberg, 2012.

[13] Gernot Schaller. *Open Quantum Systems Far from Equilibrium*. Springer, Switzerland, 2014.

[14] Akihito Ishizaki and Graham R. Fleming. Theoretical examination of quantum coherence in a photosynthetic system at physiological temperature. *Proceedings of the National Academy of Sciences*, 106(41):17255–17260, 2009.

[15] M B Plenio and S F Huelga. Dephasing-assisted transport: quantum networks and biomolecules. *New Journal of Physics*, 10(11):113019, 2008.

[16] Masoud Mohseni, Patrick Rebentrost, Seth Lloyd, and Alán Aspuru-Guzik. Environment-assisted quantum walks in photosynthetic energy transfer. *The Journal of Chemical Physics*, 129(17):174106, 2008.

[17] Patrick Rebentrost, Masoud Mohseni, Ivan Kassal, Seth Lloyd, and Alán Aspuru-Guzik. Environment-assisted quantum transport. *New Journal of Physics*, 11(3):033003, 2009.

[18] F. Caruso, A. W. Chin, A. Datta, S. F. Huelga, and M. B. Plenio. Highly efficient energy excitation transfer in light-harvesting complexes: The fundamental role of noise-assisted transport. *The Journal of Chemical Physics*, 131(10):105106, 2009.

[19] A W Chin, A Datta, F Caruso, S F Huelga, and M B Plenio. Noise-assisted energy transfer in quantum networks and light-harvesting complexes. *New Journal of Physics*, 12(6):065002, 2010.

[20] Ivan Kassal and Alán Aspuru-Guzik. Environment-assisted quantum transport in ordered systems. *New Journal of Physics*, 14(5):053041, 2012.

[21] Yonatan Dubi. Interplay between dephasing and geometry and directed heat flow in exciton transfer complexes. *The Journal of Physical Chemistry C*, 119(45):25252–25259, 2015.

[22] P. W. Anderson. Absence of diffusion in certain random lattices. *Physical Review*, 109:1492–1505, Mar 1958.

[23] F. L. Semi ao, K. Furuya, and G. J. Milburn. Vibration-enhanced quantum transport. *New Journal of Physics*, 12(8):083033, 2010.

[24] Avinash Kolli, Edward J. O'Reilly, Gregory D. Scholes, and Alexandra Olaya-Castro. The fundamental role of quantized vibrations in coherent light harvesting by cryptophyte algae. *The Journal of Chemical Physics*, 137(17):174109, 2012.

[25] A. W. Chin, J. Prior, R. Rosenbach, F. Caycedo-Soler, S. F. Huelga, and M. B. Plenio. The role of non-equilibrium vibrational structures in electronic coherence and recoherence in pigment–protein complexes. *Naure Physics*, 9, 2013.

[26] James Lim, Mark Tame, Ki Hyuk Yee, Joong-Sung Lee, and Jinhyoung Lee. Phonon-induced dynamic resonance energy transfer. *New Journal of Physics*, 16(5):053018, 2014.

[27] E. K. Irish, R. Gómez-Bombarelli, and B. W. Lovett. Vibration-assisted resonance in photosynthetic excitation-energy transfer. *Physical Review A*, 90:012510, Jul 2014.

[28] N. Killoran, S. F. Huelga, and M. B. Plenio. Enhancing light-harvesting power with coherent vibrational interactions: A quantum heat engine picture. *The Journal of Chemical Physics*, 143(15):155102, 2015.

[29] Zhedong zhang and Jin Wang. Origin of long-lived quantum coherence and excitation dynamics in pigment-protein complexes. *Scientific Reports*, 6, 2016.

[30] Hohjai Lee, Yuan-Chung Cheng, and Graham R. Fleming. Coherence dynamics in photosynthesis: Protein protection of excitonic coherence. *Science*, 316(5830):1462–1465, 2007.

[31] Sarah Mostame, Patrick Rebentrost, Alexander Eisfeld, Andrew J Kerman, Dimitris I Tsomokos, and Alán Aspuru-Guzik. Quantum simulator of an open quantum system using superconducting qubits: exciton transport in photosynthetic complexes. *New Journal of Physics*, 14(10):105013, 2012.

[32] R. de J. León-Montiel, M. A. Quiroz-Juárez, R. Quintero-Torres, J. L. Dominguez-Juárez, H. M. Moya-Cessa, J. P. Torres, and J. L. Aragón. Noise-assisted energy transport in electrical oscillator networks with off-diagonal dynamical disorder. *Scientific Reports*, 5, 2015.

[33] D. N. Biggerstaff, R. Heilmann, M. Grafe A. A. Zecevik, M. A. Broome, A. Fedrizzi, S. Nolte, A. Szameit, A. G. White, and I. Kassal. Enhancing co-

herent transport in a photonic network using controllable decoherence. *Nature Communications*, 7, 2016.

[34] Sarah Mostame, Joonsuk Huh, Christoph Kreisbeck, Andrew J. Kerman, Takatoshi Fujita, Alexander Eisfeld, and Alán Aspuru-Guzik. Emulation of complex open quantum systems using superconducting qubits. *Quantum Information Processing*, 16(2):44, 2016.

[35] A. Potočnik, A. Bargerbos, F. A. Y. N. Schröder, S. A. Khan, M. C. Collodo, S. Gasparinetti, Y. Salathé, C. Creatore, C. Eichler, H. E. Türeci, A. W. Chin, and A. Wallraff. Studying light-harvesting models with superconducting circuits. *Nature Communications*, 9, 2018.

[36] Bi-Xue Wang, Ming-Jie Tao, Qing Ai, Tao Xin, Neill Lambert, Dong Ruan, Yuan-Chung Cheng, Franco Nori, Fu-Guo Deng, and Gui-Lu Long. Quantum simulation of photosynthetic energy transfer. *arXiv:1801.09475*, 2018.

[37] G. H. Richards, K. E. Wilk, P. M. G. Curmi, H. M. Quiney, and J. A. Davis. Coherent vibronic coupling in light-harvesting complexes from photosynthetic marine algae. *The Journal of Physical Chemistry Letters*, 3(2):272–277, 2012. PMID: 26698327.

[38] Hong-Guang Duan, Valentyn I. Prokhorenko, Richard J. Cogdell, Khuram Ashraf, Amy L. Stevens, Michael Thorwart, and R. J. Dwayne Miller. Nature does not rely on long-lived electronic quantum coherence for photosynthetic energy transfer. *Proceedings of the National Academy of Sciences*, 114(32):8493–8498, 2017.

[39] D. Gelbwaser-Klimovsky and A. Aspuru-Guzik. On thermodynamic inconsistencies in several photosynthetic and solar cell models and how to fix them. *Chemical Science*, 8, 2017.

[40] R. Alicki and R. Kosloff. Introduction to quantum thermodynamics: History and prospects. *arXiv:1801.08314*, 2018.

[41] Francesco Giazotto, Tero T. Heikkila, Arttu Luukanen, Alexander M. Savin, and Jukka P. Pekola. Opportunities for mesoscopics in thermometry and refrigeration: Physics and applications. *Rev. Mod. Phys.*, 78:217–274, Mar 2006.

[42] N.A. Roberts and D.G. Walker. A review of thermal rectification observations and models in solid materials. *International Journal of Thermal Sciences*, 50(5):648 – 662, 2011.

[43] Nianbei Li, Jie Ren, Lei Wang, Gang Zhang, Peter Hanggi, and Baowen Li. Colloquium: Phononics: Manipulating heat flow with electronic analogs and beyond. *Rev. Mod. Phys.*, 84:1045–1066, Jul 2012.

[44] Giuliano Benenti, Giulio Casati, Keiji Saito, and Robert S. Whitney. Fundamental aspects of steady-state conversion of heat to work at the nanoscale. *Physics Reports*, 694:1 – 124, 2017.

[45] B. Roche, P. Roulleau, T. Jullien, Y. Jompol, I. Farrer, D. A. Ritchie, and D. C. Glattli. Harvesting dissipated energy with a mesoscopic ratchet. *Nature Communications*, 6, 2015.

[46] Holger Thierschmann, Rafael Sánchez, Björn Sothmann, Fabian Arnold, Christian Heyn, Wolfgang Hansen, Hartmut Buhmann, and Laurens W. Molenkamp. Three-terminal energy harvester with coupled quantum dots. *Nature Nanotechnology*, 10, 2015.

[47] Lei Wang and Baowen Li. Thermal logic gates: Computation with phonons. *Phys. Rev. Lett.*, 99:177208, Oct 2007.

[48] P. Pfeffer, F. Hartmann, S. Hofling, M. Kamp, and L. Worschech. Logical stochastic resonance with a coulomb-coupled quantum-dot rectifier. *Phys. Rev. Applied*, 4:014011, Jul 2015.

[49] Johannes Roßnagel, Samuel T. Dawkins, Karl N. Tolazzi, Obinna Abah, Eric Lutz, Ferdinand Schmidt-Kaler, and Kilian Singer. A single-atom heat engine. *Science*, 352(6283):325–329, 2016.

[50] B. Karimi and J. P. Pekola. Otto refrigerator based on a superconducting qubit: Classical and quantum performance. *Phys. Rev. B*, 94:184503, Nov 2016.

[51] Shabir Barzanjeh, Matteo Aquilina, and André Xuereb. Manipulating the flow of thermal noise in quantum devices. *Phys. Rev. Lett.*, 120:060601, Feb 2018.

[52] Teemu Ojanen and Antti-Pekka Jauho. Mesoscopic photon heat transistor. *Phys. Rev. Lett.*, 100:155902, Apr 2008.

[53] Karl Joulain, Jérémie Drevillon, Younès Ezzahri, and Jose Ordonez-Miranda. Quantum thermal transistor. *Phys. Rev. Lett.*, 116:200601, May 2016.

[54] T. Werlang, M. A. Marchiori, M. F. Cornelio, and D. Valente. Optimal rectification in the ultrastrong coupling regime. *Phys. Rev. E*, 89:062109, Jun 2014.

[55] Zhong-Xiao Man, Nguyen Ba An, and Yun-Jie Xia. Controlling heat flows among three reservoirs asymmetrically coupled to two two-level systems. *Phys. Rev. E*, 94:042135, Oct 2016.

[56] Jose Ordonez-Miranda, Younes Ezahri, and Karl Joulain. Quantum thermal diode based on two interacting spinlike systems under different excitations. *Phys. Rev. E*, 95:022128, Feb 2017.

[57] Yuecheng Shen, Matthew Bradford, and Jung-Tsung Shen. Single-photon diode by exploiting the photon polarization in a waveguide. *Phys. Rev. Lett.*, 107:173902, Oct 2011.

[58] B Karimi, J P Pekola, M Campisi, and R Fazio. Coupled qubits as a quantum heat switch. *Quantum Science and Technology*, 2(4):044007, 2017.

[59] Alberto Ronzani, Bayan Karimi, Jorden Senior, Yu-Cheng Chang, Joonas T. Peltonen, ChiiDong Chen, and Jukka P. Pekola. Tunable photonic heat transport in a quantum heat valve. *arXiv:1801.09312*, 2018.

[60] Erwin Kreyszig. *Introductory functional analysis with applications*. Wiley, 1978.

[61] Ramamurti Shankar. *Mathematical methods for physicists*. Springer, US, 2nd edition, 1995.

[62] G. B. Arfken and H. J. Weber. *Mathematical methods for physicists*. Elsevier, New Delhi, 6th edition, 2005.

[63] Peter Szekeres. *A Course in Modern Mathematical Physics - Groups, Hilbert Space and Differential Geometry*. Cambridge University Press, Cambridge, 2004.

[64] David J. Griffiths. *Introduction to Quantum Mechanics*. Pearson, NJ, 2005.

[65] J. J. Sakurai and Jim J. Napolitano. *Modern Quantum Mechanics*. Pearson, UK, 2nd edition, 2014.

[66] George Finlay Simmons. *Differential equations with applications and historical notes*. Textbooks in mathematics (Boca Raton Fla.). Chapman and Hall/CRC, 3rd edition, 2017.

[67] Christian Constanda. *Differential Equations: A Primer for Scientists and Engineers*. Springer Undergraduate Texts in Mathematics and Technology. Springer International Publishing, 2th edition, 2017.

[68] Andrei D. Polyanin and Valentin F. Zaitsev. *Handbook of Ordinary Differential Equations: Exact Solutions, Methods, and Problems*. Chapman and Hall/CRC, 3rd edition, 2018.

[69] Claude Cohen-Tannoudji, Bernard Diu, and Franck Laloë. *Quantum Mechanics*, volume Volume I. John Wiley and Sons, 1977.

[70] William H. Louisell. *Quantum Statistical Properties of Radiation (Wiley Classics Library)*. Wiley-Interscience, 1990.

[71] William C. Schieve and Lawrence P. Horwitz. *Quantum statistical mechanics*. Cambridge University Press, 1 edition, 2009.

[72] Michael A. Nielsen and Isaac L. Chuang. *Quantum computation and quantum information*. Cambridge University Press, 10th anniversary ed edition, 2010.

[73] Karl Blum. *Density Matrix Theory and Applications*. Springer Series on Atomic, Optical, and Plasma Physics 64. Springer-Verlag Berlin Heidelberg, 3 edition, 2012.

[74] Mehran Kardar. *Statistical Physics of Particles*. Cambridge University Press, Cambridge, 2007.

[75] Ravinder R. Puri. *Mathematical methods of quantum optics*. Springer Series in Optical Sciences. Springer, 1st edition, 2010.

[76] Roger Bowley and Mariana Sanchez. *Introductory Statistical Mechanics, Second Edition*. Oxford University Press, USA, 2nd edition, 2000.

[77] Frederick Reif. *Fundamentals of Statistical and Thermal Physics*. Waveland Press, reprint edition, 2009.

[78] Pierre Meystre and Murray Sargent. *Elements of quantum optics*. Springer, 4th edition, 2007.

[79] Miguel Orszag. *Quantum optics: including noise reduction, trapped ions, quantum trajectories, and decoherence*. Springer, 2nd edition, 2007.

[80] G. Lindblad. On the generators of quantum dynamical semigroups. *Commun. math. Phys.*, 48, 1976.

[81] V. Gorini, A. Kossakowski, and E. C. G. Sudarshan. Completely positive dynamical semigroups of n-level systems. *J. Math. Phys.*, 17, 1976.

[82] Robert Alicki. Invitation to quantum dynamical semigroups. *arXiv:quant-ph/0205188*, 2002.

[83] Jin-Sheng Peng and Gao-Xiang Li. *Introductionto to Modern Quantum Optics*. World Scientific, 1998.

[84] Howard J. Carmichael. *Statistical Methods in Quantum Optics 1: Master Equations and Fokker-Planck Equations*. Texts and Monographs in Physics. Springer-Verlag Berlin Heidelberg, 1 edition, 1999.

[85] W. Weidlich. Liouville-space formalism for quantum systems in contact with reservoirs. *Physik*, 241(4):325–339, 1971.

[86] Petrosky T. and Prigogine I. *The Liouville Space Extension of Quantum Mechanics*, pages 1–120. Wiley-Blackwell, 2007.

[87] Berthold-Georg Englert and Giovanna Morigi. *Five Lectures on Dissipative Master Equations*, pages 55–106. Springer Berlin Heidelberg, Berlin, Heidelberg, 2002.

[88] Shai Machnes and Martin B. Plenio. Stanislaw kryszewski and justyna czechowska-kryszk. *arXiv:0801.1757*, 2008.

[89] Angel Rivas, A Douglas K Plato, Susana F Huelga, and Martin B Plenio. Markovian master equations: a critical study. *New Journal of Physics*, 12(11):113032, 2010.

[90] Ronnie Kosloff. Quantum thermodynamics: A dynamical viewpoint. *Entropy*, 15(6):2100–2128, 2013.

[91] Jochen Gemmer, M. Michel, and Günter Mahler. *Quantum thermodynamics: emergence of thermodynamic behavior within composite quantum systems*. Lecture notes in physics 784. Springer-Verlag Berlin Heidelberg, 2 edition, 2009.

[92] Sai Vinjanampathy and Janet Anders. Quantum thermodynamics. *Contemporary Physics*, 57(4):545–579, 2016.

[93] James Millen and André Xuereb. Perspective on quantum thermodynamics. *New Journal of Physics*, 18(1):011002, 2016.

[94] Peter Hertel. *Quantum theory and statistical thermodynamics : principles and worked examples*. Graduate texts in physics. Springer, 2017.

[95] Robert Alicki and Ronnie Kosloff. Introduction to quantum thermodynamics: History and prospects. *arXiv:1801.08314*, 2018.

[96] Inés de Vega and Daniel Alonso. Dynamics of non-markovian open quantum systems. *Rev. Mod. Phys.*, 89:015001, Jan 2017.

[97] Heinz-Peter Breuer, Elsi-Mari Laine, Jyrki Piilo, and Bassano Vacchini. Colloquium: Non-markovian dynamics in open quantum systems. *Rev. Mod. Phys.*, 88:021002, Apr 2016.

[98] C.H. Fleming and B.L. H. Non-markovian dynamics of open quantum systems: Stochastic equations and their perturbative solutions. *Annals of Physics*, 327(4):1238 – 1276, 2012.

[99] D. Tamascelli, A. Smirne, S. F. Huelga, and M. B. Plenio. Nonperturbative treatment of non-markovian dynamics of open quantum systems. *Phys. Rev. Lett.*, 120:030402, Jan 2018.

[100] Heinz-Peter Breuer. Non-markovian quantum dynamics and the method of correlated projection superoperators. *arXiv:0707.0172*, 2007.

[101] Aidan Strathearn, Peter Kirton, Dainius Kilda, Jonathan Keeling, and Brendon W. Lovett. Efficient non-markovian quantum dynamics using time-evolving matrix product operators. *arXiv:1711.09641*, 2017.

[102] Yusui Chen, J. Q. You, and Ting Yu. Exact non-markovian master equations for multiple qubit systems: Quantum-trajectory approach. *Phys. Rev. A*, 90:052104, Nov 2014.

[103] E. Ferraro, M. Scala, R. Migliore, and A. Napoli. Non-markovian dissipative dynamics of two coupled qubits in independent reservoirs: Comparison between exact solutions and master-equation approaches. *Phys. Rev. A*, 80:042112, Oct 2009.

[104] I Sinayskiy, E Ferraro, A Napoli, A Messina, and F Petruccione. Non-markovian dynamics of an interacting qubit pair coupled to two independent bosonic baths. *Journal of Physics A: Mathematical and Theoretical*, 42(48):485301, 2009.

[105] Bassano Vacchini and Heinz-Peter Breuer. Exact master equations for the non-markovian decay of a qubit. *Phys. Rev. A*, 81:042103, Apr 2010.

[106] Andrea Smirne and Bassano Vacchini. Nakajima-zwanzig versus time-convolutionless master equation for the non-markovian dynamics of a two-level system. *Phys. Rev. A*, 82:022110, Aug 2010.

[107] H. Z. Shen, M. Qin, Xiao-Ming Xiu, and X. X. Yi. Exact non-markovian master equation for a driven damped two-level system. *Phys. Rev. A*, 89:062113, Jun 2014.

[108] E. T. Jaynes and F. W. Cummings. Comparison of quantum and semiclassical radiation theories with application to the beam maser. *Proceedings of the IEEE*, 51(1):89–109, Jan 1963.

[109] Charles R. Johnson Roger A. Horn. *Topics in matrix analysis*. Cambridge University Press, 1994.

[110] Shai Machnes and Martin B. Plenio. Surprising interactions of markovian noise and coherent driving. *arXiv:1408.3056*, 2014.

[111] Morag Am-Shallem, Amikam Levy, Ido Schaefer, and Ronnie Kosloff. Three approaches for representing lindblad dynamics by a matrix-vector notationg. *arXiv:1510.08634*, 2015.

[112] Carlos Navarrete-Benlloch. Open systems dynamics: Simulating master equations in the computer. *arXiv:1504.05266*, 2015.

[113] J. Johansson, P. Nation, and F. Nori. Qutip 2: A python framework for the dynamics of open quantum system. *Comput. Phys. Commun.*, 184, 2013.

[114] Pedro D. Manrique, Ferney Rodriguez, Luis Quiroga, and Neil F. Johnson. Nonequilibrium quantum systems: Divergence between global and local descriptions. *Advances in Condensed Matter Physics*, Volume 2015, 2014.

[115] Amikam Levy and Ronnie Kosloff. The local approach to quantum transport may violate the second law of thermodynamics. *EPL (Europhysics Letters)*, 107(2):20004, 2014.

[116] Patrick P Hofer, Marta Perarnau-Llobet, L David M Miranda, Geraldine Haack, Ralph Silva, Jonatan Bohr Brask, and Nicolas Brunner. Markovian master equations for quantum thermal machines: local versus global approach. *New Journal of Physics*, 19(12):123037, 2017.

[117] J. Onam Gonzalez, Luis A. Correa, Giorgio Nocerino, Jose P. Palao, Daniel Alonso, and Gerardo Adesso. Testing the validity of the local and global gkls master equations on an exactly solvable model. *Open Systems & Information Dynamics*, 24(04):1740010, 2017.

[118] J. Z. Bernád and J. M. Torres. Partly invariant steady state of two interacting open quantum systems. *Phys. Rev. A*, 92, 2015.

[119] M Scala, R Migliore, and A Messina. Dissipation and entanglement dynamics for two interacting qubits coupled to independent reservoirs. *Journal of Physics A: Mathematical and Theoretical*, 41(43):435304, 2008.

[120] Jie-Qiao Liao, Jin-Feng Huang, and Le-Man Kuang. Quantum thermalization of two coupled two-level systems in eigenstate and bare-state representations. *Phys. Rev. A*, 83:052110, 2011.

[121] M. Scala, E. Ferraro, A. Napoli, A. Messina, L. L. Sánchez-Soto, and R. Migliore. Dissipative dynamics of two coupled qubits: a short review of some recent results. *Optics and Spectroscopy*, 111(4):553, 2011.

[122] J. P. Santos and F. L. Semiao. Master equation for dissipative interacting qubits in a common environment. *Phys. Rev. A*, 89:022128, 2014.

[123] G.L. Decordi and A. Vidiella-Barranco. Two coupled qubits interacting with a thermal bath: A comparative study of different models. *Optics Communications*, 387:366 – 376, 2017.

[124] B. Bellomo, R. Messina, and M. Antezza. Dynamics of an elementary quantum system in environments out of thermal equilibrium. *EPL (Europhysics Letters)*, 100(2):20006, 2012.

[125] Bruno Bellomo, Riccardo Messina, Didier Felbacq, and Mauro Antezza. Quantum systems in a stationary environment out of thermal equilibrium. *Phys. Rev. A*, 87:012101, Jan 2013.

[126] József Zsolt Bernád and Juan Mauricio Torres. Partly invariant steady state of two interacting open quantum systems. *Phys. Rev. A*, 92:062114, Dec 2015.

[127] S. J. D. Phoenix and P. L. Knight. Periodicity, phase, and entropy in models of two-photonresonance. *J. Opt. Soc. Am. B*, 7(1):116–124, Jan 1990.

[128] J. K. Moqadam and R. Portugal. Quantum walks on a circle with optomechanical systems. *Quantum Inf Process*, 14, 2015.

[129] B. C. Travaglione and G. J. Milburn. Implementing the quantum random walk. *Phys. Rev. A*, 65:032310, Feb 2002.